Dynamic Modeling of the Interfacial Properties Due to the Combined Chemical Reaction and Diffusive Transport in Reactive Nonuniform Liquid Systems

Zur Erlangung des akademischen Grades eines

DOKTORS DER INGENIEURWISSENSCHAFTEN (DR.-ING.)

von der KIT-Fakultät für Chemieingenieurwesen und Verfahrenstechnik des Karlsruher Instituts für Technologie (KIT)
genehmigte

DISSERTATION

von
M.Sc. Joe Hajjar
aus Bauchrieh, Libanon

Tag der mündlichen Prüfung: 14.11.2024

Erstgutachterin: Prof. Dr. rer. nat. habil. Sabine Enders
Zweitgutachter: Prof. Dipl.-Ing. Dr. techn. Hans-Jörg Bart

“

The important thing is not to stop questioning. Curiosity has its own reason for existing. One cannot help but be in awe when he contemplates the mysteries of eternity, of life, of the marvelous structure of reality. It is enough if one tries merely to comprehend a little of this mystery every day.

”

Albert Einstein

Acknowledgments

I wish to thank everyone who has helped and supported me personally and professionally during my dissertation process.

Words cannot express my gratitude to my professor Prof. Dr. rer. nat. habil. Sabine Enders for her invaluable feedback. I also could not have undertaken this journey without the many valuable and helpful discussions I have had with her.

I am also grateful to Prof. Dipl.-Ing. Dr. techn. Hans-Jörg Bart for the supervision of this work and the associated effort.

Lastly, to my parents, for seeing this through with patience, love and understanding. Their belief in me has kept my spirits and motivation high during the whole process.

Abstract

Liquid-liquid extraction is among the most common initial thermal separation techniques in chemical and process engineering. The proper description of the phase equilibria, the mass transfer across the interface and the interfacial properties of the involved liquid systems is crucial for process design and optimization. In particular, and regarding reactive liquid extraction processes, chemical equilibrium system states as well as reaction kinetics are additionally the subject of study and should be properly predicted. Mass transfer and chemical kinetics will lead the reactive nonuniform system to reach a final stable system state, at which the combined phase and chemical equilibrium states are reached.

The interfacial properties of liquid nonuniform systems at phase equilibrium can be calculated by combining the incompressible version of the Density Gradient Theory with an appropriate g^E-model. A generalized chemical potential, which is the starting point for describing mass transfer and kinetics in reactive, heterogeneous and multicomponent systems, is derived.

In this work, a generalized and thermodynamically consistent theoretical framework that embodies the combined reaction and transport associated with reactive nonuniform systems is developed and introduced for the first time. Rate equations, which are formulated with activities, are combined with the modified and generalized Cahn-Hilliard equation. The theoretical treatment is exemplified by conceptual and theoretical model calculations involving a simple chemical reaction and for both limiting situations in which, on the one hand, the rate of reaction is effectively instantaneous and, on the other hand, the reaction is much slower than the rate of diffusion. Chemical reactions occurring in the interface between coexisting bulk phases are predicted and their impact on the dynamics of the whole system is studied. Interfacial properties, such as interfacial tensions and interfacial concentration profiles, are also calculated at each time step of the evolution of the reactive system towards its final stable state. Concerning the first limiting situation, interfacial chemical reactions have a marked impact on the overall reacting system. The chemical reaction reaches chemical equilibrium first in both bulk phases, and then at the interface between them. Opposing results emerge for the second limiting situation, in which the interfacial chemical reaction has no impact on the dynamics of the system.

Zusammenfassung

Die Flüssig-Flüssig-Extraktion gehört zu den am häufigsten verwendeten thermischen Trennverfahren im Bereich Chemieingenieurwesen und Verfahrenstechnik. Die korrekte Beschreibung der Phasengleichgewichte, des Stofftransportes über die Grenzfläche und der Grenzflächeneigenschaften der beteiligten flüssigen Systeme ist entscheidend für die Prozessauslegung und -optimierung. Im Falle der Reaktivextraktion müssen die chemischen Gleichgewichtszustände und die Reaktionskinetik zusätzlich berücksichtigt und korrekt vorhergesagt werden. Stofftransport und Reaktionskinetik führen das Reaktivsystem zu einem Superpositionszustand, also zur Überlagerung von Phasen- und chemischen Gleichgewicht.

Die Grenzflächeneigenschaften von flüssigen-heterogenen Systemen im Phasengleichgewicht können mit der inkompressiblen Dichtegradiententheorie in Kombination mit einem geeigneten g^E-Modell berechnet werden. Ein verallgemeinertes chemisches Potential, welches den Ausgangspunkt für die Beschreibung des Stofftransportes und der Reaktionskinetik in reaktiven, heterogenen und Mehrkomponentensystemen bildet, ist abgeleitet.

Im Rahmen dieser Arbeit wird zum ersten Mal eine verallgemeinerte und thermodynamisch konsistente Theorie, welche die Überlagerung von Reaktion und Stofftransport im Zusammenhang mit reaktiven und heterogenen Systemen darstellt, entwickelt und eingeführt. Ratengleichungen, welche mit Aktivitäten formuliert sind, werden mit der modifizierten und verallgemeinerten Cahn-Hilliard-Gleichung kombiniert. Die theoretische Vorstellung wird anhand von konzeptionellen und theoretischen Modellrechnungen am Beispiel einer einfachen chemischen Reaktion und für beiden Grenzfälle, in denen einerseits die Reaktion viel schneller abläuft als die Diffusion und andererseits die Reaktionsgeschwindigkeit viel kleiner ist als die Diffusionsgeschwindigkeit, demonstriert. Chemische Reaktionen, welche an der Grenzfläche zwischen koexistierenden Bulkphasen stattfinden, werden vorhergesagt und ihren Einfluss auf die dynamische Entwicklung des gesamten Systems untersucht. Grenzflächeneigenschaften wie Grenzflächenspannungen und Konzentrationsprofile werden in jedem Zeitschritt der Entwicklung des Reaktivsystems zu dem Superpositionszustand ebenfalls berechnet. Bezüglich des ersten Grenzfalles haben Grenzschichtreaktionen einen deutlichen Einfluss auf das gesamte Reaktivsystem. Die chemische Reaktion erreicht das chemische Gleichgewicht erst in beiden Bulkphasen, dann in der Grenzfläche. Gegensätzliche Ergebnisse ergeben sich für den zweiten Grenzfall, in dem die Grenzschichtreaktion keinen Einfluss auf die Dynamik des Systems hat.

Table of Contents

1 Introduction

Conventional production processes in the chemical, petrochemical and pharmaceutical industries are characterized by a sequential interconnection of unit operations to implement various basic process engineering operations, such as reaction or separation. The greatest effort in technical manufacturing and production processes is related to the upstream and downstream separation processes. Capital and operational expenditures can become very high depending on the chemical and thermodynamic properties of the involved systems.

Thermal separation processes have a wide range of application. For instance, liquid-liquid extraction, also known as solvent extraction, is among the most common initial separation techniques and is a method to separate chemical components or metal complexes based on their relative solubilities in two different and practically immiscible liquids. A net transfer of one or more species generally from an aqueous phase into an organic liquid one takes place. The advantages of such thermal separation techniques are the lower complexity in process design, a wide operating window of process parameters, and the good knowledge and understanding of the entire process. Furthermore, reactive separation processes are characterized by the simultaneous combination of reaction and separation in one single apparatus. They can reduce the number of subsequent separation steps compared to those needed in classical and conventional production processes, thus also reducing the number of required separation units. Reactive distillation, reactive absorption, reactive adsorption, reactive extraction, reactive crystallization, and reactive pervaporation are the well-known important examples of reactive separations. They are receiving considerable attention from theorists and industries due to the process intensification they generate. The main advantage of these integrated systems is a possible shift of the chemical equilibrium towards the side of the reaction products caused by their simultaneous separation from the reacting mixture, thus increasing reaction conversion and enhancing reaction selectivity. However, and due to the strong interactions of chemical reactions, heat, and mass transfer, reactive separation processes require complex thermodynamic modeling and process simulation, and lead to a limited applications window, an

extensive equipment design effort, and an increased operational complexity. The thermodynamic modeling of reactive separation processes aims essentially at predicting and properly describing the phase equilibrium, the chemical equilibrium, the reaction kinetics, the mass transfer, and the interface, all of which are mostly associated with multicomponent as well as multiphase reactive nonuniform systems. The efficiency of such separation techniques will be affected by many dynamic properties, namely the interfacial properties of the involved multicomponent and heterogeneous systems in the reactive separation process.

In particular, the reactive liquid extraction process is a liquid-liquid extraction that is intensified through a mechanism involving a chemical reaction. Liquid-liquid extraction and reactive liquid extraction are basic unit operations in chemical engineering. They are performed using a variety of apparatus such as countercurrent distribution equipment, e.g., mixer-settler cascades, or extraction columns. The interfacial properties of multicomponent and practically immiscible liquid systems have received considerable attention from the chemical, petrochemical, and pharmaceutical industries. An accurate description of liquid interfaces is important for process and product design. Continuum methods can also accommodate the time and distance scales and the variety of phenomena, such as chemical reactions and mass and heat transfer, that must be considered in practical manufacturing processes and the modeling and design of unit operations.

Mass transfer across fluid interfaces and chemical kinetics can be described by nonlinear diffusion equations and rate equations, respectively. The rate equations link the reaction rate of a chemical reaction with the activities of the reactants. In order to describe industrially relevant reactive nonuniform systems, diffusive mobilities and reaction rate coefficients, which are found in diffusion and rate equations, respectively, should usually be adjusted to experimental data. Furthermore, a thermodynamically consistent treatment of reactive systems requires the activities and chemical potentials found in both reaction and diffusion models to be described with the same thermodynamic model that also accounts for the intermolecular interactions leading to the liquid state of matter.

The interface is characterized by a layer with a smooth spatial variation in the thermodynamic state variables and in one of the intensive scalar properties of the nonuniform system, such as composition or density, between the homogeneous bulk phases. The Helmholtz energy of an

inhomogeneous system is thus given by a functional of density or composition and their spatial gradients, while being only a function of these variables in homogeneous systems. Reaching a final and stable phase equilibrium system state requires mass transfer of the involved components across the interface between uniform bulk phases and is particularly influenced by its internal structure. The Helmholtz energy functional leads to the density and concentration profiles in the interface, which play an important role in both liquid-liquid extraction and reactive liquid extraction processes. Whenever multiple phases are present in reactive processes, the interfacial properties can affect the reaction kinetics. For instance, chemical reactions can take place in homogeneous bulk phases as well as at the interface between them. In the latter case, the activities of the reactants, which are found in the rate equations, will depend on the density and concentration gradients within the interface, thus also affecting the overall kinetics.

In this work, a unified thermodynamic theory of reaction and diffusion in heterogeneous reactive liquid systems is introduced. The general and thermodynamically consistent theoretical treatment embodies the combined reaction and transport associated with reactive liquid extraction processes. The modified and generalized Cahn-Hilliard equation is combined with kinetic rate equations, which are formulated with activities rather than concentrations. Within the applied diffusion model, the flux of each component in the mixture is not solely proportional to the spatial gradient of its chemical potential, but results from additive contributions of spatial gradients of the chemical potentials of all involved components in the spirit of non-equilibrium thermodynamics. Chemical reactions occurring in the interfacial layer between homogeneous bulk phases are also predicted. The general model leads to a set of partial differential equations describing the spatial and temporal evolution of the concentrations of all the involved components in the interface, and the temporal evolution of their concentrations in the uniform bulk phases. The obtained equations are thus used to investigate the dynamics of the interfacial profiles in reactive nonuniform systems. Based on these profiles, the evolution of other interfacial properties such as the interfacial tension over time can also be obtained. The spatial and temporal evolution of the concentration profiles in the interface will be discussed in detail, and their impact, together with that of the interfacial chemical reaction, on the dynamics of the whole reactive system will be studied.

In contrast to previous work, phase equilibrium states will not be predicted using solubilities, but the chemical potentials of each of the components in each of the phases that it is present in

the system will rather be set equal. Moreover, the equilibrium constant of the occurring chemical reactions, the chemical kinetics and the mass transfer are described by activities and chemical potentials in a thermodynamically consistent manner. Therefore, a simplifying, concentration-based description, which is usually applied in the literature, will not be considered in this work. In addition, the uniform bulk phases, the interface between them, the combined phase and chemical equilibrium states, the reaction kinetics as well as the mass transfer across the interface are uniformly described by the same thermodynamic model.

The generalized concept is exemplified by theoretical and conceptual model calculations, and the resulting differential equations are solved numerically in typical situations for reactive liquid systems. In this work, the application of this generalized concept is confined to modeling both limiting cases of reacting mixtures in which the rate of reaction is effectively instantaneous, and in which diffusion is much faster than the rate of reaction. Furthermore, sensitivity analysis in terms of the applied thermodynamic and kinetic parameters is performed, and the obtained predictions and calculations are compared to a standard example. The impact of the various thermodynamic and kinetic parameters of the theoretical framework on the dynamics of the reactive systems will also be discussed in detail. In summary, this work presents a generalized and conceptual tool for the prediction of diverse and combined equilibrium states in complex multicomponent and multiphase reactive systems. It is also able to describe and predict the dynamics of these nonuniform systems, consisting of bulk phases and interface, that lead to their evolution towards these final equilibrium states.

2 Review of the Literature

First, reactive liquid extraction is discussed in the literature mainly concerning the extraction of organic compounds, such as acetic acid [1-5], butyric acid [3], formic acid [3], propionic acid [3], citric acid [6-8], amino acids [9], DL-phenylalanine [10,11], and penicillin V [12], from dilute solutions with complexing agents. The reactive extraction of organic acids with conventional solvents leads to very small partition coefficients. Therefore, and due to the strong molecular interactions between amine and acid, tertiary amines are mainly used as extracting agents for the reactive extraction of organic acids (e.g., [13-22]). These strong molecular interactions lead to the formation of complexes of both compounds. Due to the high affinity of the amine as an organic base, an enhanced reaction selectivity is thus achieved. Therefore, using amines as agents for the extraction of organic acids can significantly increase the partition coefficient [23]. Consequently, amines as extracting agents are also applied in various other fields, such as in the hydrometallurgy for the extraction of metal salts [24] or in the processing of nuclear fuels [25]. However, not all amines are suitable for the reactive extraction of organic acids from aqueous solutions. For instance, and compared to secondary and tertiary amines, primary amines have an undesired high solubility in water, while secondary amines tend to form amides upon regeneration of the solvent within the distillation section of the process. Moreover, and in contrast to tertiary amines, quaternary ammonium compounds have significantly smaller distribution coefficients [26], but, as opposed to the other amines, they can react with both dissociated and undissociated states of the acid [27], whereas tertiary amines can only react with the undissociated one. This is why the reactive extraction of organic acids from aqueous solutions with tertiary amines should be performed at low pH. Furthermore, and by closely examining the number and nature of the involved components, one can deduce that the thermodynamic modeling (e.g., [28-34]) of the liquid-liquid equilibrium (hereafter abbreviated LLE) as well as the experimental investigation (e.g., [35-37]) of the reactive systems represent a major challenge. The reactive system generally consists of an aqueous and an organic phase (e.g., toluene [29-32] and methyl isobutyl ketone [29,30,32,33]), in which the acid to be extracted and the amine as complexing agent are distributed. Therefore, quaternary mixtures

must be considered, and a quaternary distribution equilibrium must be described, although there is low aqueous solubility of the tertiary amine and the organic solvent.

In many cases, the activity coefficients of the ions in the reactive system are described by the Pitzer equations [38] for the excess Gibbs energy of strong electrolytes in aqueous solutions [28-34], in which the interactions between the ions are given by a modified Debye-Hückel contribution. In addition, binary and ternary interaction parameters, which have to be adjusted to experimental data, are used to describe the interactions between nonionic compounds or between ions and nonionic compounds. For the purpose of achieving a thermodynamically correct treatment of reactive nonuniform systems, the chemical potentials of each of the ions as well as the nonionic compounds in each of the phases that it is present must be set equal, thus correctly predicting phase equilibrium. However, Ziegenfuß and Maurer [28] and Kirsch et al. [29-34] opt for a simplified modeling by assuming negligible solubilities of the ions in the organic phase or of the organic solvent in the aqueous phase.

In addition to properly modeling the LLE, numerous phenomena related to the reactive system should also be considered: the chemical equilibrium states of the various chemical reactions that are taking place, the dissociation of the acid in the aqueous phase, the dimerization of the acid in the organic phase, the protonation of the amine, the complex formation, its kinetics, the reaction mechanism, and the autoprotolysis of water. The dissociation of the acid in the aqueous phase into its conjugate base and a hydrogen ion can be described by the acid dissociation constant. Moreover, the dimerization of the acid in the organic phase can be described by the acid dimerization constant, which is determined via spectroscopic investigations [28]. The protonation of the amine as well as the formation of the complex take place at the interface. The chemical reaction gradually produces the complex mostly from the acid molecules that did not form dimers and did not dissociate. The water molecules can also take part in the complex formation [32]. The produced complex is then solvated by the solvent molecules of the organic phase. Furthermore, its formation can also be described using equilibrium constants. However, not even the actual reaction mechanism leading to the production of the complex is always known. Quantitative descriptions of the reaction mechanism are technically possible by means of infrared spectroscopy, but the obtained spectra are very complex and ambiguous, thus leading to various interpretations. Nevertheless, conclusions about the stoichiometry of the complex formation and the qualitative position of equilibrium can be drawn [29,30]. The very low

solubilities of water, acid, and ions in the organic phase, and of the amine and solvent in the aqueous phase justify the assumption that the chemical reaction producing the complex will take place at the interface between the uniform bulk phases, since there will be only at the interface a sufficient amount of all the reactants required for the complex formation.

Second, the reactive extraction of heavy metals from aqueous solutions with complexing agents is also a topic discussed in the literature concerning the field of hydrometallurgy. Specifically, the extraction of zinc ions from aqueous solutions using the cation exchanger di(2-ethylhexyl)phosphoric acid in various diluents (e.g., in dodecane [39-40], decalin [40] or kerosene [41]) is the main subject of study. As proposed by the EFCE, this system is also considered as the test system [42] for the reactive extraction process due to several reasons: it is inexpensive and easily available, allows safe and stable processing, the phase and chemical equilibrium system states as well as the reaction kinetics are known, and the physical properties of the system are available over a wide concentration range [43]. The main focus usually lies on determining the stoichiometry of the chemical reaction producing the desired metal complex from both metal and ion exchanger. The valency of the metal and the degree of association of the ion exchanger are usually known, while the metal complex is in principle not. The produced complex determines the number of protons that are exchanged between the cation exchanger di(2-ethylhexyl)phosphoric acid and the metal cation, thus also determining the pH-dependence of the whole reaction. Furthermore, the ion exchanger di(2-ethylhexyl)phosphoric acid is found as a monomer in aromatic solvents, but as a dimer in aliphatic ones [44,45]. This obviously affects the stoichiometry of the metal complex formation. Moreover, nonidealities in the aqueous phase can be calculated using the Pitzer equations [38], and in the organic phase by means of the solubility parameters of the regular solution model according to Hildebrand and Scott [46]. In addition, the coextraction of water, which occurs, for example, in the reactive extraction of nickel [47], must be considered within the stoichiometry of the complex formation. The metal concentrations in the aqueous phase (metal ions) as well as in the organic phase (metal complex) are experimentally measurable, for example via atomic absorption spectroscopy. However, and in order to calculate the equilibrium constant of the reaction producing the complex, the concentration of the ion exchanger at chemical equilibrium (i.e., after the reactive extraction process has taken place) is also required. This concentration provides information about the maximum exchange capacity of the ion exchanger, but it also highly depends on the

produced metal complex. Furthermore, slope analysis is often used to determine the metal complex. However, it is assumed that the concentration of the ion exchanger at chemical equilibrium is equal to its initial concentration. This assumption can only be justified if the amount of metal to be extracted is very small compared to the initial amount of ion exchanger, which is, for technically relevant extraction processes, however, not desirable, given that full loadings of the ion exchanger are aimed for. In the case of high ion exchanger loadings, the metal complex must then be determined experimentally, for example via FTIR spectroscopy. In addition, Bart [48] investigated the quaternary system zinc chloride-hydrogen chloride-di(2-ethylhexyl)phosphoric acid-isododecane and compared the equilibrium concentration of zinc in the organic phase calculated with the concentration-based equilibrium constant of the chemical reaction to the one calculated with the activity-based equilibrium constant. A better agreement between modeling and experiment can be obtained by applying the activity-based equilibrium constant [48]. Bart [49] also provides a detailed overview of the reactive extraction of heavy metals from aqueous solutions using complexing agents.

Phase and chemical equilibria are important states for the characterization of the beforementioned reactive nonuniform systems. A proper description of the kinetics of the various reaction mechanisms is also crucial. The chemical kinetics of the reactive system zinc ion-di(2-ethylhexyl)phosphoric acid in various diluents (e.g., heptane [50], kerosene [51], or cumene [52]) is described and discussed in the literature. However, rate equations are mostly formulated with concentrations instead of activities. Moreover, it is assumed that the chemical reaction producing the metal complex always takes place at the interface between the aqueous and organic phases, which can also be experimentally proven [53]. The kinetic parameters found in the rate equations can be determined with a Nitsch cell [54].

There are two limiting cases for the description of mass transfer and chemical kinetics in reactive systems. The first one is the case in which the rate of reaction is effectively instantaneous, thus the transport of the reactants to and from the interface is very slow. The other limiting case is where the chemical reaction is much slower than the rate of transport of the various educts and products in the reactive system. The rate-determining step can be experimentally determined by using a two-phase stirred cell, analogous to the Lewis cell [55], with which the influence of the stirrer speed on the mass transfer rate between both phases is studied. If, on the one hand, the mass transfer rate does not depend on the stirrer speed, then the second limiting case, in which

the reaction is much slower than the rate of transport, will be observed. If, on the other hand, the mass transfer rate increases by increasing the stirrer speed, then the first limiting case, in which the reaction is much faster than the rate of transport, will be observed.

The engineering and scientific communities have opposing theoretical views about fluid interfaces between coexisting bulk phases. The first theoretical view considers a sharp interface that has been arbitrarily restricted to zero thickness. Thus, it is assumed that two adjoining phases are homogeneous up to their common interface, where physical properties of the system show a singularity, given the abrupt change. This assumption has led to the development of the two-film theory of Lewis and Whitman [56] for stationary processes, the penetration theory of Higbie [57] for transient processes, and the surface renewal theory, introduced by Danckwerts [58]. The two-film theory and the resistance-in-series model consider a small volume that includes two fluid phases and the interface between them, as illustrated in Figure 1.

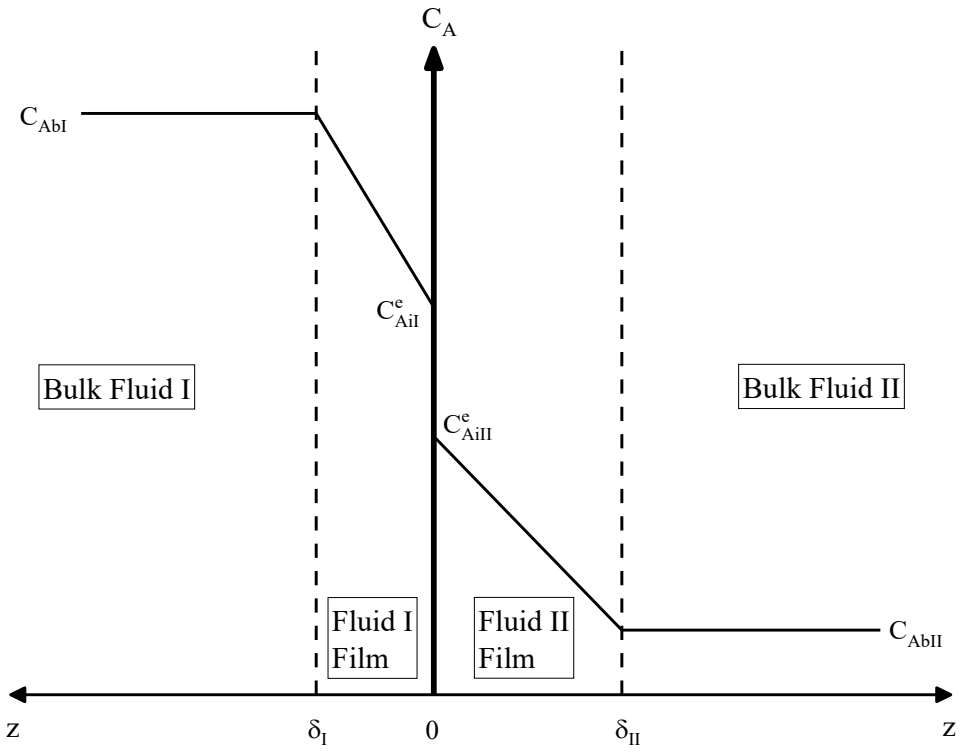

Figure 1. Two-film representation of the local interface between two fluids [56], taken from [59].

The model assumes that there is a thin film or boundary layer of thickness δ_I that lies between the local bulk of fluid I and the interface adjacent to it. The local concentration of component A in the bulk phase of fluid I is equal to C_{AbI}. Furthermore, a linear concentration profile is assumed to exist across the film of fluid I so that the concentration of component A at the interface is equal to C_{AiI}^{e}. The sharp interface between fluid I and fluid II, represented by a thick solid and vertical line in Figure 1, is taken to be at $z = 0$, with z being the spatial coordinate in a direction perpendicular to the planar interface. A second thin film or boundary layer of thickness δ_{II} on the other side of the interface, the one corresponding to fluid II, is also assumed. And again, a linear concentration profile is postulated to exist across the film of fluid II. The concentration of A in the film of fluid II right at the interface ($z = 0$) is equal to C_{AiII}^{e} and the concentration of component A in the local bulk phase of fluid II is C_{AbII}. The compositions are presumed to be uniform with respect to z in both bulk phases. In addition, the two-film model assumes phase equilibrium exactly at the interface (i.e., at $z = 0$), which explains the superscripts e used in both interfacial concentrations C_{AiI}^{e} and C_{AiII}^{e} of component A. It is also postulated that these concentrations are related through a solubility relationship like Henry's law for gas-liquid systems, or a partition coefficient for liquid-liquid systems. The theory considers that the resistance to mass transfer is found in the thin film adjacent to the interface, and that molecular diffusion takes place through the film with the difference in concentrations as the driving force. The two-film theory has been extensively applied to describe the combined reaction and transport associated with liquid-liquid reactions, and to model liquid-liquid interfaces for the purpose of describing the kinetics of chemical reactions in reactor models (e.g., in [60,61]).

Within the two-film model, the involved fluids are assumed to be stationary so that a steady state flux between both fluids will be established. However, industrial processes are mostly unsteady state processes. In such cases, the contact time between bulk phases is too short to achieve a stationary state. This phenomenon is not generally considered by the two-film model. An alternative approach is to assume that the one fluid in contact with the other changes after some period of time, being replaced by fresh fluid from the bulk. In this case, the diffusion process is not at steady state anymore, and the component flux will thus vary over time. Therefore, the penetration theory assumes unsteady state mass transfer to a fluid element as long as it is in contact with the other phase. The basic assumptions of the penetration theory are that

equilibrium is also reached at the interface, and that each of the fluid elements stays in contact with the other phase for the same constant period of time. The unsteady state diffusion of the components to the fluid element will occur under these circumstances. Moreover, Danckwerts [58] modified Higbie's penetration theory [57] and stated that a portion of the mass transfer surface is replaced by a new surface through the motion of eddies in the bulk phase. The amount of time that the fluid elements spend at the interface before being replaced by new ones is not constant anymore, but is rather described by some age distribution function. The net flux is then obtained by integration over this age distribution function. This model is referred to as surface renewal model.

The mass transfer coefficients derived from the two-film theory, the penetration theory, or the surface renewal theory are time-averaged mass transfer coefficients and have to be fitted to experimental data. If the fluid dynamic conditions, the flow geometry, the involved components, and other system parameters change, then a new adjustment is required, because the extrapolation of the adjusted mass transfer coefficients to meet the new system conditions will mostly not provide good modeling results. Nonideal effects and behavior, such as turbulent flows, the pH-dependence of the mass transfer resistance, or pronounced differences between mass transfer coefficients of different compounds, are not considered by the very simplified models and thus have to be experimentally described, which can lead to a very complicated procedure requiring a lot of experiments [62]. If other mass transfer models that take proper account of thermodynamic nonidealities and consider the driving force for diffusion as being a gradient in chemical potentials rather than concentrations are applied, then a much better description of the mass transfer in the system can be achieved. For instance, Samant and Ng [63] studied the effects of chemical kinetics and mass transfer on reactive extraction processes, and modeled the LLE, the chemical equilibrium system state, the reaction kinetics, and the mass transfer in a thermodynamically consistent manner by using activity-based models and by applying the UNIQUAC activity coefficient model [64]. They [63] opted for hypothetical model calculations. The performance of extractive reactors and liquid-liquid extractive reaction processes that are controlled by kinetics and mass transfer is discussed and investigated [63]. The two-film model in combination with the Maxwell-Stefan diffusion formulation [65,66] are applied to describe multicomponent mass transfer [63]. The effects of mass transfer and kinetics are described in terms of Damköhler number matrices for mass transfer and reaction,

respectively, together with the conventional first and second Damköhler numbers [63]. Various design guidelines and reactor attributes, including the choice of the dispersed and continuous phases, mean droplet size of the dispersed phase, phase holdups, and residence time, are also presented [63].

The second theoretical view considers an interface with a smooth spatial variation in one of the intensive scalar properties of the nonuniform system, such as composition or density. Unfortunately, the thickness and the internal structure of the interfacial region between two coexisting fluids cannot generally be determined experimentally due to its very small size. It remains for thermodynamic models to give insights into the spatial resolution of the interfacial layer on a molecular level. Theoretical approaches like density functional methods are discussed (e.g., [67]). Within these methods, the Helmholtz energy of an inhomogeneous system is described as a functional of density or composition and their spatial gradients. The constrained minimization of this functional leads to the interfacial properties of the nonuniform system, such as the interfacial tension or the interfacial concentration profiles, at phase equilibrium. In addition, and for the purpose of achieving numerical simplicity, the Helmholtz energy density can also be expanded in a Taylor series. Cahn and Hilliard [68] addressed the quantification of these ideas, although a key concept is due to van der Waals [69]. Cahn and Hilliard [68] considered the Helmholtz energy of a system of nonuniform composition or density, and expanded the Helmholtz energy density of this system in a Taylor series about the Helmholtz energy of a homogeneous solution. This theoretical framework [68] is referred to as the density gradient theory of inhomogeneous systems (hereafter abbreviated DGT). The concept of a gradient energy is introduced. Poser and Sanchez [70] then generalized the DGT to multicomponent nonuniform systems. The DGT [68-70] has been widely used in combination with equations of state (e.g., [71-80]) to calculate the interfacial properties for liquid-vapor interfaces at vapor-liquid equilibrium (VLE) and liquid-liquid interfaces at liquid-liquid equilibrium (LLE). Moreover, liquids are assumed incompressible. This leads to a constant system volume. The difference between the Helmholtz energy and the Gibbs energy is then also a constant, and both quantities become equally suitable for describing the system. Based on this assumption, Enders and Quitzsch [81] formulated the incompressible version of the DGT (inc-DGT) for the purpose of combining the DGT with a g^E-model, whereas g^E stands for the excess Gibbs energy. They [81] expanded the Gibbs energy of a nonuniform system, rather than its

Helmholtz energy, in a Taylor series about the Gibbs energy of a solution of uniform concentration. Interfacial properties of incompressible liquid-liquid systems at LLE can thus be predicted with outstanding accuracy (e.g., [82-91]).

Furthermore, mass transfer across fluid interfaces or chemical reactions occurring in reactive heterogeneous systems cause the interfacial properties of the overall system to evolve over time. Nonlinear diffusion, driven by gradients in chemical potential rather than gradients in concentration, is important for modeling mass transfer in nonideal systems and mixtures. The classical formulations of the chemical potential must be supplemented by a gradient term, which accounts for the spatial variation of density or composition in inhomogeneous systems. The generalized and modified Cahn-Hilliard diffusion equation has been extensively used in combination with various thermodynamic models to describe mass transfer across the interface in nonuniform systems (e.g., [92-97]). In addition, a very good agreement between predictions and experimental data obtained from a Nitsch cell was found [93-97]. The selective enrichment of components at the interface, together with its impact on the diffusion rate across the interface and on the equilibration time of the studied liquid mixtures, was also investigated [96,97].

The dynamics of the interfacial properties of a specific reactive liquid system, in which the esterification reaction of 1-hexanol with acetic acid to hexyl acetate and water takes place, were studied experimentally and theoretically [98,99]. Two phases were involved in the reactive extraction process, and the evolution of the interfacial properties of the reactive liquid system over time was modeled by combining the inc-DGT with rate equations [98,99]. Danzer and Enders [98,99] considered a very slow chemical reaction and assumed that it can only take place in both liquid bulk phases, thus, no reaction in the interface was modeled. Moreover, they [98,99] did not incorporate any diffusion equation into their model, given that they [98,99] proposed a quasistationary approach to describe the dynamics of the inhomogeneous reactive liquid system they [98,99] have investigated. In addition, Alfarraj and Nauman [100] simulated the reaction-induced phase separation occurring by spinodal decomposition and based on the formation of impact polystyrene. They [100] combined nonlinear diffusion driven by gradients in chemical potential with a reaction model. The rate equations, which they [100] applied, are formulated with concentrations rather than activities. Alfarraj and Nauman [100] showed that their simulation qualitatively predicts experimentally observed results. Recently, Nagl et al. [101] also modeled the combined diffusion and reaction associated with reactive nonuniform

systems. They [101] considered the catalyzed aldol condensation of acetone to diacetone alcohol with further dehydration to mesityl oxide. They [101] opted for a thermodynamically consistent model by using rate equations that are formulated with activities rather than concentrations, and in combination with the modified and generalized Cahn-Hilliard equation. Nagl et al. [101] found very good agreement between their predictions and experimental data, but did not study the impact of the interfacial chemical reaction on the reactive system.

As pointed out above, operations such as the reactive extraction of organic acids from aqueous solutions by solutions of high molecular amines, or the reactive extraction of heavy metals with complexing agents involve chemical reactions taking place at the interface between coexisting bulk phases. A generalized theory that predicts interfacial chemical reactions is thus of crucial importance. The dynamics of reactive nonuniform systems will depend on the rates of diffusion and reaction. Situations will arise in which diffusion and reaction rates are comparable or have different values. Therefore, the purpose of this work is to develop a generalized and thermodynamically consistent theory that embodies the combined reaction and transport associated with reactive nonuniform systems in reactive extraction processes.

3 Theory

3.1 Applied models

The considered nonuniform system is characterized by specifying its uniform and constant temperature T and an externally applied uniform and constant pressure p. Furthermore, and because liquid mixtures are assumed incompressible, the system volume V is thus also a constant. Therefore, the difference between the Helmholtz energy and the Gibbs energy will be a constant, and both quantities are equally suitable for describing the system. In what follows, the Gibbs energy is chosen for this purpose. As a starting point, the general and one-dimensional continuity equation in its differential form, expressing the rate of change of the mole fraction, x_i, of component i in the mixture, with respect to time, t, is taken:

$$\frac{\partial x_i}{\partial t} = -\nabla j_i + R_i \tag{1}$$

where ∇ represents the spatial gradient, j_i is the flux of component i, and R_i is the reaction term that describes sources or sinks of the ith-component. Convective flows are neglected and the flux j_i is considered as a flux that arises due to diffusion.

3.1.1 Molecular diffusion*

Fickian diffusion [103] acts to flatten concentration gradients in a system that will be driven towards an equilibrium state, at which concentrations are everywhere uniform. It is, therefore, strictly limited to ideal mixtures. Fickian diffusion thus cannot be applied for nonuniform, multiphase systems, since, even at phase equilibrium, there will be concentration gradients between the coexisting phases, yet no net diffusion can be observed. To correct this issue, a more general diffusion model, in which molecular diffusion of the various components is driven

* Taken from [102]

by gradients in chemical potential rather than concentration, should be applied since the chemical potential is what becomes everywhere uniform in a nonideal and heterogeneous system at phase equilibrium.

A multicomponent system composed of NC chemical components is considered. The amount of substance of component i is denoted by n_i, and the index $i = 1, 2, \dots, NC$ enumerates components. Molecular diffusion for which the total amount of substance, n, does not change over time will be considered:

$$n = \sum_{i=1}^{NC} n_i = \text{const} \tag{2}$$

In particular, a suitable and moving coordinate system is selected such that the total flux, j, is equal to zero:

$$j = \sum_{i=1}^{NC} j_i = 0 \tag{3}$$

in accord with eq. (2). The diffusion model is derived by incorporating Onsager's approach [104], and in a similar manner to the derivation presented in [105] for mineral solutions. This derived diffusion term is also applied in the literature (e.g., [101]).

Molecular diffusion pushes the system towards an equilibrium state, at which no more gradients of the chemical potential are observed, and the smallest possible Gibbs energy is achieved. The thermodynamic forces acting on the corresponding components are opposite to the spatial gradients of their chemical potentials, and the resulting fluxes are given by the Onsager-type relation:

$$j_i = -\sum_{l=1}^{NC} L_{il} \nabla \mu_l \quad \text{for} \quad i = 1, 2, \dots, NC \tag{4}$$

in which the index $l = 1, 2, \dots, NC$ enumerates components, μ_l denotes the chemical potential of component l, $-\nabla \mu_l$ is the thermodynamic force, and L_{il} is the Onsager matrix of kinetic coefficients, which is given by the following expression:

$$L_{il} = \begin{pmatrix} L_{11} & L_{12} & \cdots & L_{1l} & \cdots & L_{1NC} \\ L_{21} & L_{22} & \cdots & L_{2l} & \cdots & L_{2NC} \\ \vdots & \vdots & \ddots & \vdots & \vdots & \vdots \\ L_{i1} & L_{i2} & \cdots & L_{il} & \cdots & L_{iNC} \\ \vdots & \vdots & \vdots & \vdots & \ddots & \vdots \\ L_{NC1} & L_{NC2} & \cdots & L_{NCl} & \cdots & L_{NCNC} \end{pmatrix} \tag{5}$$

In order to be consistent with the second law of thermodynamics, it is assumed that L_{il} is a positive semidefinite matrix. Moreover, the matrix L_{il} is assumed symmetric:

$$L_{il} = L_{li} \quad \text{for} \quad i, l = 1, 2, \dots, NC \tag{6}$$

in analogy with Onsager's reciprocal relations [104]. By closely examining eq. (4), one expects that the driving force for diffusion $-\nabla\mu_l$ yields a flux of component l in the opposite direction to the force and fluxes of all other components $i \neq l$. In other words, $L_{il} > 0$ for $i = l$, and $L_{il} < 0$ for $i \neq l$.

By substituting eq. (4) into eq. (3), the following expression for the total flux results:

$$j = -\sum_{i=1}^{NC}\sum_{l=1}^{NC} L_{il}\nabla\mu_l = -\sum_{l=1}^{NC}\left(\sum_{i=1}^{NC} L_{il}\right)\nabla\mu_l \tag{7}$$

An additional restriction is imposed:

$$\sum_{i=1}^{NC} L_{il} = 0 \quad \text{for} \quad l = 1, 2, \dots, NC \tag{8}$$

so that the total flux given by eq. (7) automatically vanishes in accord with eq. (3) and irrespective of the specific values of $\nabla\mu_l$. As a consequence of the restriction given by eq. (8), only the off-diagonal elements of the matrix L_{il} in eq. (5) need to be specified.

A new expression for the component flux j_i can thus be introduced. The symmetry relation given by eq. (6) and the restriction given by eq. (8) imply that eq. (4) is equivalent to:

$$j_i = \sum_{l=1}^{NC} L_{il}\nabla(\mu_i - \mu_l) \quad \text{for} \quad i = 1, 2, \dots, NC \tag{9}$$

The latter equation indicates that the driving force for diffusion is a gradient in the difference of chemical potentials. In fact, simpler expressions for the flux j_i can be derived if differences of chemical potentials are used. It is, therefore, more convenient to deal with eq. (9) instead of the main eq. (4).

Chemical diffusion of unlike chemical species i and l is only possible if both species are present in a given mixture. Therefore, the kinetic coefficients L_{il} must depend on concentration and must vanish if either $n_i = 0$ or $n_l = 0$, for $i, l = 1, 2, \dots, NC$. It is then useful to introduce a set of positive diffusive mobilities, M_{il}, such that:

$$L_{il} = -M_{il}\frac{n_i n_l}{n} \quad \text{for} \quad i \neq l \quad \text{and} \quad i, l = 1, 2, \dots, NC \tag{10}$$

where $M_{il} = M_{li}$ in accord with the symmetry relation given by eq. (6). The values L_{ii} are uniquely deduced from eq. (8). Substitution of eq. (10) into eq. (9) yields the following expression for the diffusive flux of component i in a multicomponent system:

$$j_i = -\sum_{l=1}^{NC} M_{il}\frac{n_i n_l}{n}\nabla(\mu_i - \mu_l) \quad \text{for} \quad i = 1, 2, \dots, NC \tag{11}$$

Eq. (11) is then inserted into a sourceless continuity equation for the amount of substance of component i:

$$\frac{\partial n_i}{\partial t} = -\nabla j_i \quad \text{for} \quad i = 1, 2, \dots, NC \tag{12}$$

which yields:

$$\frac{\partial n_i}{\partial t} = \nabla\left[\sum_{l=1}^{NC} M_{il}\frac{n_i n_l}{n}\nabla(\mu_i - \mu_l)\right] \quad \text{for} \quad i = 1, 2, \dots, NC \tag{13}$$

and given a constant total amount of substance (eq. (2)), one can reduce eq. (13) to the equations for mole fractions such that an NC-component system can be described by $NC - 1$ equations:

$$\frac{\partial x_i}{\partial t} = \nabla\left[\sum_{l=1}^{NC} M_{il} x_i x_l \nabla(\mu_i - \mu_l)\right] \quad \text{for} \quad i = 1, 2, \dots, NC - 1 \tag{14}$$

By applying the incompressible version of the density gradient theory (inc-DGT), which will be further discussed in subsubchapter 3.5.3, the diffusive mobility M_{il} will have units of $\frac{\mathrm{mol}^3}{\mathrm{J.m}^4.\mathrm{s}}$. It is adjusted to experimental data, which are usually obtained from diffusive mass transfer experiments using a Nitsch-cell [54], for instance in [96,97,101]. Furthermore, and because liquids at constant temperature are considered, it is assumed that the diffusive mobilities will have the same value in both liquid bulk phases as well as at the interface between them.

In addition, it can be noted that by applying eq. (14) to a two-component mixture, the well-known nonlinear Cahn-Hilliard equation for an isotropic binary system results [106]:

$$\frac{\partial x_2}{\partial t} = \nabla[M_{12}(1-x_2)x_2\nabla(\mu_2-\mu_1)] \tag{15}$$

However, the term $M_{12}(1-x_2)x_2$ in eq. (15) replaces the mobility used by them [106]. Therefore, eq. (14) is the modified and generalized Cahn-Hilliard equation.

Returning to the binary case, and by assuming an ideal mixture, the following expression for the difference of the chemical potentials $\mu_2-\mu_1$ results:

$$\mu_2-\mu_1 = \frac{\partial g}{\partial x_2} \tag{16}$$

with g being the molar Gibbs energy. Eq. (15) can then be written as:

$$\frac{\partial x_2}{\partial t} = \nabla\left[M_{12}(1-x_2)x_2\frac{\partial^2 g}{\partial {x_2}^2}\nabla x_2\right] \tag{17}$$

Also, since for an ideal mixture:

$$g = (1-x_2)\mu_{10} + x_2\mu_{20} + RT[(1-x_2)\ln(1-x_2) + x_2\ln x_2] \tag{18}$$

the following equation results:

$$\frac{\partial x_2}{\partial t} = \nabla(RTM_{12}\nabla x_2) \tag{19}$$

which is a similar expression to Fick's second law of diffusion. Therefore, eq. (15) or the more general eq. (14) reduce to Fickian diffusion in the case of ideal mixtures. μ_{10} and μ_{20} in eq. (18)

are the chemical potentials of the pure species 1 and 2, respectively, at system temperature and pressure, and R is the universal gas constant.

3.1.2 Chemical reaction*

The most general description of a chemical reaction network considers a number NC of distinct chemical components reacting via a number NR of chemical reactions. No change in total moles upon reaction is assumed, in accord with eq. (2). Applying eq. (2) allows writing balances in mole fractions rather than mole balances for the chemical species involved in the reaction network. The rate of change in mole fraction can be expressed as the sum of the rates of change in mole fractions due to the various chemical reactions that are taking place in the reacting mixture:

$$\frac{\partial x_i}{\partial t} = \sum_{j=1}^{NR} \frac{\partial x_{i,j}}{\partial t} = \sum_{j=1}^{NR} \upsilon_{i,j} r_j \quad \text{for} \quad i = 1, 2, \dots, NC-1 \tag{20}$$

where j is the reaction index running from 1 to NR, $\upsilon_{i,j}$ is the stoichiometric coefficient of component i in the jth-reaction, and r_j is the reaction rate of reaction j. By convention, the stoichiometric coefficient $\upsilon_{i,j}$ is negative for the educts and positive for the products of reaction j. The reaction rate r_j is given by a power law, which is formulated by activities rather than concentrations for the purpose of introducing a thermodynamically consistent treatment of reactive systems. Therefore, the partial orders of reaction for the numerous components will be equal to the absolute value of their stoichiometric coefficients. The rate equation that links the reaction rate of the chemical reaction j with the activities of its educts is thus written as:

$$r_j = k_j \prod_{m=1}^{N_j} a_{m,j}^{|\upsilon_{m,j}|} \quad \text{for} \quad j = 1, 2, \dots, NR \tag{21}$$

in which N_j is the total number of educts in reaction j, $m = 1, 2, \dots, N_j$ enumerates the educts of reaction j, and k_j is the reaction rate coefficient of the jth-reaction. Furthermore, $a_{m,j}$ in

* Taken from [59]

eq. (21) is the activity of educt m in the jth-reaction and $|v_{m,j}|$ is the absolute value of its stoichiometric coefficient. In the case of real mixtures, activities rather than concentrations will be applied to describe the "effective concentration" of a component in the mixture. The activities, $a_{m,j}$, can be expressed by chemical potentials according to the following expression:

$$a_{m,j} = \exp\left(\frac{\mu_{m,j} - \mu_{m0,j}}{RT}\right) \quad \text{for} \quad m = 1, 2, \dots, N_j \quad \text{and} \quad j = 1, 2, \dots, NR \tag{22}$$

where $\mu_{m,j}$ is the chemical potential of educt m in reaction j and $\mu_{m0,j}$ is the chemical potential of the pure species m at system temperature and pressure. Substitution of eq. (22) into eq. (21) with a subsequent mathematical treatment yields the following equation for the reaction rate of reaction j:

$$r_j = k_j \exp\left(\sum_{m=1}^{N_j} |v_{m,j}| \left(\frac{\mu_{m,j} - \mu_{m0,j}}{RT}\right)\right) \quad \text{for} \quad j = 1, 2, \dots, NR \tag{23}$$

The reaction rate coefficient, k_j, has units of s^{-1}. Furthermore, reaction rate coefficients are usually adjusted to experimental data of chemical reactions taking place in homogeneous solutions at a given initial feed composition. However, and by expressing the rate equations with activities, which are a measure of the "effective concentration" of a species in a mixture, the adjusted rate coefficient, k_j, can also be applied to describe the kinetics of heterogeneous systems with varying feed compositions, including the interface between liquid bulk phases. Therefore, the reaction rate coefficient, k_j, will not depend on concentration anymore. It will thus only depend on temperature, and, given a specific and constant temperature of the whole system, it will have the same value in both liquid bulk phases as well as at the interface between them.

By substituting eq. (23) into eq. (20), the following expression for the rate of change in mole fraction due to chemical reaction in a multicomponent system with respect to time results:

$$\frac{\partial x_i}{\partial t} = \sum_{j=1}^{NR} v_{i,j} k_j \exp\left(\sum_{m=1}^{N_j} |v_{m,j}| \left(\frac{\mu_{m,j} - \mu_{m0,j}}{RT}\right)\right) \quad \text{for} \quad i = 1, 2, \dots, NC - 1 \tag{24}$$

Eq. (24) leads to the generalization of the framework introduced in [101].

3.1.3 Dynamic model*

A general dynamic equation can now be specified to account for the combined reaction and transport phenomena associated with liquid-liquid chemical reactions in multicomponent and inhomogeneous mixtures. Expressions for the rate of change in mole fraction due to diffusion and reaction with respect to time, which are given by eq. (14) and eq. (24), respectively, have been derived. These two equations are inserted into the general and one-dimensional continuity equation as a contribution for the diffusive and reactive terms in eq. (1). The dynamic model can thus be written as:

$$\frac{\partial x_i}{\partial t} = \nabla\left[\sum_{l=1}^{NC} M_{il} x_i x_l \nabla(\mu_i - \mu_l)\right] + \sum_{j=1}^{NR} \upsilon_{i,j} k_j \exp\left(\sum_{m=1}^{N_j} |\upsilon_{m,j}| \left(\frac{\mu_{m,j} - \mu_{m0,j}}{RT}\right)\right) \qquad (25)$$

$$\text{for} \quad i = 1, 2, \dots, NC - 1$$

Eq. (25) is the central one of the treatment. It is solved numerically to obtain the spatial and temporal evolution of the mole fraction x_i. In addition, the component continuity equations given by eq. (25) are not independent due to the condition of constant total amount of substance, n, expressed by eq. (2), which is automatically supported by all solutions of eq. (25). Moreover, and given that eq. (25) is an equation for mole fractions, a multicomponent system of NC distinct chemical components is thus described by $NC - 1$ equations, because the summation equation $\sum_{i=1}^{NC} x_i = 1$ has to be fulfilled at every point in space and time.

The resulting component continuity equations (eq. (25)) form a system of coupled nonlinear partial differential equations that have to be solved numerically in order to describe the evolution of reactive nonuniform liquid systems.

Furthermore, mass transfer coefficients of individual components in reactive heterogeneous liquid systems can be calculated, and adequate formulations of typical dimensionless quantities that are used in chemical reaction engineering, such as the Hatta number or the enhancement and utilization factors, can also be derived.

* Taken from [102]

3.2 Phase equilibrium

The criteria for phase equilibrium were established over 100 years ago by Gibbs [107], who defined a phase as a continuous and homogeneous region in which no spatial gradients of the thermodynamic state variables are observed. Phase equilibrium, which is formally reached for $t \to +\infty$, is achieved when thermal equilibrium, mechanical equilibrium, and diffusive equilibrium are simultaneously fulfilled in a thermodynamic system. Consequently, the criteria for phase equilibrium are that the temperature and pressure of the numerous phases I, II, …, NP of the nonuniform system are equal, with NP being the total number of phases present in the system, and that the chemical potentials of each of the components in each of the phases that it is present are equal:

$$T^I = T^{II} = \cdots = T^{NP} \tag{26}$$

$$p^I = p^{II} = \cdots = p^{NP} \tag{27}$$

$$\mu_i{}^I = \mu_i{}^{II} = \cdots = \mu_i{}^{NP} \quad \text{for} \quad i = 1, 2, \ldots, NC \tag{28}$$

Furthermore, the intensive properties of the system are not independent but related. The Gibbs-Duhem equation describes the relationship between infinitesimal changes in temperature, pressure, and chemical potential of the involved components in a thermodynamic system:

$$\sum_{i=1}^{NC} n_i d\mu_i = -SdT + Vdp \tag{29}$$

in which S is the entropy of the system.

3.3 Critical point

The history of the calculation of critical points starts with the work of Gibbs [107], who established the critical point conditions for a binary mixture by deriving mathematical relationships between thermodynamic properties at the critical point. The criterion for the critical point of binary mixtures is that the following condition has to be satisfied:

$$\left(\frac{\partial^2 g}{\partial {x_1}^2}\right)_{T,p} = 0 \quad \text{and} \quad \left(\frac{\partial^3 g}{\partial {x_1}^3}\right)_{T,p} = 0 \tag{30}$$

Beegle et al. [108] studied the stability of a pure fluid and a multicomponent mixture at a given state, and provided a general description of the mathematics involved in defining stable system states through the use of Legendre transformations applied to the internal energy of the system.

Reid and Beegle [109] subsequently introduced a formulation expressing the critical conditions in terms of Legendre transforms, in which two matrix determinants must be simultaneously equated with zero. This is the method implemented in this work. The criticality conditions defining the location of the critical point of a system can thus be expressed by using Legendre transforms. Within this formulation, several equivalent sets of independent variables in the Legendre transformation are found. By applying mole fractions as working variables to specify critical point criteria, and by ordering the independent set of variables for the internal energy U for a ternary system such that the internal energy is given by the following function [109]:

$$U = f(S, V, n_1, n_2, n) \tag{31}$$

the 2$^{\text{th}}$ order Legendre transform of U will be, therefore, the total Gibbs energy G, and the first criticality condition that must be fulfilled at the critical point results [109]:

$$D_2 = \begin{vmatrix} \left(\frac{\partial^2 g}{\partial {x_1}^2}\right)_{T,p,x_2} & \left(\frac{\partial^2 g}{\partial x_1 \partial x_2}\right)_{T,p} \\ \left(\frac{\partial^2 g}{\partial x_2 \partial x_1}\right)_{T,p} & \left(\frac{\partial^2 g}{\partial {x_2}^2}\right)_{T,p,x_1} \end{vmatrix} = 0 \tag{32}$$

where D_2 is the matrix determinant related to the 2$^{\text{th}}$ order Legendre transform of the total internal energy of the system, which is given by eq. (31). In addition, the second criticality condition is given by [109]:

$$\begin{vmatrix} \left(\frac{\partial^2 g}{\partial {x_1}^2}\right)_{T,p,x_2} & \left(\frac{\partial^2 g}{\partial x_1 \partial x_2}\right)_{T,p} \\ \left(\frac{\partial D_2}{\partial x_1}\right)_{T,p,x_2} & \left(\frac{\partial D_2}{\partial x_2}\right)_{T,p,x_1} \end{vmatrix} = 0 \tag{33}$$

Eq. (32) and eq. (33) are applied in this work to calculate the critical point of a ternary mixture.

3.4 Chemical equilibrium

A simple case of general chemical reaction networks, in which systems composed of merely reversible reactions, will be considered. In particular, a reaction network consisting of two chemical reactions ($NR = 2$ in eq. (20)) will be the subject of study. The chemical equation of the reaction can then be written in the generic form:

$$\sum_{m=1}^{N_+} \left|\upsilon_{m,+}\right| X_m \underset{k_-}{\overset{k_+}{\rightleftharpoons}} \sum_{m=1}^{N_-} \left|\upsilon_{m,-}\right| Y_m \tag{34}$$

where $j = +$ is the reaction index of the forward reaction and $j = -$ is the reaction index of the backward reaction. X_m is the symbol for the mth-chemical species of the $+$th-chemical reaction, Y_m is the symbol for the mth-chemical species of the $-$th-chemical reaction, and $\left|\upsilon_{m,+}\right|$ and $\left|\upsilon_{m,-}\right|$ are the absolute values of their stoichiometric coefficients, respectively. k_+ and k_- are the reaction rate coefficients of the forward and backward reactions, respectively, and the total number of components is given by: $NC = N_+ + N_-$.

Chemical equilibrium is reached when the forward chemical reaction proceeds at the same rate as the backward chemical reaction. It corresponds to a steady system state, at which both educts and products are present in concentrations which have no further tendency to change with time. The reaction rates of forward and backward reactions thus become equal.

Assuming that the chemical reaction is carried out at constant temperature and pressure, the derivative of the Gibbs energy with respect to the reaction coordinate, which parameterizes reaction process at the level of the molecular species involved, vanishes at chemical equilibrium. This criterion is both necessary and sufficient to describe chemical equilibrium states. At constant temperature and pressure, the Gibbs energy will depend only on the extent of reaction ξ, which measures the reaction progress in terms of the composition of the reacting mixture, and can only decrease according to the second law of thermodynamics. In order to meet the thermodynamic condition for chemical equilibrium, the Gibbs energy must be stationary, meaning that the partial derivative of G with respect to ξ must be equal to zero:

$$\left(\frac{\partial G}{\partial \xi}\right)_{T,p} = 0 \tag{35}$$

Furthermore, the Gibbs energy total differential is given by the following expression:

$$dG = Vdp - SdT + \sum_{i=1}^{NC} \mu_i dn_i \tag{36}$$

Inserting $dn_i = \upsilon_i d\xi$ into eq. (36) gives a stoichiometric coefficient υ_i (negative for educts, positive for products) and a differential that denotes the chemical reaction occurring to an infinitesimal extent ($d\xi$). At constant temperature ($dT = 0$) and pressure ($dp = 0$), eq. (36) thus leads to:

$$\left(\frac{\partial G}{\partial \xi}\right)_{T,p} = \sum_{i=1}^{NC} \upsilon_i \mu_i \tag{37}$$

In the case of real mixtures, activities rather than concentrations will be applied, and the chemical potentials can be expressed in terms of activities:

$$\mu_i = \mu_{i0}^* + RT \ln a_i \quad \text{for} \quad i = 1, 2, \ldots, NC \tag{38}$$

where μ_{i0}^* is the standard chemical potential of the pure species i at system temperature and pressure. By substituting these chemical potentials in eq. (37), the relationship becomes:

$$\begin{aligned} \left(\frac{\partial G}{\partial \xi}\right)_{T,p} &= \sum_{i=1}^{NC} \upsilon_i \mu_{i0}^* + RT \ln\left(\prod_{i=1}^{NC} {a_i}^{\upsilon_i}\right) \\ &= \sum_{i=1}^{NC} \upsilon_i \mu_{i0}^* + RT \ln\left(\frac{\prod_{m=1}^{N_-} {a_{m,-}}^{|\upsilon_{m,-}|}}{\prod_{m=1}^{N_+} {a_{m,+}}^{|\upsilon_{m,+}|}}\right) \end{aligned} \tag{39}$$

where $a_{m,+}$ and $a_{m,-}$ are the activities of the chemical species X_m and Y_m, respectively. Furthermore, the sum $\sum_{i=1}^{NC} \upsilon_i \mu_{i0}^*$ is given by:

$$\sum_{i=1}^{NC} \upsilon_i \mu_{i0}^* = \Delta_r g^* \tag{40}$$

which is the standard molar Gibbs energy change $\Delta_r g^*$ of reaction. At chemical equilibrium, and in accord with eq. (35), both eq. (39) and eq. (40) lead to the following expression:

$$0 = \Delta_r g^* + RT \ln K \tag{41}$$

in which $K = \prod_{i=1}^{NC} {a_i}^{\upsilon_i}$ is the equilibrium coefficient for the reaction, which, according to eq. (41), can be related to the standard molar Gibbs energy change of reaction by the following equation:

$$K = \prod_{i=1}^{NC} {a_i}^{\upsilon_i} = \frac{\prod_{m=1}^{N_-} {a_{m,-}}^{|\upsilon_{m,-}|}}{\prod_{m=1}^{N_+} {a_{m,+}}^{|\upsilon_{m,+}|}} = \exp\left(\frac{-\Delta_r g^*}{RT}\right) \tag{42}$$

By applying eq. (24) to the chemical reaction network given by eq. (34), and for $t \to +\infty$ at which chemical equilibrium is formally reached and the rate of change in mole fraction of component i with respect to time vanishes ($\frac{\partial x_i(t\to+\infty)}{\partial t} = 0$), the equilibrium coefficient K can also be given by the ratio of the reaction rate coefficients according to the following expression:

$$K = \prod_{i=1}^{NC} {a_i}^{\upsilon_i} = \frac{\prod_{m=1}^{N_-} {a_{m,-}}^{|\upsilon_{m,-}|}}{\prod_{m=1}^{N_+} {a_{m,+}}^{|\upsilon_{m,+}|}} = \frac{k_+}{k_-} \tag{43}$$

As described in subsubchapter 3.1.2, the reaction rate coefficients only depend on temperature. Therefore, the equilibrium coefficient K will also depend only on temperature.

3.5 Density Gradient Theory

3.5.1 Pure components

The DGT was first formulated by van der Waals [69], who considered the liquid-vapor interface of a pure substance as a finite region in which the density changes continuously. Cahn and Hilliard [68] rediscovered and applied the DGT for the calculation of interfacial properties of pure substances. The DGT provides an expression for the Helmholtz energy F of nonuniform systems. Within the theoretical framework of the DGT, the Helmholtz energy density $\bar{f}$ in a region of nonuniform density will depend both on the local density ρ and on the density of the immediate environment. Therefore, $\bar{f}$ can be expressed as the sum of two contributions, which are functions of the local density and the local density gradients, respectively. The basic assumption of the DGT is that the density gradient in a direction perpendicular to the interface is small compared with the reciprocal of the intermolecular distance. In that case, the density ρ

and its derivatives can be taken as independent variables. The Helmholtz energy density $\bar{f}$ can thus be expanded in a Taylor series about $\bar{f}_0$, the Helmholtz energy density of a solution of uniform density ρ. Leading terms in the expansion for $\bar{f}$ are [68]:

$$\begin{aligned}\bar{f}(\rho, \nabla\rho, \nabla^2\rho) = \bar{f}_0(\rho) &+ \sum_{i=1}^{3} \underbrace{\left(\frac{\partial \bar{f}}{\partial\left(\frac{\partial\rho}{\partial x_i}\right)}\right)_0}_{=L_i} \left(\frac{\partial\rho}{\partial x_i}\right) \\ &+ \sum_{i=1}^{3}\sum_{j=1}^{3} \underbrace{\left(\frac{\partial \bar{f}}{\partial\left(\frac{\partial^2\rho}{\partial x_i \partial x_j}\right)}\right)_0}_{=\kappa_{ij}{}^{(1)}} \left(\frac{\partial^2\rho}{\partial x_i \partial x_j}\right) \\ &+ \frac{1}{2}\sum_{i=1}^{3}\sum_{j=1}^{3} \underbrace{\left(\frac{\partial^2 \bar{f}}{\partial\left(\frac{\partial\rho}{\partial x_i}\right)\partial\left(\frac{\partial\rho}{\partial x_j}\right)}\right)_0}_{=\kappa_{ij}{}^{(2)}} \left(\frac{\partial\rho}{\partial x_i}\right)\left(\frac{\partial\rho}{\partial x_j}\right)\end{aligned} \tag{44}$$

where terms in derivatives higher than the second are neglected and the subscripts i and j in eq. (44) are employed to denote the successive substitution of the x, y and z components in a Cartesian coordinate system for the variable x_i. In addition, the subscript zero in eq. (44) indicates the value of the parameter in a homogeneous solution of uniform density.

For an isotropic medium, the Helmholtz energy must be invariant to the symmetry operations of reflection ($x_i \to -x_i$) and of rotation about a fourfold axis ($x_i \to x_j$) such that the polarization vector L_i and the tensors $\kappa_{ij}{}^{(1)}$ and $\kappa_{ij}{}^{(2)}$ in eq. (44) will satisfy the following conditions [68]:

$$L_i = 0 \tag{45}$$

$$\kappa_{ij}{}^{(1)} = \kappa_{ij}{}^{(2)} = 0 \quad \text{for} \quad i \neq j \tag{46}$$

$$\kappa_{ij}{}^{(1)} = \kappa_1 = \left(\frac{\partial \bar{f}}{\partial \nabla^2\rho}\right)_0 \quad \text{for} \quad i = j \tag{47}$$

$$\kappa_{ij}{}^{(2)} = \kappa_2 = \left(\frac{\partial^2 \bar{f}}{(\partial|\nabla\rho|)^2}\right)_0 \quad \text{for} \quad i = j \tag{48}$$

Hence, eq. (44) reduces to [68]:

$$\bar{f}(\rho, \nabla\rho, \nabla^2\rho) = \bar{f}_0(\rho) + \kappa_1\nabla^2\rho + \kappa_2(\nabla\rho)^2 \tag{49}$$

The total Helmholtz energy is obtained by integrating over the volume of the solution [68]:

$$\begin{aligned} F &= \int_V \bar{f}\, dV \\ &= \int_V \left[\bar{f}_0(\rho) + \kappa_1\nabla^2\rho + \kappa_2(\nabla\rho)^2\right] dV \end{aligned} \tag{50}$$

The divergence theorem is applied to eliminate the term in $\nabla^2\rho$ from eq. (50) [68]:

$$\int_V (\kappa_1\nabla^2\rho)\, dV = -\int_V \frac{d\kappa_1}{d\rho}(\nabla\rho)^2\, dV + \int_S (\kappa_1\nabla\rho \cdot n)\, dS \tag{51}$$

where S is the external surface, at which effects will be neglected. Therefore, a boundary of integration in eq. (50) is chosen in such a manner that $\nabla\rho \cdot n$ in eq. (51), where n is the outward pointing unit normal at each point on the boundary, will be zero at the boundary. The surface integral in eq. (51) thus vanishes and eq. (50) can be written as [68]:

$$F = \int_V \left[\bar{f}_0(\rho) + \underbrace{\left(-\frac{d\kappa_1}{d\rho} + \kappa_2\right)}_{=\kappa}(\nabla\rho)^2\right] dV \tag{52}$$

Eq. (52) reveals that the Helmholtz energy of a nonuniform system can be expressed as the sum of two contributions, one being the Helmholtz energy that this system would have in a uniform and homogeneous solution, and the other a "gradient energy", which is a function of the local density [68].

Moreover, a flat interface of area A between two coexisting liquid and vapor bulk phases of density ρ^L and ρ^V is considered. ρ^L and ρ^V are the densities of a pure liquid and its vapor, respectively. By applying eq. (52) to the one-dimensional density change across the interface, the following expression for the Helmholtz energy of the system results [68]:

$$F = A\int_{-\infty}^{+\infty} \left[\bar{f}_0(\rho) + \kappa\left(\frac{d\rho}{dz}\right)^2\right] dz \tag{53}$$

where z is the one-dimensional interfacial coordinate in a direction perpendicular to the planar interface. The surface tension, σ, or the specific interfacial Helmholtz energy, is by definition the difference per unit area of interface between the actual Helmholtz energy of the system and that which it would have if the properties of the bulk phases were continuous throughout [68]:

$$\sigma = \int_{-\infty}^{+\infty} \left[\overline{\Delta\Omega}(\rho) + \kappa \left(\frac{d\rho}{dz} \right)^2 \right] dz \tag{54}$$

in which $\overline{\Delta\Omega}(\rho)$ is the grand thermodynamic potential defined by:

$$\overline{\Delta\Omega}(\rho) = \overline{f_0}(\rho) - \rho\mu^e + p^e \tag{55}$$

where the superscript e denotes the equilibrium value of the parameter, and μ^e is referred to the same standard state as $\overline{f_0}$. At equilibrium, the integral in eq. (54) is a minimum. By substituting the integrand of eq. (54) in the Euler-Lagrange equation, a differential equation, whose solutions are the density profiles corresponding to stationary values of the integral, results [68]:

$$\overline{\Delta\Omega}(\rho) - \kappa \left(\frac{d\rho}{dz} \right)^2 = \text{const} \tag{56}$$

The constant in eq. (56) must be zero since $\overline{\Delta\Omega}(\rho)$ and $\frac{d\rho}{dz}$ both tend to zero as $z \to \pm\infty$. Therefore, for a minimum value of σ [68]:

$$\overline{\Delta\Omega}(\rho) = \kappa \left(\frac{d\rho}{dz} \right)^2 \tag{57}$$

and eq. (54) can thus be written as [68]:

$$\sigma^{VLE} = 2 \int_{-\infty}^{+\infty} \overline{\Delta\Omega}(\rho)\, dz \tag{58}$$

Furthermore, numerical analysis is facilitated by transforming the equations from z-space to ρ-space. Eq. (57) can be applied to change the variable of integration in eq. (58) from z to ρ. The following expression results [68]:

$$\sigma^{VLE} = 2 \int_{\rho^V}^{\rho^L} \sqrt{\kappa \overline{\Delta\Omega}(\rho)}\, d\rho \tag{59}$$

In addition, the density variation across the interface at equilibrium, as determined by eq. (57), is such that [68]:

$$\frac{d\rho}{dz} = \sqrt{\frac{\overline{\Delta\Omega}(\rho)}{\kappa}} \tag{60}$$

which leads to the interfacial density profile of a pure component:

$$z - z_0 = \int_{\rho(z_0)}^{\rho(z)} \sqrt{\frac{\kappa}{\overline{\Delta\Omega}(\rho)}}\, d\rho \tag{61}$$

where z_0 is an arbitrarily chosen reference coordinate for integration, and $\rho(z) \in [\rho^V, \rho^L]$.

3.5.2 Mixtures

Poser and Sanchez [70] generalized the DGT to multicomponent mixtures. The main assumption they [70] adopted in order to evaluate F is that the entropy of the nonuniform system will only be a function of the local density and thus independent of density gradients. As a starting point, the internal energy U is employed and effects of density gradients on U will be evaluated in a mean-field approximation. The internal energy per unit volume for a multicomponent system with pairwise additive interactions is given by [70]:

$$\frac{U(r)}{V} = \frac{1}{2}\sum_{i=1}^{NC}\sum_{j=1}^{NC} \varepsilon_{ij}(r) \tag{62}$$

in which r is the position vector and ε_{ij} represents the interaction energy of components i and j, which is given by [70]:

$$\varepsilon_{ij}(r) = \rho_i(r) \int \rho_j(r+s) u_{ij}(s)\, ds \tag{63}$$

where ρ_i and ρ_j are the partial densities of components i and j, respectively, s is the intermolecular distance, and u_{ij} is the intermolecular interaction potential between components

i and j, which is assumed to be spherically symmetric. By neglecting third and higher order terms, $\rho_j(r+s)$ in eq. (63) is expanded in a Taylor series around $s = 0$ [70]:

$$\rho_j(r+s) = \rho_j(r) + (s \cdot \nabla)\rho_j + \frac{1}{2}(s \cdot \nabla)^2 \rho_j \tag{64}$$

Substitution of eq. (64) into eq. (63) with a subsequent integration yields the following expression for the interaction energy ε_{ij} [70]:

$$\varepsilon_{ij}(r) = -\rho_i(r)\rho_j(r){\kappa_0}^{ij} + \rho_i(r) \int \left[(s \cdot \nabla)\rho_j + \frac{1}{2}(s \cdot \nabla)^2 \rho_j\right] u_{ij}(s)\, ds \tag{65}$$

with

$${\kappa_0}^{ij} = -4\pi \int_{\sigma_{ij}}^{+\infty} s^2 u_{ij}(s)\, ds \tag{66}$$

in which ${\sigma_{ij}}^3$ is the repulsive core volume between both components i and j. Since u_{ij} is spherically symmetric, the following properties result [70]:

$$\int (s \cdot \nabla)^b \rho_j u_{ij}(s)\, ds = 0 \quad b \text{ odd} \tag{67}$$

$$\int (s \cdot \nabla)^b \rho_j u_{ij}(s)\, ds \neq 0 \quad b \text{ even} \tag{68}$$

so that after integration, eq. (65) becomes [70]:

$$\varepsilon_{ij}(r) = -\rho_i(r)\rho_j(r){\kappa_0}^{ij} - \rho_i(r)\nabla^2\rho_j(r){\kappa_2}^{ij} \tag{69}$$

with

$${\kappa_2}^{ij} = -\frac{2\pi}{3} \int_{\sigma_{ij}}^{+\infty} s^4 u_{ij}(s)\, ds \tag{70}$$

The internal energy per unit volume (eq. (62)) can thus be written as:

$$\frac{U(r)}{V} = -\frac{1}{2}\sum_{i=1}^{NC}\sum_{j=1}^{NC} \rho_i(r)\rho_j(r){\kappa_0}^{ij} - \frac{1}{2}\sum_{i=1}^{NC}\sum_{j=1}^{NC} \rho_i(r)\nabla^2\rho_j(r){\kappa_2}^{ij} \tag{71}$$

As mentioned above, the entropy of the nonuniform system is only a function of the local density. Therefore, the local Helmholtz energy density $\overline{f_0}(r)$ will be defined as [70]:

$$\overline{f_0}(r) = -\frac{1}{2}\sum_{i=1}^{NC}\sum_{j=1}^{NC}\rho_i(r)\rho_j(r){\kappa_0}^{ij} - T\frac{S(\rho_1,\rho_2,\dots,\rho_{NC})}{V} \tag{72}$$

where S in eq. (72) is the entropy of the system. The Helmholtz energy density of an inhomogeneous system is thus given by the following expression [70]:

$$\begin{aligned}\bar{f}(r) &= \frac{U(r)}{V} - T\frac{S(\rho_1,\rho_2,\dots,\rho_{NC})}{V} \\ &= \overline{f_0}(r) - \frac{1}{2}\sum_{i=1}^{NC}\sum_{j=1}^{NC}\rho_i(r)\nabla^2\rho_j(r){\kappa_2}^{ij}\end{aligned} \tag{73}$$

Furthermore, the total Helmholtz energy is obtained by integrating over the volume of the nonuniform system:

$$F = \int_V \left[\overline{f_0}(r) - \frac{1}{2}\sum_{i=1}^{NC}\sum_{j=1}^{NC}\rho_i(r)\nabla^2\rho_j(r){\kappa_2}^{ij}\right] dV \tag{74}$$

which, for a system with a planar interface of area A, can be written as:

$$F = A\int_{-\infty}^{+\infty}\left[\overline{f_0}(z) - \frac{1}{2}\sum_{i=1}^{NC}\sum_{j=1}^{NC}\rho_i(z)\frac{d^2\rho_j(z)}{dz^2}{\kappa_2}^{ij}\right] dz \tag{75}$$

Further simplification of eq. (75) can be achieved by partial integration of the second term in the integral ($\frac{d\rho_j}{dz} = 0$ for $z \to \pm\infty$) [70]:

$$F = A\int_{-\infty}^{+\infty}\left(\overline{f_0}(z) + \frac{1}{2}\sum_{i=1}^{NC}\sum_{j=1}^{NC}{\kappa_2}^{ij}\frac{d\rho_i}{dz}\frac{d\rho_j}{dz}\right) dz \tag{76}$$

and the expression for the surface tension, σ, for a planar interface will be [70]:

$$\sigma = \int_{-\infty}^{+\infty}\left(\overline{\Delta\Omega} + \frac{1}{2}\sum_{i=1}^{NC}\sum_{j=1}^{NC}{\kappa_2}^{ij}\frac{d\rho_i}{dz}\frac{d\rho_j}{dz}\right) dz \tag{77}$$

where $\overline{\Delta\Omega}$ in eq. (77) is the grand thermodynamic potential and the generalized form of eq. (55), given by [70]:

$$\overline{\Delta\Omega} = \overline{f}_0(z) - \sum_{i=1}^{NC} \rho_i(z) {\mu_i}^e + p^e \tag{78}$$

Moreover, and at equilibrium, the integral in eq. (77) is a minimum. By substituting the integrand I of eq. (77) in the Euler-Lagrange equation:

$$\frac{\partial I\left(z, \rho_i(z), \frac{d\rho_i(z)}{dz}\right)}{\partial \rho_i} - \frac{d}{dz}\left(\frac{\partial I\left(z, \rho_i(z), \frac{d\rho_i(z)}{dz}\right)}{\partial\left(\frac{d\rho_i}{dz}\right)}\right) = 0 \quad \text{for} \quad i = 1, 2, \dots, NC \tag{79}$$

NC-coupled differential equations result [70]:

$$\frac{\partial \overline{\Delta\Omega}}{\partial \rho_i} - \frac{1}{2}\sum_{j=1}^{NC} {\kappa_2}^{ij} \frac{d^2\rho_j}{dz^2} = 0 \quad \text{for} \quad i = 1, 2, \dots, NC \tag{80}$$

These differential equations are multiplied by $\frac{d\rho_i}{dz}$ and summed over all species i [70]:

$$\frac{d}{dz}\left(\overline{\Delta\Omega} - \frac{1}{2}\sum_{i=1}^{NC}\sum_{j=1}^{NC} {\kappa_2}^{ij} \frac{d\rho_i}{dz}\frac{d\rho_j}{dz}\right) = 0 \tag{81}$$

which upon integration yields [70]:

$$\overline{\Delta\Omega} = \frac{1}{2}\sum_{i=1}^{NC}\sum_{j=1}^{NC} {\kappa_2}^{ij} \frac{d\rho_i}{dz}\frac{d\rho_j}{dz} \tag{82}$$

and eq. (77) can thus be written, for instance concerning a liquid-vapor interface, as [70]:

$$\sigma^{VLE} = 2\int_{-\infty}^{+\infty} \overline{\Delta\Omega}\, dz \tag{83}$$

Furthermore, eq. (82) can be rewritten as:

$$\frac{d\rho_1}{dz} = \sqrt{\frac{2\overline{\Delta\Omega}}{\sum_{i=1}^{NC}\sum_{j=1}^{NC} {\kappa_2}^{ij} \frac{d\rho_i}{d\rho_1}\frac{d\rho_j}{d\rho_1}}} \tag{84}$$

Using this result to effect a change of variables in eq. (83) yields the following expression:

$$\sigma^{VLE} = \int_{\rho_1{}^V}^{\rho_1{}^L} \sqrt{2\kappa' \overline{\Delta\Omega}}\, d\rho_1 \tag{85}$$

with

$$\kappa' = \sum_{i=1}^{NC} \sum_{j=1}^{NC} \kappa_2{}^{ij} \frac{d\rho_i}{d\rho_1} \frac{d\rho_j}{d\rho_1} \tag{86}$$

Eq. (84) can also be formally integrated to yield the partial density profiles of the various components across the interface in a multicomponent nonuniform system:

$$z - z_0 = \int_{\rho_1(z_0)}^{\rho_1(z)} \sqrt{\frac{\kappa'}{2\overline{\Delta\Omega}}}\, d\rho_1 \tag{87}$$

where κ' is given by eq. (86), and $\rho_1(z) \in [\rho_1{}^V, \rho_1{}^L]$. In order to predict the interfacial properties of the system, the pure component parameter $\kappa_2{}^{ii} = \kappa_{ii}$ is treated as an adjustable parameter and chosen to match experimental surface tensions of the pure component i at a temperature between the triple point and the critical point. If $\kappa_2{}^{ij} = \kappa_{ij}$ is assumed to be given by the geometric mean approximation [70]:

$$\kappa_{ij} = \sqrt{\kappa_{ii}\kappa_{jj}} \tag{88}$$

a useful simplification in the Euler-Lagrange equations (eq. (80)) can be achieved. Eq. (80) then reduces to a system of $(NC-1)$-nonlinear equations [70]:

$$\sqrt{\kappa_{ii}} \left(\frac{\partial \overline{\Delta\Omega}}{\partial \rho_1}\right)_{\rho_{j\neq 1}} - \sqrt{\kappa_{11}} \left(\frac{\partial \overline{\Delta\Omega}}{\partial \rho_i}\right)_{\rho_{j\neq i}} = 0 \quad \text{for} \quad i = 2, 3, \ldots, NC \tag{89}$$

To evaluate the integrals in eq. (85) and eq. (87), the partial densities ρ_i of the various components across the interface must first be obtained. For this purpose, eq. (89) is the minimization condition for eq. (85) with which the coupled partial densities ρ_i of the numerous components in the interface are calculated.

3.5.3 Incompressible Density Gradient Theory (inc-DGT)

The incompressible density gradient theory (inc-DGT) was developed and applied to mixtures for the purpose of combining the DGT with a g^E-model. Within the framework of the inc-DGT, it is assumed that pressure has no impact on density. This applies to liquid-liquid systems, which are considered incompressible. In that case, the difference between the Helmholtz energy and the Gibbs energy becomes a constant, and both quantities are equally suitable for describing the system. Based on this assumption, the molar Gibbs energy g of a heterogeneous system, rather than its Helmholtz energy density, can be expanded in a Taylor series about g_0, the molar Gibbs energy of a solution of uniform concentration. If the density is not considered anymore, then the mole fractions of the various components in a mixture will be the only thermodynamic state variables whose values will change across the interface between the adjoining bulk phases. Therefore, the Gibbs energy of the nonuniform system is given by the following functional [81]:

$$G = \int_V \bar{g}(T, x_i, \nabla x_i)\, dV \tag{90}$$

where $\bar{g}$ is the Gibbs energy density. The inc-DGT can now be combined with a g^E-model rather than an equation of state, as in its original formulation, which implies that the nonuniform system has gradients in concentration and not in density anymore (eq. (90)). However, the interfacial properties of pure components can no longer be predicted with the inc-DGT, since pure components only form a VLE but not a LLE. Therefore, only their densities will change across the interface. Moreover, the pressure dependence obviously cannot be neglected anymore, whenever VLE states are predicted. In fact, the inc-DGT is combined with a g^E-model, with which the phase properties of pure components cannot be predicted either. While in the original formulation of the DGT, the number of variables is equal to the number of components in the mixture, in the case of the inc-DGT, it is reduced by one because the summation equation has to be fulfilled at every point in space and time. However, the parameter κ loses its physical meaning within the inc-DGT, and has to be adjusted to experimental interfacial tensions of binary mixtures, whereas in the original DGT, it can be theoretically calculated if a specific expression for the intermolecular interaction potential is provided (eq. (70)), or treated as an adjustable parameter and chosen to match experimental surface tensions of pure components at a temperature between the triple point and the critical point.

Within the theoretical framework of the inc-DGT, the grand thermodynamic potential is now given by the difference between the molar Gibbs energy g_0, rather than the Helmholtz energy density, as in eq. (55) and eq. (78), of a homogeneous solution of uniform composition, and the molar Gibbs energy which the nonuniform system would have if the properties of the bulk phases were continuous throughout [81]:

$$\Delta\Omega = g_0(z) - \sum_{i=1}^{NC} x_i(z)\mu_i{}^e \tag{91}$$

Therefore, the interfacial tension is then given by the difference per unit area of interface between the actual Gibbs energy of the nonuniform system, rather than its Helmholtz energy, as in eq. (54) and eq. (77), and that which it would have if the properties of the coexisting bulk phases were continuous throughout. The expression for the interfacial tension at LLE is derived in a similar manner to the one at VLE in subsubchapter 3.5.2 if the mole fraction is substituted for the partial density. Concerning a binary system, the interfacial tension is thus written as:

$$\sigma^{LLE} = \int_{x_1{}^I}^{x_1{}^{II}} \sqrt{2\kappa_{12}\Delta\Omega}\, dx_1 \tag{92}$$

where κ_{12} is the influence parameter of the binary mixture 1-2. Furthermore, the concentration profiles across the interface at equilibrium are given by the following expression:

$$z - z_0 = \int_{x_1(z_0)}^{x_1(z)} \sqrt{\frac{\kappa_{12}}{2\Delta\Omega}}\, dx_1 \tag{93}$$

where $x_1(z) \in [x_1{}^I, x_1{}^{II}]$. Since the incompressible version of the DGT (inc-DGT) is applied in this work, the influence parameter, κ_{12}, has units of $\frac{\mathrm{J.mol}}{\mathrm{m^4}}$ rather than $\frac{\mathrm{J.m^5}}{\mathrm{mol^2}}$ in the original framework of the DGT. The spatial coordinate perpendicular to the interface, z, has thus been transformed to include the molar density of the system, which cannot be determined whenever g^E-models are applied. Therefore, coordinate z will have units of $\frac{\mathrm{mol}}{\mathrm{m^2}}$. To obtain the interfacial coordinate in m, z has to be divided by the difference between the molar densities of the coexisting liquid bulk phases.

3.5.4 Chemical potential*

To apply the generalized theoretical treatment of reactive nonuniform and multicomponent systems (eq. (25)), explicit expressions for the chemical potentials of the various components are required. These are derived from the system Gibbs energy, G, given by eq. (90). The dependence of g on ∇x_i provides the conceptual framework for a generalized chemical potential that incorporates interfacial energies. Conventional and classical formulations of the chemical potential must thus be supplemented by a gradient term, whenever inhomogeneous systems are studied. To determine an expression for the chemical potential, a small variation of the amount of substance, n_i, of the numerous components must be considered. A generalized chemical potential will be, therefore, introduced:

$$\mu_i = \left(\frac{\delta G}{\delta n_i}\right)_{T,p,n_{j\neq i}} = \left(\frac{\partial G}{\partial n_i}\right)_{T,p,n_{j\neq i}} - \nabla\left(\frac{\partial G}{\partial(\nabla n_i)}\right)_{T,p,\nabla n_{j\neq i}} \quad \text{for} \quad i = 1, 2, \dots, NC \tag{94}$$

where the δ notation denotes the variational derivative. Eq. (94) parallels the traditional definition of chemical potential but variational differentiation is substituted for ordinary partial differentiation. The generalized chemical potentials given by eq. (94) satisfy Euler's theorem:

$$\sum_{i=1}^{NC} x_i \mu_i = g \tag{95}$$

as well as the Gibbs-Duhem equation (eq. (29)) at constant temperature and pressure:

$$\sum_{i=1}^{NC} x_i \nabla \mu_i = 0 \tag{96}$$

A mechanism is now determined through which chemical as well as phase equilibrium can be approached in a system in which interfacial or surface effects, as previously characterized by a gradient energy, are important. For a given molar Gibbs energy, g, the gradient-dependent chemical potentials are first calculated by using eq. (94). Then, they are inserted into eq. (25) to derive the dynamics of reactive nonuniform liquid systems. In nonequilibrium thermodynamic systems, the chemical potential varies spatially and thus serves as the driving force for diffusion and chemical reaction.

* Taken from [59] and [102]

3.6 Model example and numerical methods*

In this work, a simple illustration of eq. (25) is given by a conceptual model example assuming a three-component inhomogeneous liquid system with components A, B and C ($NC = 3$) at a constant temperature $T = 298.15$ K. In addition, a simple chemical reaction network consisting of two chemical reactions is considered, namely:

$$\frac{1}{2}A + \frac{1}{2}B \underset{k_2}{\overset{k_1}{\rightleftharpoons}} C \tag{97}$$

in which half of component A and half of component B react to produce component C and vice versa, until the chemical equilibrium is reached. A special feature of the chosen model example (eq. (97)) is that there will be no change in total moles upon reaction, which is consistent with the restriction imposed by eq. (2). Eq. (25) can thus be applied to describe the dynamics of the nonuniform system. Furthermore, it is assumed that the temperature will not change upon reaction. The enthalpy of reaction is thus assumed to be zero. Concerning the chemical reaction given by eq. (97), $NR = 2$ and j runs from 1 to 2: $j = 1$ is the reaction index for the forward reaction, in which A and B are consumed to form C, and $j = 2$ is the reaction index for the backward reaction, in which C is consumed to produce components A and B. The number of educts in the forward reaction is thus $N_1 = 2$ and the one in the backward reaction is $N_2 = 1$. Accordingly, k_1 is the reaction rate coefficient for the forward reaction and k_2 is the reaction rate coefficient for the backward reaction. In addition, it is assumed that both components A and B form a miscibility gap, while components A and C as well as components B and C will be miscible in each other. In what follows, components A and B are treated as independent. The Gibbs energy density $\bar{g}$ in eq. (90) will thus depend on temperature, the two independent mole fractions x_A and x_B, and their gradients ∇x_A and ∇x_B:

$$G = \int_V \bar{g}(T, x_A, x_B, \nabla x_A, \nabla x_B)\, dV \tag{98}$$

where the following expression for g is introduced in the spirit of the inc-DGT of ternary liquid mixtures:

* Taken from [59] and [102]

$$g = g_0 + \frac{1}{2}\kappa_R(\nabla x_A)^2 + \kappa_{RS}\nabla x_A \nabla x_B + \frac{1}{2}\kappa_S(\nabla x_B)^2 \tag{99}$$

Here, g_0 is the molar Gibbs energy of a homogeneous solution of uniform composition x_A and x_B. It accounts for both the configurational and the nonideal (or excess) contributions to the Gibbs energy and is given by the following expression:

$$g_0 = \sum_{i=1}^{3} x_i \mu_{i0} + RT \sum_{i=1}^{3} x_i \ln x_i + g^E \tag{100}$$

in which g^E is the excess molar Gibbs energy. For the sake of simplicity, a simple g^E-model, the Porter equation, will be assumed in this work:

$$\frac{g^E}{RT} = A_{AB}x_A x_B + A_{AC}x_A x_C + A_{BC}x_B x_C \tag{101}$$

where $x_C = 1 - x_A - x_B$ and A_{AB}, A_{AC} and A_{BC} are the temperature-dependent and adjustable Porter coefficients. More realistic thermodynamic models for g^E that describe and incorporate the nonideal and complex phase behavior of real mixtures and systems can also be considered but will not be further discussed in this work. When modeling with a g^E-model, the pressure dependence of the activity coefficient will be neglected; it is then only a function of temperature and composition. Therefore, the criterion of mechanical equilibrium (eq. (27)) cannot be solved, which means that the densities of the coexisting phases cannot be calculated when g^E-models are applied, in contrast to modeling by means of equations of state. The activity coefficient of component i, γ_i, accounts for the deviation of a mixture of chemical substances from ideal behavior, and is related to the excess Gibbs energy G^E by the following thermodynamic relation:

$$\ln \gamma_i = \left(\frac{\partial \left(\frac{G^E}{RT} \right)}{\partial n_i} \right)_{T,p,n_{j \neq i}} \tag{102}$$

which, applied to eq. (101), yields the following analytical expressions for the activity coefficients γ_A, γ_B and γ_C of components A, B and C, respectively, by means of the Porter equation:

$$\ln \gamma_A = A_{AB}(1 - x_A)x_B + A_{AC}(1 - x_A)x_C - A_{BC}x_B x_C \tag{103}$$

$$\ln \gamma_B = A_{AB} x_A (1 - x_B) - A_{AC} x_A x_C + A_{BC} (1 - x_B) x_C \tag{104}$$

$$\ln \gamma_C = -A_{AB} x_A x_B + A_{AC} x_A (1 - x_C) + A_{BC} x_B (1 - x_C) \tag{105}$$

The gradient terms in eq. (99) represent the lowest-order corrections to the molar Gibbs energy of a homogeneous solution, g_0, for concentration gradients, and thus describe the interfacial energy associated with the phase boundaries. The gradient energy parameters or the influence parameters of the ternary mixture are denoted by κ_R, κ_{RS} and κ_S. Moreover, the gradient terms in eq. (99) should give a positive contribution to g_0 for arbitrary directions of ∇x_A and ∇x_B. This implies the following restrictions and necessary conditions concerning the influence parameters:

$$\kappa_R > 0 \tag{106}$$

$$\kappa_S > 0 \tag{107}$$

$$\kappa_{RS} < \sqrt{\kappa_R \kappa_S} \tag{108}$$

if σ^{LLE} is to be positive. Furthermore, stable equilibrium system states can be calculated, and LLE is achieved by constrained minimization of the functional given by eq. (98). The material balance constraints are derived from the condition that $\frac{1}{V}\int_V x_A \, dV$ and $\frac{1}{V}\int_V x_B \, dV$ must be conserved for components A and B, respectively. Therefore, the calculus of variations is applied and leads to a set of differential Euler-Lagrange equations, which are derived in a similar manner to the ones in subchapter 3.5:

$$\left(\frac{\partial \Delta\Omega}{\partial x_A}\right)_{x_B} - \frac{1}{2}\kappa_R \nabla^2 x_A - \frac{1}{2}\kappa_{RS} \nabla^2 x_B = 0 \tag{109}$$

$$\left(\frac{\partial \Delta\Omega}{\partial x_B}\right)_{x_A} - \frac{1}{2}\kappa_{RS} \nabla^2 x_A - \frac{1}{2}\kappa_S \nabla^2 x_B = 0 \tag{110}$$

These equations are then solved, and the solutions are used to perform a coordinate transformation from z-space to x-space. As a result, an expression for the interfacial tension σ^{LLE} for the corresponding ternary mixture at LLE can be obtained:

$$\sigma^{LLE} = \int_{x_A{}^I}^{x_A{}^{II}} \sqrt{2\left[\kappa_R + 2\kappa_{RS}\frac{dx_B}{dx_A} + \kappa_S\left(\frac{dx_B}{dx_A}\right)^2\right]\Delta\Omega} \, dx_A \tag{111}$$

where the superscripts I and II refer to the two equilibrium liquid phases. Therefore, ${x_A}^I$ and ${x_A}^{II}$ are the equilibrium bulk compositions of phases I and II, respectively. In addition, the minimization of the Gibbs energy functional leads to an expression for the equilibrium interfacial concentration profiles across the interface:

$$z - z_0 = \int_{x_A(z_0)}^{x_A(z)} \sqrt{\frac{\left[\kappa_R + 2\kappa_{RS}\frac{dx_B}{dx_A} + \kappa_S\left(\frac{dx_B}{dx_A}\right)^2\right]}{2\Delta\Omega}}\, dx_A \tag{112}$$

In this work, the arbitrarily chosen reference coordinate for integration is set to $z_0 = 0$ at $x_A(z_0) = {x_A}^I$. Hence, the upper bound of integration, $x_A(z)$, will vary within the interface between the two equilibrium bulk compositions ${x_A}^I$ and ${x_A}^{II}$.

In eqs. (109)-(112), $\Delta\Omega$ is the grand thermodynamic potential given by eq. (91) for a ternary mixture, thus, $\Delta\Omega$ is the difference between the molar Gibbs energy of a homogeneous solution of uniform composition x_A and x_B, and the molar Gibbs energy which the nonuniform system would have if the properties of both equilibrium bulk phases I and II were continuous throughout. Therefore, μ_i^e in eq. (91) is the equilibrium chemical potential (referred to the same standard state as g_0) of component i in both bulk phases I and II, which has obviously the same value in both bulk phases given that the two phases are in equilibrium.

The interfacial tension of the binary subsystem A-B at LLE is given by eq. (92): $\int_{{x_A}^I}^{{x_A}^{II}} \sqrt{2\kappa_{AB}\Delta\Omega}\, dx_A$, to which, for consistency purposes, eq. (111) should reduce, by transitioning from the ternary to the binary system. In that case, $\frac{dx_B}{dx_A} = -1$ in eq. (111) and $x_C = 0$. The following condition thus arises:

$$\kappa_R - 2\kappa_{RS} + \kappa_S = \kappa_{AB} \tag{113}$$

In order to fulfill the condition given by eq. (113), it will be assumed that:

$$\kappa_{RS} = -\sqrt{\kappa_R \kappa_S} \tag{114}$$

and:

$$\kappa_R = \kappa_S = \frac{1}{4}\kappa_{AB} \tag{115}$$

$\kappa_{AB} > 0$ is the gradient energy parameter or influence parameter of the binary system A-B, which is chosen to match experimental interfacial tensions of that particular binary mixture that demixes.

If κ_{RS} is assumed to be given by the geometric mean approximation of eq. (114), and κ_R and κ_S are assumed to be given by eq. (115), a useful simplification in the Euler-Lagrange equations (eq. (109) and eq. (110)) can be achieved. These equations then reduce to the following algebraic form:

$$\left(\frac{\partial \Delta\Omega}{\partial x_A}\right)_{x_B} + \left(\frac{\partial \Delta\Omega}{\partial x_B}\right)_{x_A} = 0 \tag{116}$$

Eq. (116) is the minimization condition with which the coupled molar fractions of all three components A, B and C in the interface at LLE can be calculated.

Substitution of eq. (114) and eq. (115) into eq. (99) leads to the final expression for the molar Gibbs energy of the ternary inhomogeneous system:

$$g = g_0 + \frac{1}{8}\kappa_{AB}(\nabla x_A)^2 - \frac{1}{4}\kappa_{AB}\nabla x_A \nabla x_B + \frac{1}{8}\kappa_{AB}(\nabla x_B)^2 \tag{117}$$

Furthermore, inserting eq. (114) and eq. (115) into eq. (111) and eq. (112) leads to the following expression for the interfacial tension, σ^{LLE}, between both equilibrium liquid bulk phases I and II:

$$\sigma^{LLE} = \int_{x_A{}^I}^{x_A{}^{II}} \sqrt{\frac{1}{2}\kappa_{AB}\left[1 - 2\frac{dx_B}{dx_A} + \left(\frac{dx_B}{dx_A}\right)^2\right]\Delta\Omega}\, dx_A \tag{118}$$

and to the following expression for the equilibrium concentration profiles in the interface:

$$z - z_0 = \int_{x_A(z_0)}^{x_A(z)} \sqrt{\frac{\kappa_{AB}\left[1 - 2\frac{dx_B}{dx_A} + \left(\frac{dx_B}{dx_A}\right)^2\right]}{8\Delta\Omega}}\, dx_A \tag{119}$$

To evaluate both integrals in eq. (118) and eq. (119), the interfacial mole fractions of components A, B and C need to be determined. This is done by solving eq. (116) in the interface.

Now that the molar Gibbs energy of the nonuniform system has been derived, the chemical potentials of all three components are calculated in accord with eq. (94), where G is obtained by applying eq. (117). The chemical potentials, μ_i, thus read as follows:

$$\begin{aligned}\mu_A = g + (1 - x_A)\left[\left(\frac{\partial g_0}{\partial x_A}\right)_{x_B} + \frac{1}{4}\kappa_{AB}(\nabla^2 x_B - \nabla^2 x_A)\right] \\ - x_B\left[\left(\frac{\partial g_0}{\partial x_B}\right)_{x_A} + \frac{1}{4}\kappa_{AB}(\nabla^2 x_A - \nabla^2 x_B)\right]\end{aligned} \tag{120}$$

$$\begin{aligned}\mu_B = g - x_A\left[\left(\frac{\partial g_0}{\partial x_A}\right)_{x_B} + \frac{1}{4}\kappa_{AB}(\nabla^2 x_B - \nabla^2 x_A)\right] \\ + (1 - x_B)\left[\left(\frac{\partial g_0}{\partial x_B}\right)_{x_A} + \frac{1}{4}\kappa_{AB}(\nabla^2 x_A - \nabla^2 x_B)\right]\end{aligned} \tag{121}$$

$$\begin{aligned}\mu_C = g - x_A\left[\left(\frac{\partial g_0}{\partial x_A}\right)_{x_B} + \frac{1}{4}\kappa_{AB}(\nabla^2 x_B - \nabla^2 x_A)\right] \\ - x_B\left[\left(\frac{\partial g_0}{\partial x_B}\right)_{x_A} + \frac{1}{4}\kappa_{AB}(\nabla^2 x_A - \nabla^2 x_B)\right]\end{aligned} \tag{122}$$

where g is given by eq. (117). As expected, Euler's theorem (eq. (95)) as well as the Gibbs-Duhem equation (eq. (96)) are satisfied by eqs. (120)-(122).

The governing equations for the mole fractions x_A and x_B are obtained by inserting the latter chemical potentials (eqs. (120)-(122)) into eq. (25), while taking the chemical reaction given by eq. (97) and the following relation: $a_i = x_i\gamma_i$ into account:

$$\begin{aligned}\frac{\partial x_A(z,t)}{\partial t} = \nabla\Bigg\{M_{AB}x_A(z,t)x_B(z,t)\nabla\Bigg[\left(\frac{\partial g_0(z,t)}{\partial x_A}\right)_{x_B} - \left(\frac{\partial g_0(z,t)}{\partial x_B}\right)_{x_A} \\ + \frac{1}{2}\kappa_{AB}\big(\nabla^2 x_B(z,t) - \nabla^2 x_A(z,t)\big)\Bigg] \\ + M_{AC}x_A(z,t)x_C(z,t)\nabla\left[\left(\frac{\partial g_0(z,t)}{\partial x_A}\right)_{x_B} + \frac{1}{4}\kappa_{AB}\big(\nabla^2 x_B(z,t) - \nabla^2 x_A(z,t)\big)\right]\Bigg\} \\ + \frac{1}{2}\Big[-k_1\sqrt{x_A(z,t)\gamma_A(z,t)}\sqrt{x_B(z,t)\gamma_B(z,t)} \\ + k_2 x_C(z,t)\gamma_C(z,t)\Big]\exp\Big(\frac{\kappa_{AB}}{8RT}\Big[\big(\nabla x_A(z,t) - \nabla x_B(z,t)\big)^2 \\ + 2\big(x_A(z,t) - x_B(z,t)\big)\nabla^2 x_A(z,t) + 2\big(x_B(z,t) - x_A(z,t)\big)\nabla^2 x_B(z,t)\Big]\Big)\end{aligned} \tag{123}$$

$$\frac{\partial x_B(z,t)}{\partial t} = \nabla\Bigg\{M_{AB}x_A(z,t)x_B(z,t)\nabla\Bigg[\left(\frac{\partial g_0(z,t)}{\partial x_B}\right)_{x_A} - \left(\frac{\partial g_0(z,t)}{\partial x_A}\right)_{x_B} + \frac{1}{2}\kappa_{AB}\left(\nabla^2 x_A(z,t) - \nabla^2 x_B(z,t)\right)\Bigg] + M_{BC}x_B(z,t)x_C(z,t)\nabla\Bigg[\left(\frac{\partial g_0(z,t)}{\partial x_B}\right)_{x_A} + \frac{1}{4}\kappa_{AB}\left(\nabla^2 x_A(z,t) - \nabla^2 x_B(z,t)\right)\Bigg]\Bigg\} + \frac{1}{2}\Big[-k_1\sqrt{x_A(z,t)\gamma_A(z,t)}\sqrt{x_B(z,t)\gamma_B(z,t)} + k_2 x_C(z,t)\gamma_C(z,t)\Big]\exp\left(\frac{\kappa_{AB}}{8RT}\Big[\left(\nabla x_A(z,t) - \nabla x_B(z,t)\right)^2 + 2\left(x_A(z,t) - x_B(z,t)\right)\nabla^2 x_A(z,t) + 2\left(x_B(z,t) - x_A(z,t)\right)\nabla^2 x_B(z,t)\Big]\right) \quad (124)$$

where $x_C(z,t) = 1 - x_A(z,t) - x_B(z,t)$. The partial differential equations given by eq. (123) and eq. (124) are the starting point for describing the dynamics of the assumed ternary reactive system A-B-C. They must be solved simultaneously for each point in space z and time t, and numerical methods must be applied to obtain $x_A(z,t)$ and $x_B(z,t)$. An equation for the third component can also be derived in a similar manner:

$$\frac{\partial x_C(z,t)}{\partial t} = \nabla\Bigg\{-M_{AC}x_A(z,t)x_C(z,t)\nabla\Bigg[\left(\frac{\partial g_0(z,t)}{\partial x_A}\right)_{x_B} + \frac{1}{4}\kappa_{AB}\left(\nabla^2 x_B(z,t) - \nabla^2 x_A(z,t)\right)\Bigg] - M_{BC}x_B(z,t)x_C(z,t)\nabla\Bigg[\left(\frac{\partial g_0(z,t)}{\partial x_B}\right)_{x_A} + \frac{1}{4}\kappa_{AB}\left(\nabla^2 x_A(z,t) - \nabla^2 x_B(z,t)\right)\Bigg]\Bigg\} + \Big[k_1\sqrt{x_A(z,t)\gamma_A(z,t)}\sqrt{x_B(z,t)\gamma_B(z,t)} - k_2 x_C(z,t)\gamma_C(z,t)\Big]\exp\left(\frac{\kappa_{AB}}{8RT}\Big[\left(\nabla x_A(z,t) - \nabla x_B(z,t)\right)^2 + 2\left(x_A(z,t) - x_B(z,t)\right)\nabla^2 x_A(z,t) + 2\left(x_B(z,t) - x_A(z,t)\right)\nabla^2 x_B(z,t)\Big]\right) \quad (125)$$

but does not provide new information. By summing eqs. (123)-(125), the following equation results: $\frac{\partial x_A(z,t)}{\partial t} + \frac{\partial x_B(z,t)}{\partial t} + \frac{\partial x_C(z,t)}{\partial t} = 0$, as expected. $\gamma_A(z,t)$, $\gamma_B(z,t)$ and $\gamma_C(z,t)$ in eqs. (123)-(125) are the activity coefficients of components A, B and C, and are calculated by

eqs. (103)-(105), respectively; thus, they are determined via g^E in eq. (101) by applying classical thermodynamic relations.

Global equilibrium refers to the stable equilibrium system state at which the combined phase and chemical equilibria are reached. At global equilibrium, the chemical potentials of all three components are constant throughout the system, and the fluxes and molecular diffusion of the numerous components vanish. In addition, the forward reaction proceeds at the same rate as the backward reaction. Therefore, the rates of change in mole fraction of the various components with respect to time will vanish ($\frac{\partial x_i(z,t\to+\infty)}{\partial t} = 0$). Moreover, the global equilibrium state depends neither on the reaction rate coefficients k_1 and k_2, nor on the diffusive mobilities M_{AB}, M_{AC} and M_{BC}, the former and latter only determining the path to the final equilibrium state. At global equilibrium, the diffusion term in eqs. (123)-(125) vanishes. By setting the left-hand side of eq. (123) or eq. (124) or eq. (125) to zero and by keeping in mind that the exponential function does not vanish, the following expression for the equilibrium coefficient, K, for the chemical reaction given by eq. (97) can be derived:

$$K(z) = \frac{x_C(z,t\to+\infty)\gamma_C(z,t\to+\infty)}{\sqrt{x_A(z,t\to+\infty)\gamma_A(z,t\to+\infty)}\sqrt{x_B(z,t\to+\infty)\gamma_B(z,t\to+\infty)}} = \frac{k_1}{k_2} \quad (126)$$

which is also in accord with the formulation given by eq. (43). The equilibrium coefficient, K, is a function of temperature, given that both reaction rate coefficients k_1 and k_2 depend only on temperature.

A numerical scheme has been developed to solve the set of partial differential equations given by eq. (123) and eq. (124), subject to an initial condition of interfacial concentration profiles as well as a boundary condition. Eq. (123) and eq. (124) are discretized by a standard explicit scheme. Therefore, a fully explicit finite difference method is adopted, in which the domain of discretization, consisting of the two coexisting homogeneous liquid bulk phases and the inhomogeneous interface between them, is divided into grid points with the unknown variables located at each point of the grid. These variables, including all the spatial derivatives, are calculated and evaluated at each grid point. In addition, Euler's method is used for time discretization. The boundary conditions are given by both bulk phases, which are homogeneous and of uniform composition. Consequently, the diffusion term as well as the mole fraction

gradients of the various components with respect to the spatial variable, z, will vanish in both coexisting bulk phases. The argument of the exponential function in eqs. (123)-(125) also vanishes and the function thus takes a value of one. For both bulk phases, in which no concentration gradients with respect to z are found, eqs. (123)-(125) reduce to the following expressions:

$$\frac{\partial x_A(z \to \pm\infty, t)}{\partial t} = \frac{1}{2}\Big[-k_1\sqrt{x_A(z \to \pm\infty, t)\gamma_A(z \to \pm\infty, t)}\sqrt{x_B(z \to \pm\infty, t)\gamma_B(z \to \pm\infty, t)} + k_2 x_C(z \to \pm\infty, t)\gamma_C(z \to \pm\infty, t)\Big] \tag{127}$$

$$\frac{\partial x_B(z \to \pm\infty, t)}{\partial t} = \frac{1}{2}\Big[-k_1\sqrt{x_A(z \to \pm\infty, t)\gamma_A(z \to \pm\infty, t)}\sqrt{x_B(z \to \pm\infty, t)\gamma_B(z \to \pm\infty, t)} + k_2 x_C(z \to \pm\infty, t)\gamma_C(z \to \pm\infty, t)\Big] \tag{128}$$

$$\frac{\partial x_C(z \to \pm\infty, t)}{\partial t} = k_1\sqrt{x_A(z \to \pm\infty, t)\gamma_A(z \to \pm\infty, t)}\sqrt{x_B(z \to \pm\infty, t)\gamma_B(z \to \pm\infty, t)} - k_2 x_C(z \to \pm\infty, t)\gamma_C(z \to \pm\infty, t) \tag{129}$$

which are the well-known rate equations of forward and backward chemical reactions occurring in a homogeneous mixture and formulated with activities rather than mole fractions. Therefore, time-dependent Dirichlet boundary conditions are applied.

Furthermore, a special case will arise when chemical reactions taking place at the interface between the coexisting liquid bulk phases are not considered and modeled anymore. The set of partial differential equations given by eq. (123) and eq. (124) will be taken again as a starting point, and the reaction term in the interface will thus be excluded. Hence, the chemical reaction will occur only in both homogeneous bulk phases I and II. The mole fraction gradients of components A and B with respect to the spatial variable z vanish in both bulk phases, the argument of the exponential function also vanishes, and the function thus takes a value of one. Consequently, eq. (123) and eq. (124) reduce to the following expressions, with which the

dynamics of the reactive nonuniform ternary system can be described without incorporating interfacial chemical reactions:

$$\begin{aligned}\frac{\partial x_A(z,t)}{\partial t} = \nabla\Bigg\{ & M_{AB}x_A(z,t)x_B(z,t)\nabla\left[\left(\frac{\partial g_0(z,t)}{\partial x_A}\right)_{x_B} - \left(\frac{\partial g_0(z,t)}{\partial x_B}\right)_{x_A}\right. \\ & \left. + \frac{1}{2}\kappa_{AB}\left(\nabla^2 x_B(z,t) - \nabla^2 x_A(z,t)\right)\right] \\ & + M_{AC}x_A(z,t)x_C(z,t)\nabla\left[\left(\frac{\partial g_0(z,t)}{\partial x_A}\right)_{x_B} + \frac{1}{4}\kappa_{AB}\left(\nabla^2 x_B(z,t) - \nabla^2 x_A(z,t)\right)\right]\Bigg\} \\ & + \frac{1}{2}\Big[-k_1\sqrt{x_A(z\to\pm\infty,t)\gamma_A(z\to\pm\infty,t)}\sqrt{x_B(z\to\pm\infty,t)\gamma_B(z\to\pm\infty,t)} \\ & + k_2 x_C(z\to\pm\infty,t)\gamma_C(z\to\pm\infty,t)\Big]\end{aligned} \tag{130}$$

$$\begin{aligned}\frac{\partial x_B(z,t)}{\partial t} = \nabla\Bigg\{ & M_{AB}x_A(z,t)x_B(z,t)\nabla\left[\left(\frac{\partial g_0(z,t)}{\partial x_B}\right)_{x_A} - \left(\frac{\partial g_0(z,t)}{\partial x_A}\right)_{x_B}\right. \\ & \left. + \frac{1}{2}\kappa_{AB}\left(\nabla^2 x_A(z,t) - \nabla^2 x_B(z,t)\right)\right] \\ & + M_{BC}x_B(z,t)x_C(z,t)\nabla\left[\left(\frac{\partial g_0(z,t)}{\partial x_B}\right)_{x_A} + \frac{1}{4}\kappa_{AB}\left(\nabla^2 x_A(z,t) - \nabla^2 x_B(z,t)\right)\right]\Bigg\} \\ & + \frac{1}{2}\Big[-k_1\sqrt{x_A(z\to\pm\infty,t)\gamma_A(z\to\pm\infty,t)}\sqrt{x_B(z\to\pm\infty,t)\gamma_B(z\to\pm\infty,t)} \\ & + k_2 x_C(z\to\pm\infty,t)\gamma_C(z\to\pm\infty,t)\Big]\end{aligned} \tag{131}$$

where $x_C(z,t) = 1 - x_A(z,t) - x_B(z,t)$.

Moreover, and in order to predict the LLE of the ternary system A-B-C, thermal equilibrium (eq. (26)) as well as diffusive equilibrium (eq. (28)) must be simultaneously fulfilled. The diffusive equilibrium condition states the equality of the chemical potentials for each component A, B, and C in both phases I and II present, which translates into the equality of activities $a_i = x_i\gamma_i$, or the isoactivity criterion, for each component in both bulk phases, whenever LLE states are to be studied and modeled. This equivalence relation can be easily deduced from eq. (38) and leads to the following equations that must be simultaneously solved in order to predict the LLE of the ternary system A-B-C:

$$x_A{}^I \gamma_A{}^I(T^I, x_A{}^I, x_B{}^I, x_C{}^I) - x_A{}^{II} \gamma_A{}^{II}(T^{II}, x_A{}^{II}, x_B{}^{II}, x_C{}^{II}) = 0 \quad (132)$$

$$x_B{}^I \gamma_B{}^I(T^I, x_A{}^I, x_B{}^I, x_C{}^I) - x_B{}^{II} \gamma_B{}^{II}(T^{II}, x_A{}^{II}, x_B{}^{II}, x_C{}^{II}) = 0 \quad (133)$$

$$x_C{}^I \gamma_C{}^I(T^I, x_A{}^I, x_B{}^I, x_C{}^I) - x_C{}^{II} \gamma_C{}^{II}(T^{II}, x_A{}^{II}, x_B{}^{II}, x_C{}^{II}) = 0 \quad (134)$$

Thermal equilibrium is indirectly fulfilled through $T = T^I = T^{II} = 298.15$ K. Furthermore, γ_A, γ_B and γ_C in both bulk phases I and II are determined by applying eqs. (103)-(105), respectively.

The minimization condition given by eq. (116) with which the equilibrium (LLE) mole fractions of all three components A, B and C at each grid point in the interface are calculated, and the phase equilibrium conditions given by eqs. (132)-(134) are numerically solved by applying Powell's conjugate direction method. A brief description of this method is presented hereafter. Assuming a function which depends on multiple variables, the objective is to find the value of those variables at which this function takes on a minimum value. Starting, for instance, at a given point in a multidimensional space and proceeding from this point in an arbitrarily direction, any function can be minimized along this direction or line. However, the problem is to find a suitable set of directions for the minimization. In addition, some functions do not get exactly to their minimum, but repeated cycles of line minimizations will induce quadratically convergence of these functions to their minimum. Powell's method implies first initializing the set of directions to the basis vectors, and then, after trying all possible directions (one iteration), changing the set of directions based on where the function got to its minimum at the previous direction. It is important to point out that the direction along which the function made its biggest decrease will be discarded. The reason is to avoid linear dependence between the old and new direction, which leads to wrong solutions of the minimization. Given a certain accuracy, the termination criterion for the iteration will be the least-squares method. Furthermore, Powell's method can be used when derivatives of the function to be minimized are not easily obtained [110]. Moreover, the critical point of the ternary system is also calculated by applying this method. First, the determinants in eq. (32) and eq. (33) are evaluated, then both criticality conditions (eq. (32) and eq. (33)) are numerically solved by applying Powell's conjugate direction method.

If the interfacial mole fractions of components A, B and C at LLE are determined, then the interfacial tension, σ^{LLE}, between both equilibrium liquid bulk phases I and II (eq. (118)) and

the equilibrium concentration profiles in the interface (eq. (119)) can be calculated. Both integrals in eq. (118) and eq. (119) are numerically evaluated by applying Romberg's method. The Romberg's integration method is based on an extended trapezoidal rule. Given a function that has to be integrated over an interval between fixed limits, this interval can be halved and the value of the function at the midpoint can be obtained. The function is then integrated over the new intervals. These two intervals can also be halved, the values of the function at the midpoints accordingly obtained, and the function over all four intervals again integrated. The Romberg's method uses this extended trapezoidal rule, and then extrapolates the successive results of the various integrals to infinite halving of the corresponding intervals so that the value of the original integral will be best determined [111].

4 Results and Discussion

4.1 Dynamic modeling of the interfacial properties - Limiting case I

In this subchapter, reactive nonuniform systems in which the chemical reaction takes place instantaneously, and thus in which the reaction is much faster than the rate of diffusion, are the subject of interest. Therefore, the diffusion term will be omitted and all three diffusive mobilities will be assigned a value of zero: $M_{AB} = M_{AC} = M_{BC} = 0$.

4.1.1 Proof of concept*

In this subsubchapter, an exemplary model calculation and numerical solution of the basic system given by eq. (123) and eq. (124) with $M_{AB} = M_{AC} = M_{BC} = 0$ is provided, which will serve as a comprehensive proof of concept. In what follows, a standard model example will be introduced. A three-component mixture made of A, B and C, in which components A and B are practically immiscible and their phase diagram has a large miscibility gap at the assumed temperature $T = 298.15$ K, is considered. Therefore, the Porter coefficient A_{AB} is assigned a value of $A_{AB} = 3.5$ in eq. (101). Furthermore, the other two Porter coefficients are set to $A_{AC} = A_{BC} = 0$ so that the binary subsystems A-C as well as B-C will form ideal mixtures. The initial state of the system is the liquid-liquid phase equilibrium, at which no chemical reaction will take place. To begin with, the corresponding phase diagram of the ternary mixture is calculated. To do so, barycentric coordinates are used such that each point within the Gibbs triangle in Figure 2 simultaneously represents x_A, x_B and x_C. The phase diagram of the ternary system A-B-C at $T = 298.15$ K is shown in Figure 2. The liquid bulk phase I is defined as the one corresponding to the left-hand side branch of the binodal curve, and the liquid bulk

* Taken from [59]

phase II as the one corresponding to the right-hand side branch of the binodal curve. The binodal concentrations of the subsystem A-B are close to 0 or 1, given the Porter coefficient A_{AB} in eq. (101) assumed for the phase equilibrium calculation.

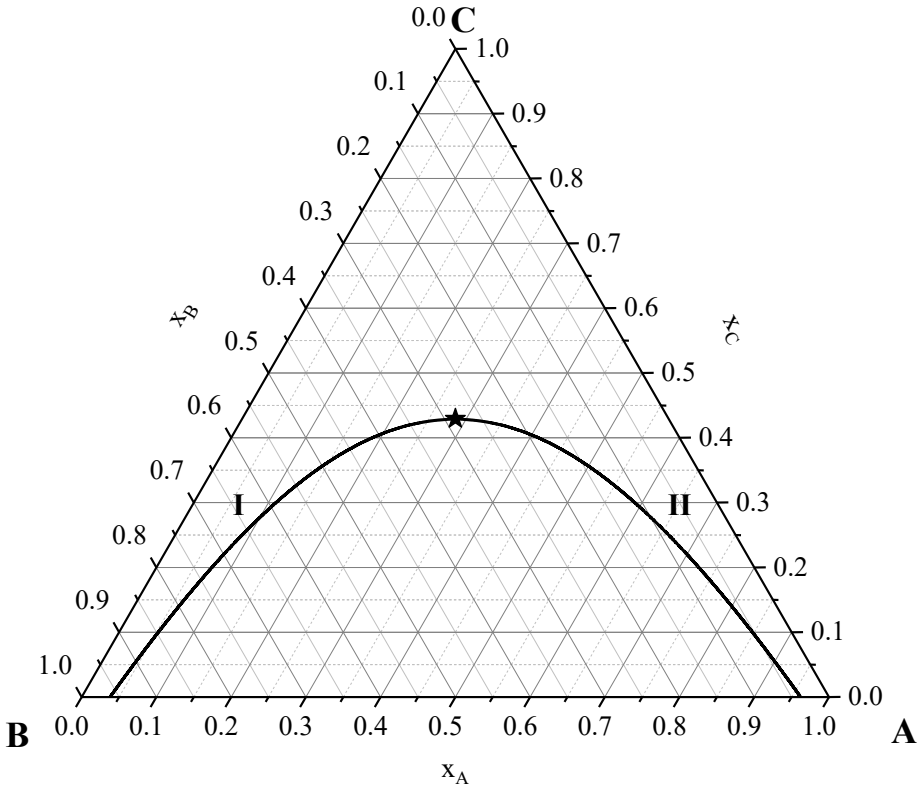

Figure 2. Phase diagram (binodal curve: black line, critical point: star) for the ternary mixture A-B-C at $T = 298.15$ K, calculated with eq. (101) by using $A_{AB} = 3.5$ and $A_{AC} = A_{BC} = 0$. The bulk phase I corresponds to the left-hand side branch of the binodal curve and the bulk phase II corresponds to the right-hand side branch of the binodal curve.

The assumption that the binary subsystems A-C and B-C form ideal mixtures leads to the symmetrical phase diagram, as depicted in Figure 2. Large miscibility gaps are typical of many nonideal systems consisting of aqueous and organic phases with chemical components incorporating large differences in polarity. Such nonuniform systems may include those involved in the reactive extraction process of organic acids from aqueous solutions by solutions of high molecular amines, in which the complex formation takes place at the interface [31]. In addition, the influence parameter of the binary subsystem A-B will be assigned a value of $\kappa_{AB} = 12 \cdot 10^{-7} \frac{\mathrm{J \cdot mol}}{\mathrm{m^4}}$, which is also typical of many liquid two-phase systems [81,83,84].

Furthermore, and to account for instantaneous reaction rates, it will be assumed that both reaction rate coefficients will have equal values of $k_1 = k_2 = 1\ \mathrm{s}^{-1}$. The chemical equilibrium constant given by eq. (126) will thus have a value of $K = 1$. Having specified all parameters needed for modeling, the dynamics of the system can now be studied by solving eq. (123) and eq. (124) at different time steps. The initial system state at time $t = 0$ is chosen to be an equilibrated (LLE) mixture of components A-B-C at infinite dilution of component C, as shown by both black points in Figure 3. These thus refer to the initial concentrations of bulk phases I and II at $t = 0$. A thought experiment, in which a catalyst is added into both bulk phases, will now be considered. Therefore, phases I and II will not correspond to liquid-liquid equilibrium bulk phases anymore, but may also refer to liquid bulk phases which are not in equilibrium.

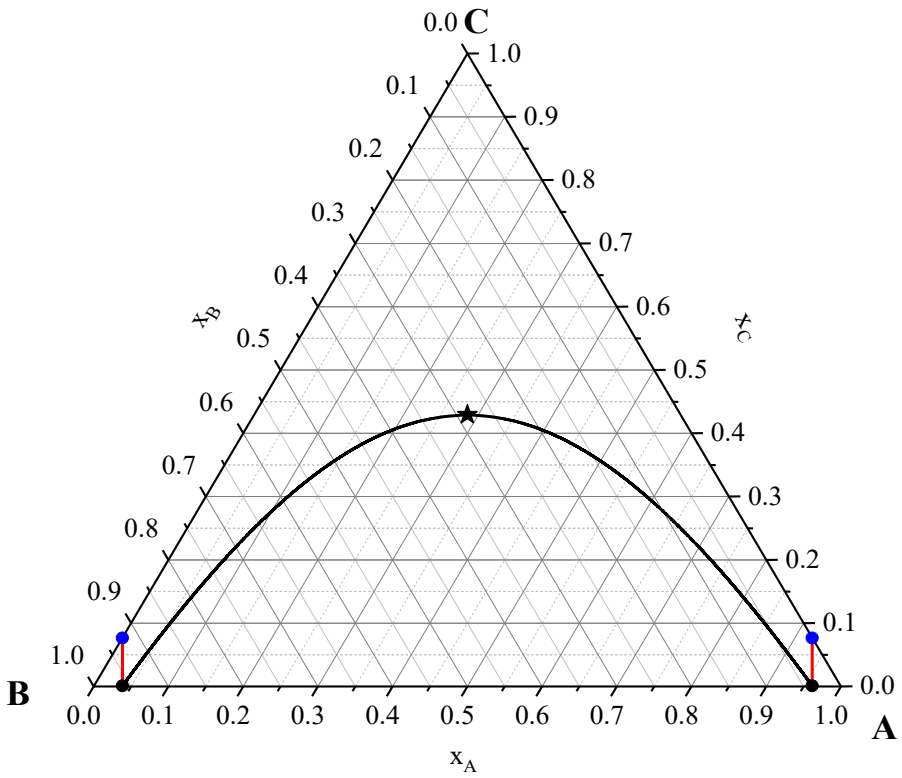

Figure 3. Phase diagram (binodal curve: black line, critical point: star) for the ternary mixture A-B-C at $T = 298.15\ \mathrm{K}$, calculated with eq. (101) by using $A_{AB} = 3.5$ and $A_{AC} = A_{BC} = 0$. The initial state before the chemical reaction starts is indicated by black points, the evolution of the bulk phase mole fractions (reaction path, calculated by solving eq. (123) and eq. (124) at $T = 298.15\ \mathrm{K}$ with $A_{AB} = 3.5$ and $A_{AC} = A_{BC} = 0$ in eq. (101), $\kappa_{AB} = 12 \cdot 10^{-7}\ \frac{\mathrm{J \cdot mol}}{\mathrm{m^4}}$, $k_1 = k_2 = 1\ \mathrm{s}^{-1}$, and $M_{AB} = M_{AC} = M_{BC} = 0$) is depicted by red lines, and the final state is represented by blue points.

In a next step, the equilibrium interfacial concentration profiles corresponding to the initial state ($t = 0$) of the chosen mixture are calculated by solving eq. (116) in the interface and subsequently evaluating the integral in eq. (119). The result is shown in Figure 4, in which a very sharp phase boundary can be observed, and the binodal mole fractions of components A and B are close to 0 or 1. In addition, bulk phase I, which is located at the left-hand side of Figure 4, is rich in component B, while bulk phase II, which is located at the right-hand side of Figure 4, is rich in component A, as also depicted by both black points in Figure 3. Furthermore, the reaction product, component C, acts as a solubilizer in the ternary, two-phase system, as can be deduced from its phase diagram in Figure 2 and from the maximum in $x_C(z, t = 0)$ shown in the inserted figure in Figure 4.

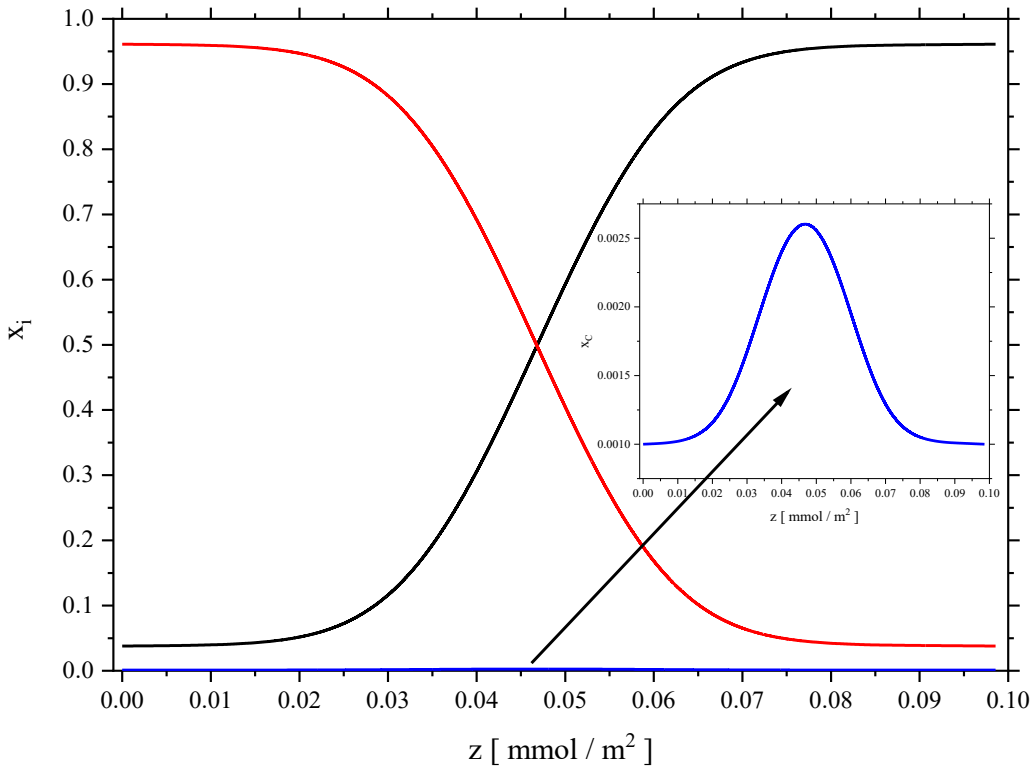

Figure 4. Equilibrium interfacial mole fraction profiles at $t = 0$ for components A (black line), B (red line) and C (blue line) at infinite dilution of component C, calculated by eq. (116) and eq. (119), in combination with eq. (101) by using $A_{AB} = 3.5$ and $A_{AC} = A_{BC} = 0$ at $T = 298.15$ K and $\kappa_{AB} = 12 \cdot 10^{-7} \frac{\text{J·mol}}{\text{m}^4}$. The inserted figure shows the mole fraction profile of component C.

The observed maximum in $x_C(z, t = 0)$ can be interpreted by the enrichment of component C in the interface. An increase in the mole fraction of component C results in greater solubility of A in B and B in A. Although component C is too low in concentration, it is strongly segregated and enriched at the interface. This is a very general finding concerning solubilizers at infinite dilution in inhomogeneous systems, with broad implications for the interfacial and physical properties of nonideal mixtures. For instance, Schäfer et al. [78] found in the ternary mixture DMF-decane-dodecene an enrichment of dodecene in the interface, and in ternary mixtures of DMF-decane-aldehyde always an enrichment of the aldehyde. Concerning the mixture composed of namely water-benzene-butan-1-ol, the enrichment of butan-1-ol was observed [84]. In addition, Danzer and Enders [90] predicted the enrichment of acetic acid in the ternary mixtures water-1-hexanol-acetic acid and water-hexyl acetate-acetic acid. In all studied ternary mixtures [78,84,90], the component exhibiting similarities in polarity with the two other components will be enriched at the interface. The similarity in polarity also explains the enrichment of component C at infinite dilution in the ternary system A-B-C, because the interaction between C and A, on the one hand, and the interaction between C and B, on the other hand, are identical according to the assumed Porter coefficients $A_{AC} = A_{BC} = 0$ in eq. (101).

By comparing the concentration profiles in Figure 1 with the interfacial concentration profiles depicted in Figure 4, the shortcomings of the two-film theory can be identified. A typical interfacial enrichment of one component in ternary mixtures [78,84,90] or multiple components in quaternary mixtures [91] cannot be predicted by applying the two-film theory.

The equilibrium concentration profiles illustrated in Figure 4 are the ones that will initiate the chemical reaction given by eq. (97). More precisely, they correspond to the initial condition ($t = 0$) required to solve the set of partial differential equations given by eq. (123) and eq. (124). By adding a small amount of catalyst into the mixture, the chemical reaction will speed up. The reaction dynamics will now be considered, and the mole fraction profiles, $x_i(z, t)$, that result from the temporal evolution of the mole fraction of the various components will now be investigated at different time steps. Figure 5 shows the calculated interfacial concentration profiles at different times. An exemplary snapshot of the mole fraction distribution for the one-dimensional numerical solution of eq. (123) and eq. (124) at $t = 0.05\,\mathrm{s}$ is illustrated in Figure 5a. Typical reactive features of the inhomogeneous ternary system are observable.

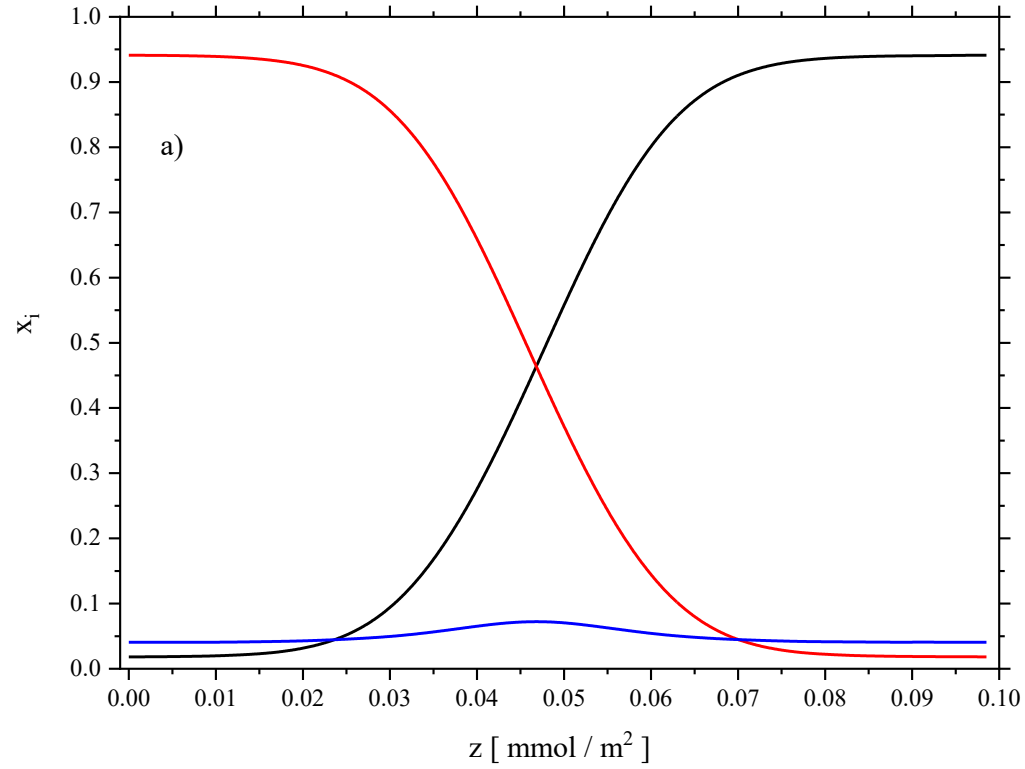
a)
x_i
z [mmol / m^2]
0.0
0.1
0.2
0.3
0.4
0.5
0.6
0.7
0.8
0.9
1.0
0.00
0.01
0.02
0.03
0.04
0.05
0.06
0.07
0.08
0.09
0.10

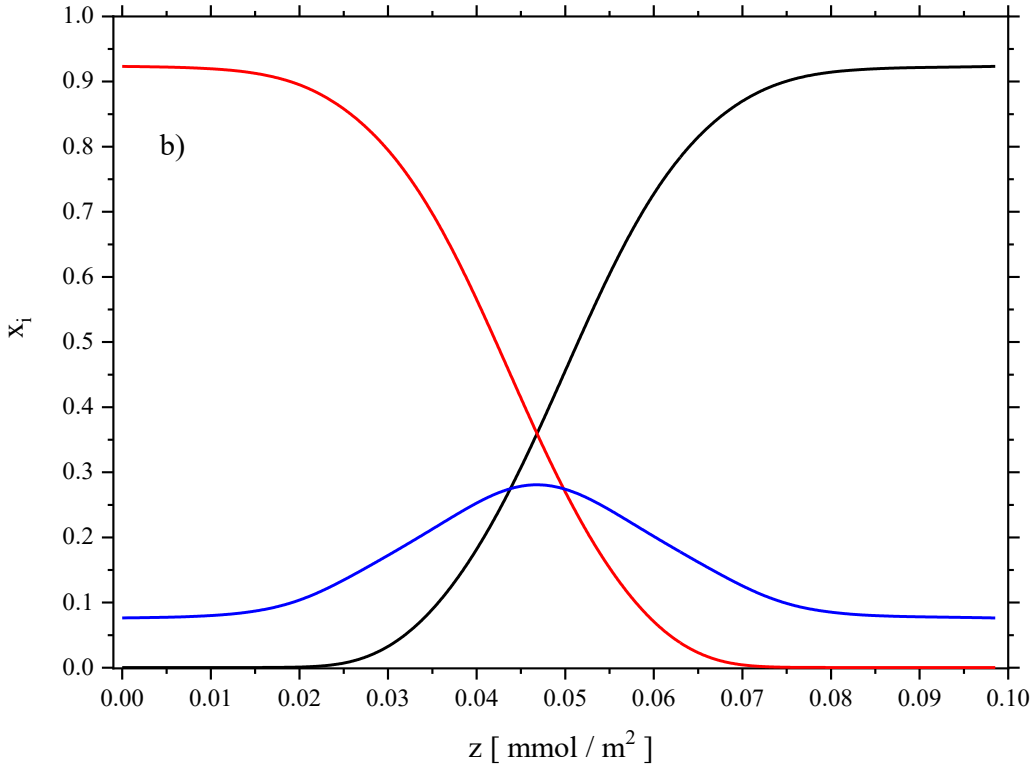
b)
x_i
z [mmol / m^2]
0.0
0.1
0.2
0.3
0.4
0.5
0.6
0.7
0.8
0.9
1.0
0.00
0.01
0.02
0.03
0.04
0.05
0.06
0.07
0.08
0.09
0.10

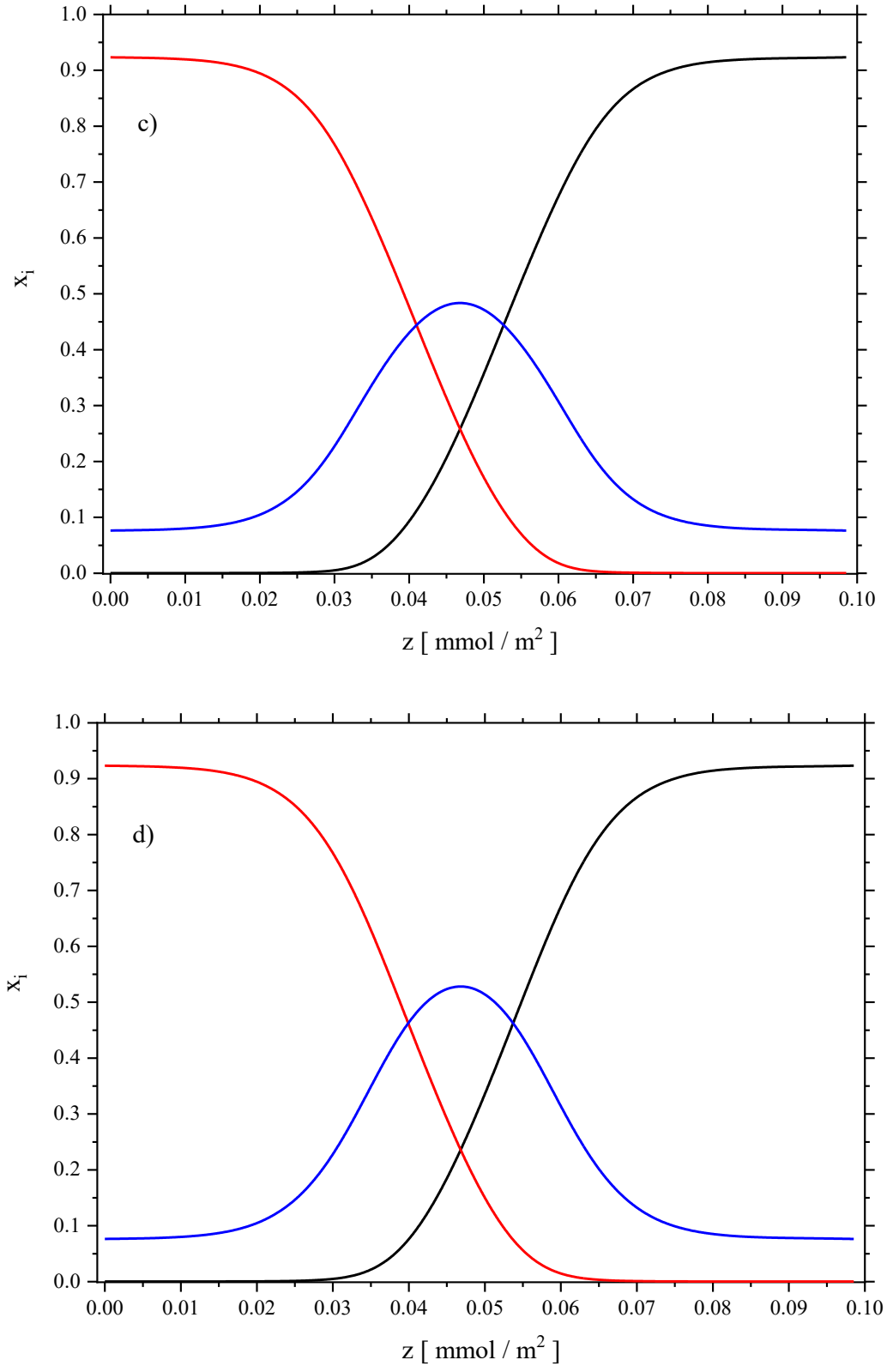

Figure 5. Interfacial mole fraction profiles at different times (a) $t = 0.05$ s, b) $t = 0.25$ s, c) $t = 0.8$ s and d) $t = 2.4$ s) for components A (black line), B (red line), and C (blue line),

calculated by solving eq. (123) and eq. (124) at $T = 298.15\,\mathrm{K}$ with $A_{AB} = 3.5$ and $A_{AC} = A_{BC} = 0$ in eq. (101), $\kappa_{AB} = 12 \cdot 10^{-7}\,\frac{\mathrm{J \cdot mol}}{\mathrm{m^4}}$, $k_1 = k_2 = 1\,\mathrm{s^{-1}}$, and $M_{AB} = M_{AC} = M_{BC} = 0$.

At first, and compared to the concentration profiles illustrated in Figure 4, the interfacial mole fraction profiles depicted in Figure 5a show that components A and B are being continuously consumed, and component C is being continuously formed, in both bulk phases I and II as well as at the interface between them.

To trace the evolution of the uniform bulk phases, more precisely of the bulk phase mole fractions using the Gibbs triangle, the instant concentrations of both phases will be permanently evaluated. The result is given by red lines in Figure 3, in which the red line on the left-hand side of the phase diagram corresponds to the evolution of bulk phase I, while the red line on the right-hand side of the phase diagram corresponds to the evolution of bulk phase II due to the occurring chemical reaction. The consumption of components A and B, and the simultaneous production of component C can also be deduced from these two red lines in Figure 3. Furthermore, the subsequent evolution of the reactive system will lead to an intermediate equilibrium system state at approximately $t = 0.25\,\mathrm{s}$. After $0.25\,\mathrm{s}$ have elapsed since the chemical reaction started, the educts and product bulk mole fractions become constant, and chemical equilibrium in both bulk phases is thus reached, but not necessarily phase equilibrium. This intermediate system state is shown in Figure 5b, from which the equilibrium bulk phase concentrations can be deduced. The same state is indicated by two blue points in Figure 3, which refer to the final bulk system state. The corresponding values of the equilibrium mole fractions of components A, B and C in bulk phases I and II in Figure 5b agree with those taken from both blue points on the left-hand side and on the right-hand side of the phase diagram in Figure 3, respectively. The mole fraction of component A in bulk phase I and of component B in bulk phase II nearly vanish. The chemical reaction has thus totally consumed one of its educts in both liquid bulk phases, as expected, given that the initial bulk phase mole fraction of component A in bulk phase I and the initial mole fraction of component B in bulk phase II were close to 0, as shown in Figure 4. Moreover, the chemical reaction reaches chemical equilibrium in both bulk phases at the same time after approximately $0.25\,\mathrm{s}$ due to the symmetry of the applied Porter equation (eq. (101) with $A_{AC} = A_{BC} = 0$), which is reflected by the phase diagram of the ternary system and the initial mole fraction profiles given in Figure 4.

Returning to the bulk phases, and at approximately $t = 0.25$ s, the final state of both bulk phases will be such that the ratio of the activity of the product to the activities of the educts, all activities raised to the power of the absolute value of the corresponding stoichiometric coefficients, which is also the equilibrium coefficient expression given by eq. (126), will take a value of 1 in both bulk phases I and II. Therefore, it can be deduced that chemical equilibrium has been reached in both coexisting liquid bulk phases.

However, the latter observation does not apply to the interface between the coexisting liquid phases. In fact, the chemical reaction is still taking place at the interface and variations in the mole fractions with respect to time are still observed. Another exemplary snapshot of the mole fractions will now be considered. A random time step at $t = 0.8$ s will be chosen. The corresponding interfacial mole fraction profiles are shown in Figure 5c. It can be observed that component C is still being continuously produced at the interface, the phase boundary is getting sharper, and the interfacial mole fractions of both educts are still decreasing; components A and B are thus continuously being consumed at the interface. The bulk phase concentrations did not evolve with time, as expected, given that chemical equilibrium has already been reached in both bulk phases. In addition, educts A and B are progressively vanishing at the interface and their mole fractions are taking a value of nearly 0 across a big portion of the interfacial layer.

The subsequent evolution will lead the ternary system to its final overall equilibrium state at approximately $t = 2.4$ s, including the interface (Figure 5d). After 2.4 s have elapsed since the chemical reaction started at $t = 0$, the educts and product interfacial mole fractions become constant, and the interfacial chemical reaction will reach chemical equilibrium, the latter having already been reached in both bulk phases after approximately 0.25 s of reaction. The system evolved into a stationary state and the stationary spatial distributions of the mole fractions corresponding to this final system state are shown in Figure 5d, from which the equilibrium interfacial and bulk mole fractions can be deduced. At this time step, namely at $t = 2.4$ s, the final state will be such that the ratio of the activity of the product to the activities of the educts, all activities raised to the power of the absolute value of the corresponding stoichiometric coefficients given by eq. (126), will now also take a value of 1 at the interface, more precisely at every point of the grid located inside the interface. Hence, the overall chemical equilibrium has been reached. For illustration purposes, the entire evolution will be shown in Figure 6.

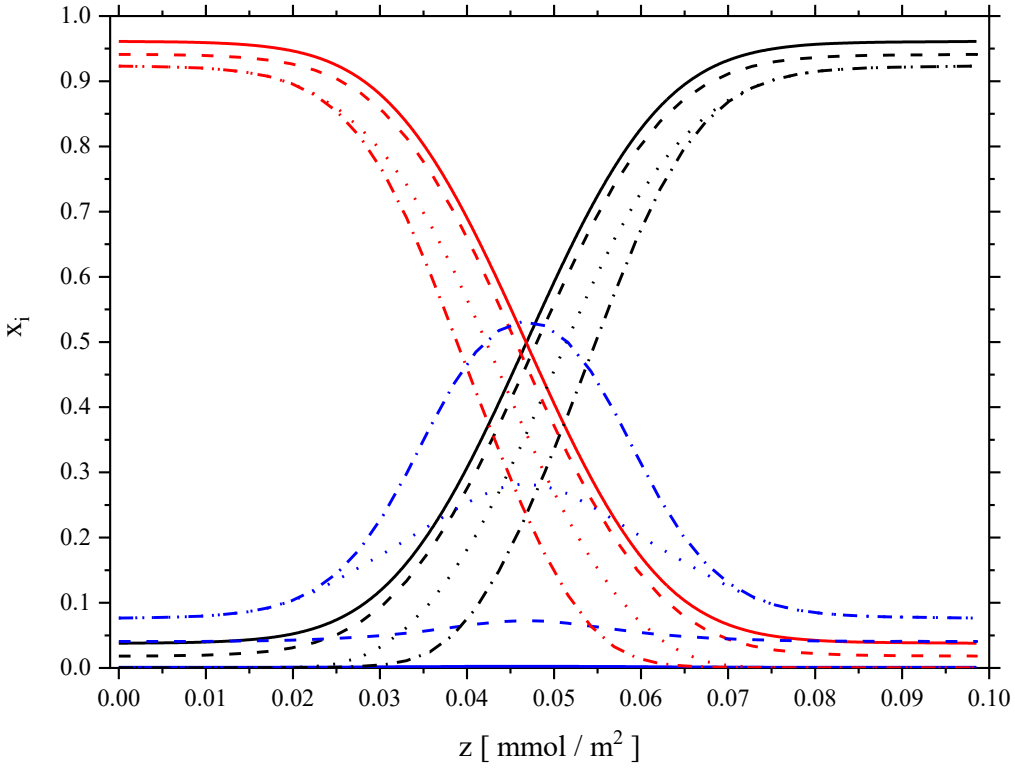

Figure 6. Interfacial mole fraction profiles for components A (black line), B (red line), and C (blue line) at different times (solid line: $t = 0$, dashed line: $t = 0.05$ s, dotted line: $t = 0.25$ s, and dashed-dotted line: $t = 2.4$ s). The calculations were performed identically to the ones in Figure 4 and Figure 5.

In addition, Figure 7 shows the calculated interfacial concentration profiles of the reaction product C at different time steps. The continuous production of C in both bulk phases as well as in the interface between them is thus depicted in Figure 7 until the overall chemical equilibrium is reached. The highest actual yield of component C is found at the center of the interface, where a pronounced maximum in the mole fraction profile of product C in Figure 5d and Figure 7 (solid line) can be found. This is exactly what can be expected, given the stoichiometry of the assumed chemical reaction (eq. (97)). The main explanation is as follows. Due to the symmetry incorporated by eq. (101) with $A_{AC} = A_{BC} = 0$, the initial spatial distribution of the mole fractions of components A and B will be such that both educts will be present in nearly equimolar amounts at the center of the interface, thus, their mole fractions will take there a value of nearly 0.5, as shown in Figure 4. Consequently, given that half of component A reacts with half of

component B to produce component C according to eq. (97), and both educts are present in an equal number of moles, the highest actual yield of component C will be at the center of the interfacial domain.

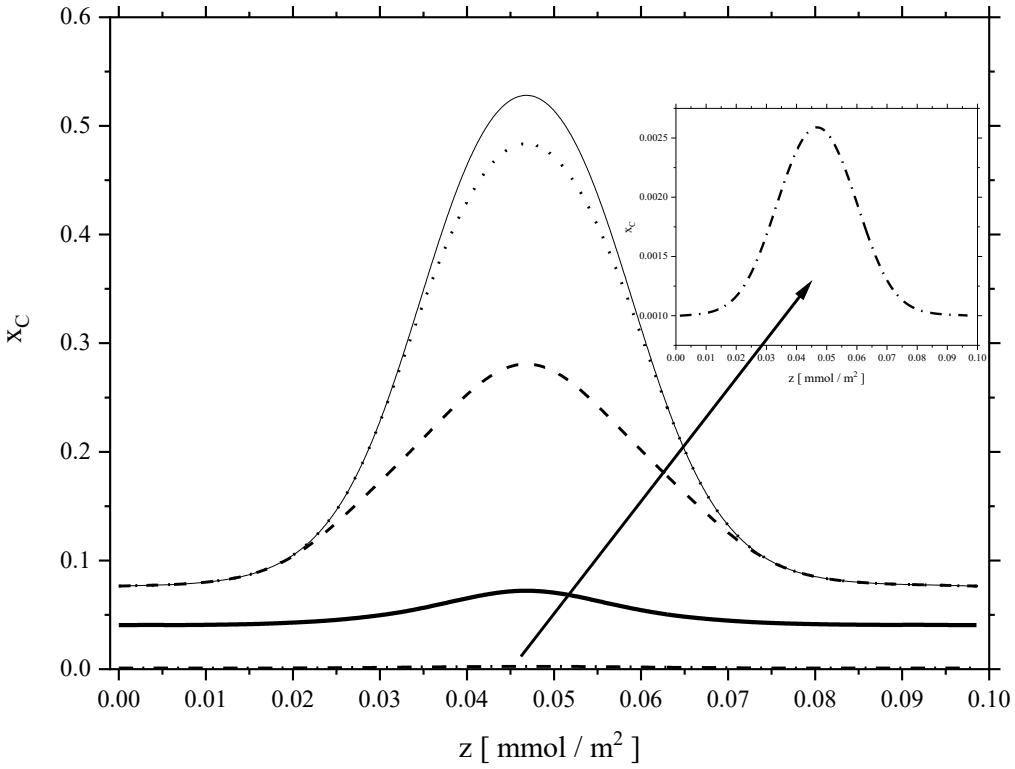

Figure 7. Interfacial mole fraction profiles for component C at different times (dashed-dotted line: $t = 0$, thick solid line: $t = 0.05$ s, dashed line: $t = 0.25$ s, dotted line: $t = 0.8$ s, and solid line: $t = 2.4$ s). The calculations were performed identically to the ones in Figure 4 and Figure 5.

Similarly, and as can also be expected, the lowest actual yield of component C will be in both bulk phases I and II, given that the initial bulk phase mole fraction of educt A in bulk phase I and of educt B in bulk phase II are close to 0, as shown in Figure 4. This result is illustrated by the two minima in the mole fraction profile of product C on the left-hand side and the right-hand side of Figure 5d and Figure 7 (solid line). Furthermore, and by closely examining the initial spatial distribution of the mole fractions of both educts A and B between the center of the interface and the two bulk phases, it can be deduced that the actual yield of component C will decrease from its maximum value at the center of the interfacial layer to its minimum value by

approaching both bulk phases, as can also be observed in Figure 7 (solid line). In addition, the evolution of the composition of both liquid bulk phases over time will be investigated, and is depicted in Figure 8 and Figure 9.

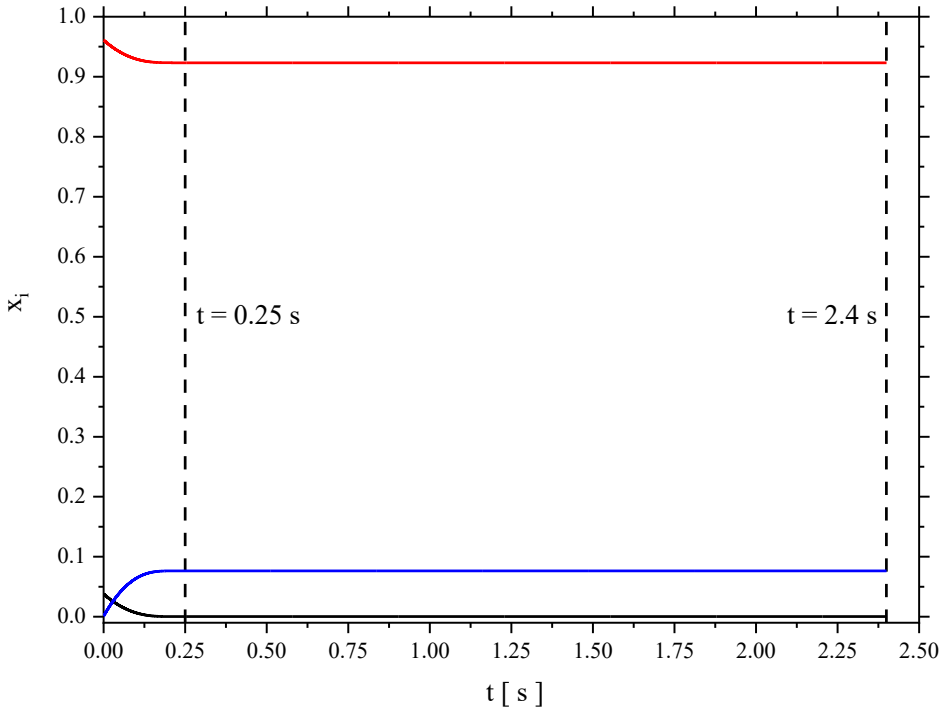

Figure 8. Time evolution of the mole fractions of components A (black line), B (red line), and C (blue line) in bulk phase I, calculated by solving eq. (123) and eq. (124) at $T = 298.15$ K with $A_{AB} = 3.5$ and $A_{AC} = A_{BC} = 0$ in eq. (101), $\kappa_{AB} = 12 \cdot 10^{-7} \frac{\text{J·mol}}{\text{m}^4}$, $k_1 = k_2 = 1\ \text{s}^{-1}$, and $M_{AB} = M_{AC} = M_{BC} = 0$. The dashed lines represent the time steps at which chemical equilibrium is reached in both bulk phases ($t = 0.25$ s) and in the interface ($t = 2.4$ s).

Figure 8 shows the change in mole fraction of components A, B and C in bulk phase I, while Figure 9 shows the change in mole fraction of components A, B and C in bulk phase II. Since the temporal evolution of the concentrations of educts A and B are interchanged by switching from phase I (Figure 8) to phase II (Figure 9), symmetrical behavior can thus also be observed. Again, this behavior can be deduced from the symmetry of the Porter equation (eq. (101) with $A_{AC} = A_{BC} = 0$). The time derivatives of all three mole fractions in bulk phases I and II vanish after approximately 0.25 s have elapsed since the chemical reaction has started, signifying that chemical equilibrium has been reached in both phases. Therefore, the bulk phase concentrations

will remain constant after $t = 0.25$ s. The whole evolution of all three concentrations in both bulk phases will be portrayed until the system has reached its final steady state at approximately $t = 2.4$ s, at which chemical equilibrium has also been reached at the interface. Both time steps are represented by vertical dashed lines in Figure 8 and Figure 9.

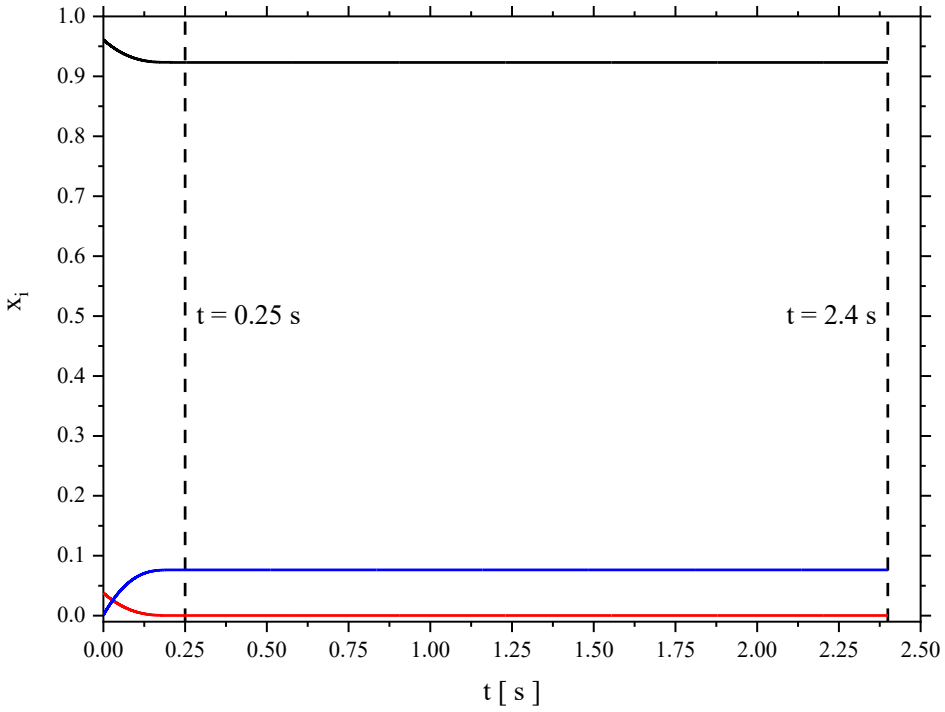

Figure 9. Time evolution of the mole fractions of components A (black line), B (red line), and C (blue line) in bulk phase II, calculated by solving eq. (123) and eq. (124) at $T = 298.15$ K with $A_{AB} = 3.5$ and $A_{AC} = A_{BC} = 0$ in eq. (101), $\kappa_{AB} = 12 \cdot 10^{-7} \frac{\text{J·mol}}{\text{m}^4}$, $k_1 = k_2 = 1\ \text{s}^{-1}$, and $M_{AB} = M_{AC} = M_{BC} = 0$. The dashed lines represent the time steps at which chemical equilibrium is reached in both bulk phases ($t = 0.25$ s) and in the interface ($t = 2.4$ s).

Moreover, it is important to account for the differences in equilibration times of the reactive system characterized by a large miscibility gap: the chemical reaction reaches chemical equilibrium first in both bulk phases I and II, then at the interface between them. This is obviously due to the spatial distribution of the various concentrations of the involved components inside the interfacial layer, compared to the unique and uniform composition of both liquid bulk phases. These results and observations are also in contrast to the two-film theory, in which it is postulated that equilibrium is reached first at the interface, and then in the corresponding bulk phases (Figure 1).

4.1.2 Impact of the Porter coefficients*

In this subsubchapter, model calculations and numerical solutions of the basic system given by eq. (123) and eq. (124) are provided, in which the values of the Porter coefficients will be varied in order to study the impact of these coefficients on the temporal evolution of the reacting ternary mixture. This will be done by comparing the obtained predictions with the standard example of subsubchapter 4.1.1. A three-component mixture composed of A, B and C is again considered, in which components A and B will be practically immiscible, while components A and C as well as components B and C will be miscible in each other. The initial system state at $t = 0$ will again be the liquid-liquid phase equilibrium state (LLE) at infinite dilution of component C, at which no chemical reaction will take place. A thought experiment, in which a catalyst is added into the mixture to speed up the chemical reaction, will then be considered.

The influence of the Porter coefficients A_{AB}, A_{AC} and A_{BC} on the dynamics of the investigated reactive system will be studied. Therefore, the reaction rate coefficients and the influence parameter of the binary subsystem A-B will be assigned the same values that have been assigned to them within the standard example in subsubchapter 4.1.1, thus $k_1 = k_2 = 1\ \mathrm{s}^{-1}$ and $\kappa_{AB} = 12 \cdot 10^{-7}\ \frac{\mathrm{J \cdot mol}}{\mathrm{m^4}}$. The chemical equilibrium constant given by eq. (126) will thus have a value of $K = 1$.

Firstly, the size of the miscibility gap between components A and B will be the subject of interest. The binary subsystems A-C as well as B-C will form ideal mixtures, thus the Porter coefficients A_{AC} and A_{BC} in eq. (101) will have a value of 0, as was also modeled in subsubchapter 4.1.1. Consequently, the Porter coefficient A_{AB} will be varied, and will be given an exemplary value of $A_{AB} = 2.04$ in eq. (101) to study the effect of a very small miscibility gap between components A and B on the reactive behavior of the ternary mixture, in contrast to the large miscibility gap assumed in subsubchapter 4.1.1 with $A_{AB} = 3.5$. To begin with, the corresponding phase diagram of the ternary system is calculated, which is shown in Figure 10. The assumption that the binary subsystems A-C and B-C form ideal mixtures leads to the symmetrical phase diagram, as depicted in Figure 10.

* Taken from [112]

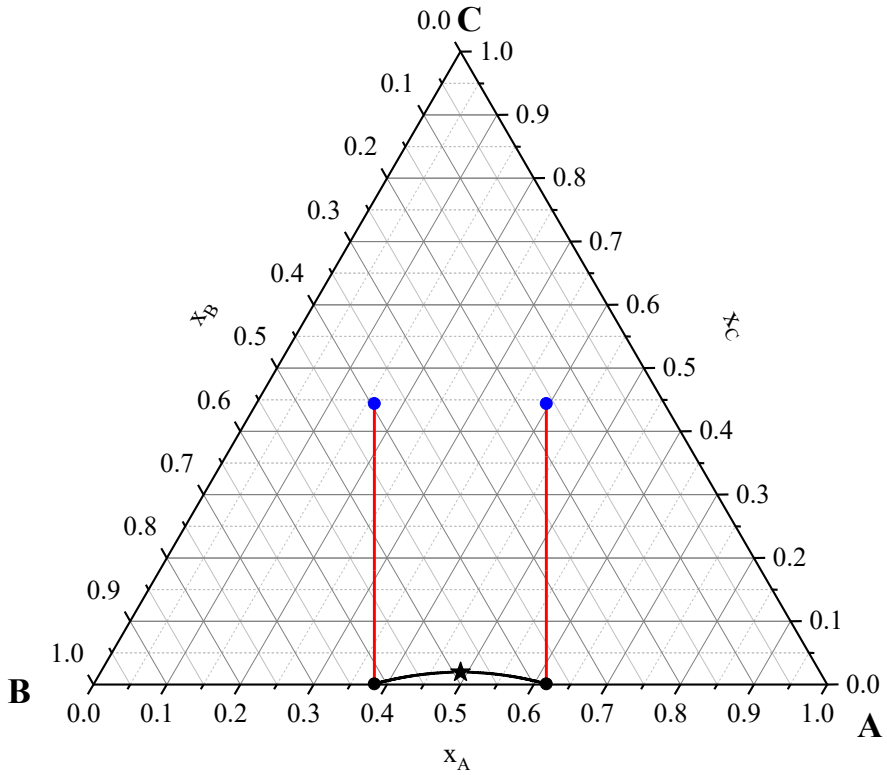

Figure 10. Phase diagram (binodal curve: black line, critical point: star) for the ternary mixture A-B-C at $T = 298.15\,\mathrm{K}$, calculated with eq. (101) by using $A_{AB} = 2.04$ and $A_{AC} = A_{BC} = 0$. The initial state before the chemical reaction starts is indicated by black points, the evolution of the bulk phase mole fractions (reaction path, calculated by solving eq. (123) and eq. (124) at $T = 298.15\,\mathrm{K}$ with $A_{AB} = 2.04$ and $A_{AC} = A_{BC} = 0$ in eq. (101), $\kappa_{AB} = 12 \cdot 10^{-7}\,\frac{\mathrm{J \cdot mol}}{\mathrm{m^4}}$, $k_1 = k_2 = 1\,\mathrm{s^{-1}}$, and $M_{AB} = M_{AC} = M_{BC} = 0$) is depicted by red lines, and the final state is represented by blue points.

The equilibrium interfacial concentration profiles corresponding to the initial state ($t = 0$) of the chosen mixture are then calculated. This is done by solving eq. (116) in the interface and subsequently evaluating the integral in eq. (119). The result is shown in Figure 11, in which a very smooth phase boundary can be observed, given the small miscibility gap found in the phase diagram of the ternary system in Figure 10. Hence, bulk phase I, which is located at the left-hand side of Figure 11, and bulk phase II, which is located at the right-hand side of Figure 11, will be both rich in component A as well as component B, as depicted by both black points in Figure 10. Furthermore, the reaction product C is enriched at the interface and acts as a solubilizer in the ternary inhomogeneous system, as can be deduced from its phase diagram in Figure 10 and in the maximum of $x_C(z, t = 0)$ shown in the inserted figure in Figure 11. The selective enrichment of component C can again be explained by the similarities in polarity that

it exhibits with the two other components A and B in the mixture, because the interaction between C and A, on the one hand, and the interaction between C and B, on the other hand, are identical according to the restriction $A_{AC} = A_{BC} = 0$ imposed in eq. (101).

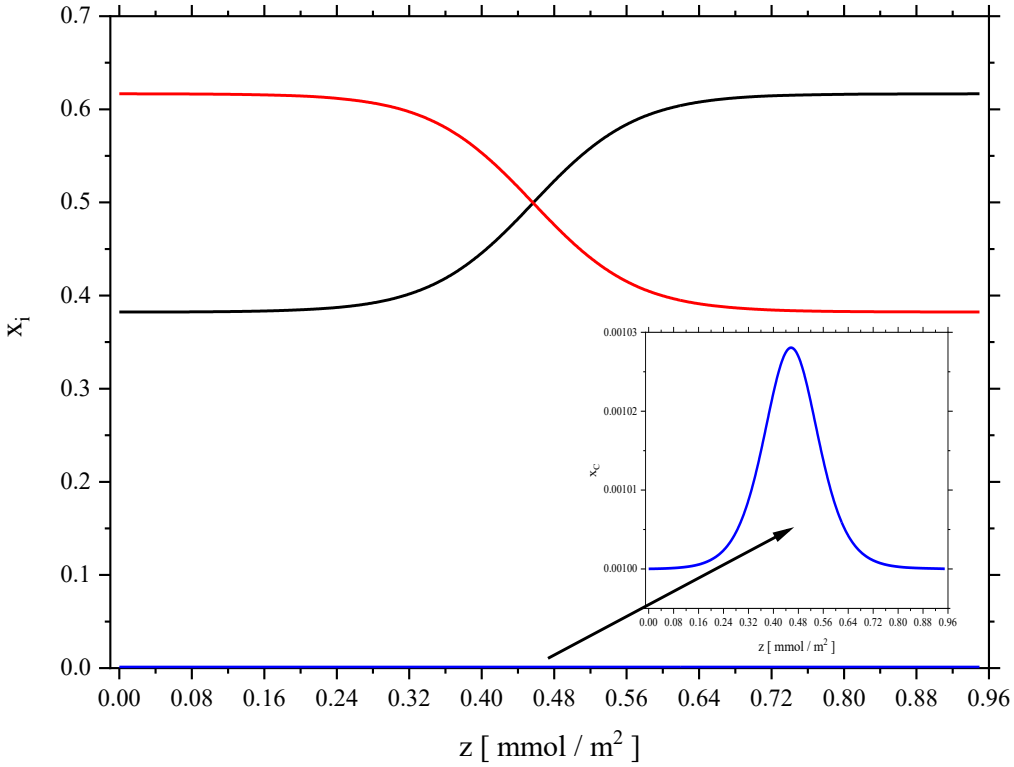

Figure 11. Equilibrium interfacial mole fraction profiles at $t = 0$ for components A (black line), B (red line) and C (blue line) at infinite dilution of component C, calculated by eq. (116) and eq. (119), in combination with eq. (101) by using $A_{AB} = 2.04$ and $A_{AC} = A_{BC} = 0$ at $T = 298.15$ K and $\kappa_{AB} = 12 \cdot 10^{-7} \frac{\text{J·mol}}{\text{m}^4}$. The inserted figure shows the mole fraction profile of component C.

The equilibrium concentration profiles at $t = 0$, shown in Figure 11, are the ones that will initiate the chemical reaction given by eq. (97). More precisely, they will correspond to the initial condition ($t = 0$) required to solve the set of partial differential equations given by eq. (123) and eq. (124).

The dynamics of the system can now be considered, and the mole fraction profiles, $x_i(z,t)$, are investigated by solving eq. (123) and eq. (124) at different time steps. Figure 12 shows the calculated interfacial concentration profiles at two different times.

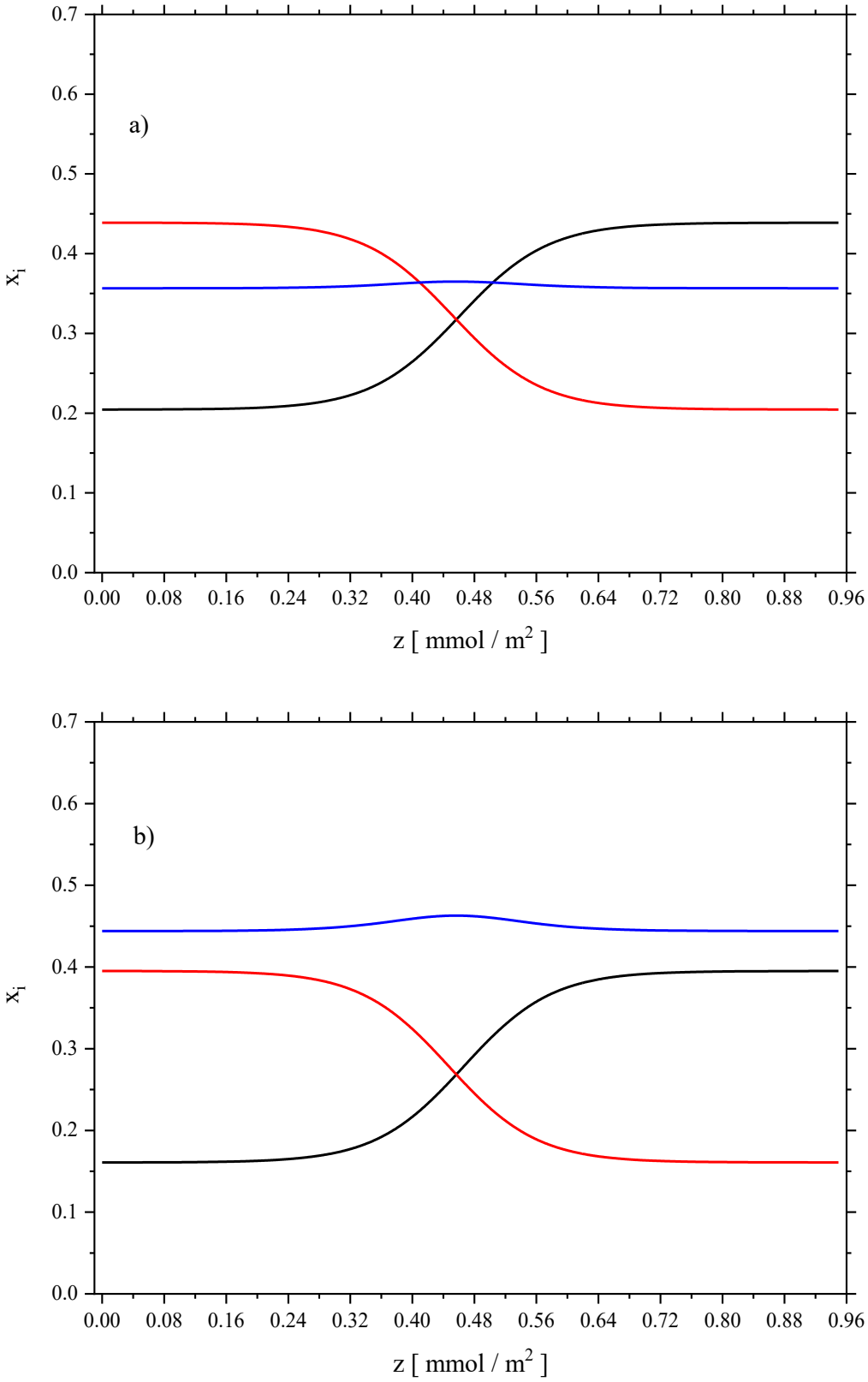

Figure 12. Interfacial mole fraction profiles at two different times (a) $t = 0.8$ s and b) $t = 3.67$ s) for components A (black line), B (red line), and C (blue line), calculated by

solving eq. (123) and eq. (124) at $T = 298.15\,\mathrm{K}$ with $A_{AB} = 2.04$ and $A_{AC} = A_{BC} = 0$ in eq. (101), $\kappa_{AB} = 12 \cdot 10^{-7}\,\frac{\mathrm{J \cdot mol}}{\mathrm{m^4}}$, $k_1 = k_2 = 1\,\mathrm{s^{-1}}$, and $M_{AB} = M_{AC} = M_{BC} = 0$.

An exemplary snapshot of the mole fraction distribution for the one-dimensional numerical solution of eq. (123) and eq. (124) at $t = 0.8\,\mathrm{s}$ is illustrated in Figure 12a. Typical reactive features of the inhomogeneous ternary system are observable. Components A and B are being continuously consumed, and component C is being continuously formed, in both bulk phases I and II as well as at the interface between them.

To trace the temporal evolution of both bulk phases, the instant bulk mole fractions of all three components A, B and C will be permanently evaluated. The result is given by red lines in Figure 10, in which the red line on the left-hand side of the phase diagram corresponds to the evolution of bulk phase I, while the red line on the right-hand side of the phase diagram corresponds to the evolution of bulk phase II due to the occurring chemical reaction. The consumption of components A and B, and the simultaneous formation of component C can also be deduced from these two red lines in Figure 10.

The subsequent evolution of the reactive system leads to an intermediate equilibrium system state at approximately $t = 3.51\,\mathrm{s}$, at which the chemical reaction reaches chemical equilibrium in both liquid bulk phases, and thus the educts and product bulk mole fractions become constant. The same state is indicated by two blue points in Figure 10, which refer to the final bulk system state. Furthermore, the chemical reaction reaches chemical equilibrium in both bulk phases at the same time due to the symmetry of the applied Porter equation (eq. (101) with $A_{AC} = A_{BC} = 0$), which is reflected by the phase diagram of the ternary system in Figure 10 and the initial mole fraction profiles given in Figure 11. At approximately $t = 3.51\,\mathrm{s}$, the final state of both bulk phases will be such that the ratio of the activity of the product to the activities of the educts, all activities raised to the power of the absolute value of the corresponding stoichiometric coefficients, which is also the equilibrium coefficient expression given by eq. (126), will take a value of 1 in both bulk phases I and II.

This intermediate equilibrium system state is immediately followed by the final overall equilibrium state at approximately $t = 3.67\,\mathrm{s}$, at which the interfacial chemical reaction also reaches chemical equilibrium, and the educts and product interfacial mole fractions become constant. However, no significant variations in the interfacial mole fractions of the three

components between $t = 3.51$ s and $t = 3.67$ s are observed, the bulk phase concentrations having obviously not evolved between both time steps, given that chemical equilibrium has already been reached in both bulk phases at $t = 3.51$ s. Therefore, only the stationary spatial distribution of the mole fractions corresponding to the final system state at $t = 3.67$ s will be portrayed in Figure 12b, from which the equilibrium interfacial and bulk mole fractions can be deduced. The corresponding values of the equilibrium mole fractions of components A, B and C in bulk phases I and II in Figure 12b agree with those taken from both blue points on the left-hand side and on the right-hand side of the phase diagram in Figure 10, respectively. Moreover, and at $t = 3.67$ s, the final state will be such that the ratio of the activity of the product to the activities of the educts, all activities raised to the power of the absolute value of the corresponding stoichiometric coefficients, will now also take a value of 1 at every point of the grid located inside the interface.

The evolution of the composition of both liquid bulk phases over time is depicted in Figure 13. Figure 13a shows the change in mole fraction of components A, B and C in bulk phase I, and Figure 13b shows the change in mole fraction of components A, B and C in bulk phase II.

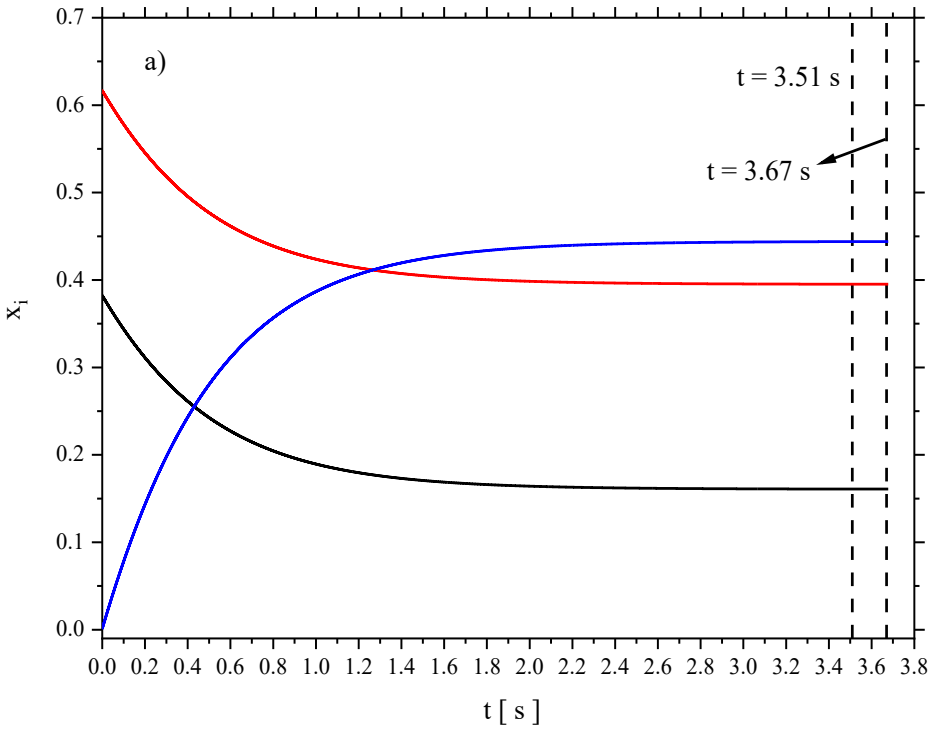

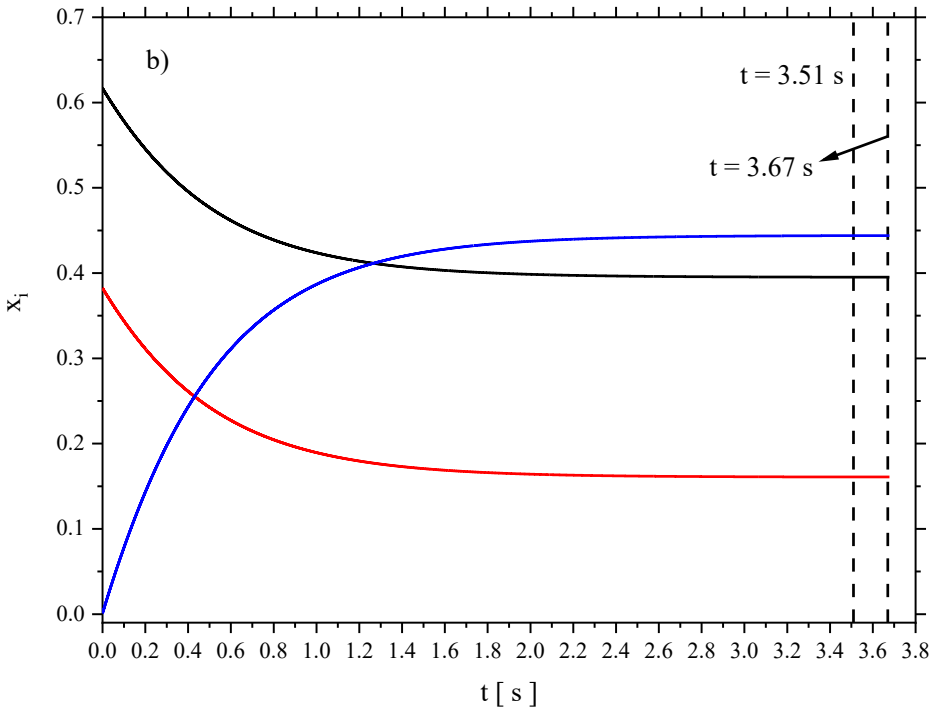

Figure 13. Time evolution of the mole fractions of components A (black line), B (red line), and C (blue line) in both bulk phases (a) bulk phase I and b) bulk phase II), calculated by solving eq. (123) and eq. (124) at $T = 298.15\ \mathrm{K}$ with $A_{AB} = 2.04$ and $A_{AC} = A_{BC} = 0$ in eq. (101), $\kappa_{AB} = 12 \cdot 10^{-7}\ \frac{\mathrm{J \cdot mol}}{\mathrm{m^4}}$, $k_1 = k_2 = 1\ \mathrm{s^{-1}}$, and $M_{AB} = M_{AC} = M_{BC} = 0$. The dashed lines represent the time steps at which chemical equilibrium is reached in both bulk phases ($t = 3.51\ \mathrm{s}$) and in the interface ($t = 3.67\ \mathrm{s}$).

Since the temporal evolutions of the bulk concentration of educts A and B are interchanged by switching from phase I to phase II in Figure 13, symmetrical behavior can thus be observed. Again, this behavior can be deduced from the symmetry of the Porter equation (eq. (101) with $A_{AC} = A_{BC} = 0$).

The main differences observed between the predictions obtained with a small miscibility gap ($A_{AB} = 2.04$) and the predictions obtained in subsubchapter 4.1.1, in which both educts form a large miscibility gap ($A_{AB} = 3.5$), will now be discussed. In both cases, the chemical reaction given by eq. (97) takes place not only in both liquid bulk phases but also at the interface between them. However, it is important to account for the differences in equilibration times between both liquid bulk phases and the interface. In subsubchapter 4.1.1, a difference of approximately $2.4\ \mathrm{s} - 0.25\ \mathrm{s} = 2.15\ \mathrm{s}$ concerning large miscibility gaps is observed, which is much more

pronounced than the difference of approximately $3.67\ \mathrm{s} - 3.51\ \mathrm{s} = 0.16\ \mathrm{s}$ observed in Figure 13 concerning small miscibility gaps. This is a very important finding regarding nonuniform reactive systems in which the chemical reaction is much faster than the rate of diffusion, and thus in which the rate of reaction is effectively instantaneous, with broad implications for the dynamics and evolution of such systems. The smaller the miscibility gap between the reaction educts is, the smaller the differences in equilibration times between bulk phases and interface will be, specifically for the assumed thermodynamical model (Porter equation) and the assumed chemical reaction (eq. (97)). This is obviously due to the high initial concentrations of both components A and B in both bulk phases I and II (Figure 11), and to the smooth interface at $t = 0$, in contrast to the predictions made in the previous subsubchapter. Furthermore, and in subsubchapter 4.1.1, the chemical reaction has totally consumed one of its educts in both liquid bulk phases, given that the initial mole fraction of component A in bulk phase I and the initial mole fraction of component B in bulk phase II were close to 0, which is due to the assumed large miscibility gap ($A_{AB} = 3.5$). However, and by modeling much smaller miscibility gaps between components A and B ($A_{AB} = 2.04$), the reaction educts in bulk phases I and II will be both sufficiently present in high initial concentrations for the chemical reaction (black points in Figure 10). This initial state will lead to a much more pronounced evolution of the bulk phase mole fractions depicted by red lines in Figure 10, and to a much higher production of component C as well as a much higher consumption of components A and B in both liquid bulk phases, as shown in Figure 10 and Figure 13, compared to the results obtained in subsubchapter 4.1.1.

In both cases, the chemical reaction reaches chemical equilibrium first in both bulk phases I and II, then at the interface between them. This is exactly what can be expected, given the stoichiometry of the assumed chemical reaction (eq. (97)). The main explanation is as follows. Regardless of the size of the assumed miscibility gap between the educts, the initial spatial distribution of the mole fractions of components A and B will be such that both educts will be present in nearly equimolar amounts at the center of the interface, thus, their mole fractions will take there a value of nearly 0.5, because of the symmetry incorporated by eq. (101) with $A_{AC} = A_{BC} = 0$, as shown in Figure 4 and Figure 11. Hence, given that half of component A reacts with half of component B to produce component C, and both educts are present in an equal number of moles, the biggest production and highest actual yield of component C will be

at the center of the interfacial region, which is depicted by a maximum in the mole fraction profile of product C in Figure 5d and Figure 12b. For this reason, the interfacial chemical reaction will reach chemical equilibrium after the bulk phase reaction. However, this effect is more or less pronounced depending on the size of the miscibility gap, as was described above. Therefore, and as long as inhomogeneous two-phase systems are the subject of study, both equilibration times will not be equal regardless of the size of the miscibility gap formed by the involved reaction educts.

For illustration purposes, the difference Δt^e in equilibration times, thus the difference between the time needed for the chemical reaction to reach equilibrium at the interface and the time it needs to reach equilibrium in both liquid bulk phases I and II, will be evaluated for different values of the Porter coefficient A_{AB}, and is plotted in Figure 14 as Δt^e over A_{AB}.

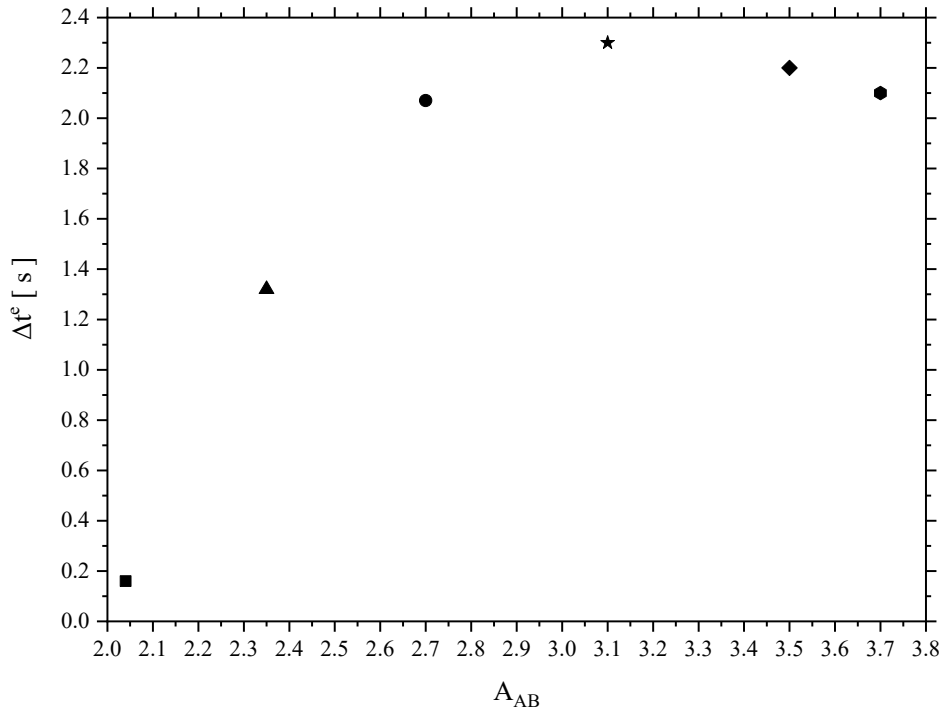

Figure 14. Difference between the time needed for the chemical reaction to reach chemical equilibrium at the interface and the time it needs to reach chemical equilibrium in both bulk phases I and II for the ternary mixture A-B-C calculated by solving eq. (123) and eq. (124) at $T = 298.15\,\mathrm{K}$ with $A_{AC} = A_{BC} = 0$ in eq. (101), $\kappa_{AB} = 12 \cdot 10^{-7}\ \frac{\mathrm{J \cdot mol}}{\mathrm{m^4}}$, $k_1 = k_2 = 1\,\mathrm{s^{-1}}$, $M_{AB} = M_{AC} = M_{BC} = 0$ and for different values of A_{AB} in eq. (101) (square: $A_{AB} = 2.04$, triangle: $A_{AB} = 2.35$, circle: $A_{AB} = 2.7$, star: $A_{AB} = 3.1$, rhombus: $A_{AB} = 3.5$ and hexagonal: $A_{AB} = 3.7$).

A very interesting reactive behavior can be deduced from the scatter plot: Figure 14 shows a maximum in the difference in equilibration times between interface and bulk phases at a given value of A_{AB}. Consequently, the prediction concerning the impact of the size of the miscibility gap on the differences in equilibration times Δt^e discussed above is only valid up to a certain value of the Porter coefficient A_{AB}, and thus up to a specific size of the miscibility gap between educts A and B. By choosing higher values of A_{AB}, and thus by modeling bigger miscibility gaps, other reactive effects and features will arise, which lead to a decrease of Δt^e with increasing A_{AB}, as shown in Figure 14. This observation is related to the general theoretical framework introduced in subchapter 3.1, and can be explained by carefully examining the argument of the exponential functions found in the governing dynamic eq. (123) and eq. (124) of the reactive ternary system. The following explanation holds true, after this specific size of the miscibility gap formed between components A and B, which corresponds to the value of A_{AB} at which the maximum of Δt^e is reached, has been exceeded. The bigger the miscibility gap between components A and B will be, the sharper the phase boundary between both bulk phases will become (because the interfacial thickness will decrease and the binodal mole fractions of components A and B will be much closer to 0 or 1), the greater the spatial gradients of components A and B inside the interface will get, and thus the higher the values of the exponential functions in eq. (123) and eq. (124) will become, the bigger the rates of change in mole fractions due to chemical reaction with respect to time will be, and thus the faster the chemical reaction will reach chemical equilibrium at the interface and, therefore, the smaller the differences in equilibration times between interface and bulk phases will be observed in Figure 14. However, it is important to understand that these predictions and interpretations apply only to reactive nonuniform systems in which the rate of reaction is effectively instantaneous.

Secondly, the ternary mixture will be studied for the case in which the binary subsystems A-C and B-C do not form ideal mixtures anymore, but components A and C as well as B and C will still be miscible in each other. Therefore, on the one hand, the Porter coefficients will be assigned the values of $A_{AC} = 0$, $A_{BC} = 1$, while, on the other hand, they will be assigned the following ones: $A_{AC} = 1$, $A_{BC} = 0$. For both cases, the reaction educts will form a large miscibility gap, and A_{AB} will have the same value of $A_{AB} = 3.5$ as in subsubchapter 4.1.1. For clarification purposes, it will be convenient to put the predictions of both separate cases in combined figures. This would improve the readability of the results significantly.

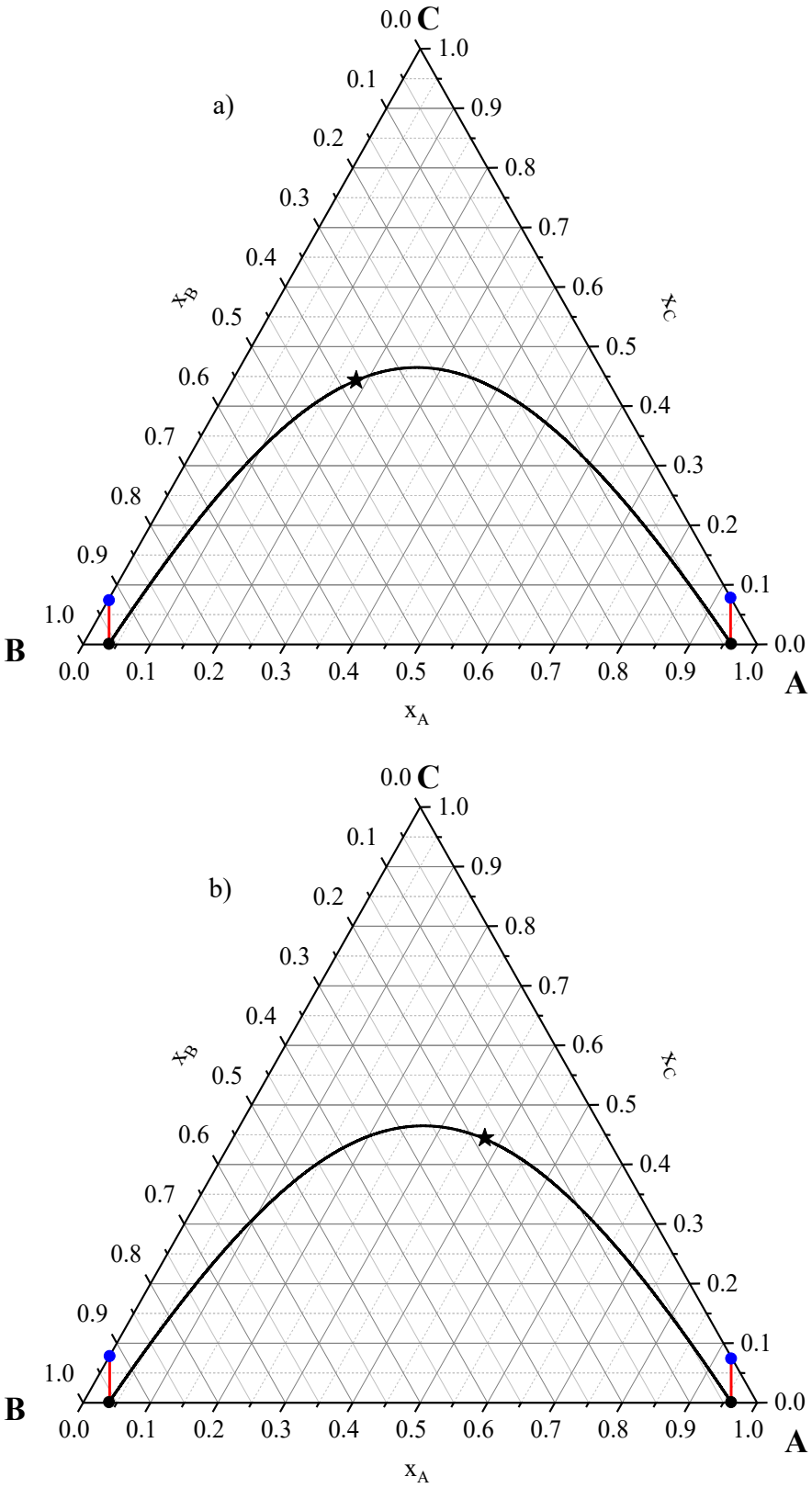

Figure 15. Phase diagram (binodal curve: black line, critical point: star) for the ternary mixture A-B-C at $T = 298.15$ K, calculated with eq. (101) by using $A_{AB} = 3.5$ and for different values

of A_{AC} and A_{BC} in eq. (101) (a) $A_{AC} = 0$, $A_{BC} = 1$ and b) $A_{AC} = 1$, $A_{BC} = 0$). The initial state before the chemical reaction starts is indicated by black points, the evolution of the bulk phase mole fractions (reaction path, calculated by solving eq. (123) and eq. (124) at $T = 298.15$ K with $A_{AB} = 3.5$ and for different values of A_{AC} and A_{BC} (a) $A_{AC} = 0$, $A_{BC} = 1$ and b) $A_{AC} = 1$, $A_{BC} = 0$) in eq. (101), $\kappa_{AB} = 12 \cdot 10^{-7} \frac{\text{J·mol}}{\text{m}^4}$, $k_1 = k_2 = 1\ \text{s}^{-1}$, and $M_{AB} = M_{AC} = M_{BC} = 0$) is depicted by red lines, and the final state is represented by blue points.

The corresponding phase diagrams and the equilibrium interfacial concentration profiles that are related to the initial state of the system at $t = 0$ are first calculated. The results are shown in Figure 15 and Figure 16, respectively. Both figures show that the symmetry of the system, more precisely of the ternary phase diagram, has now been broken. Figure 16a shows the initial interfacial concentration profiles for all three components with $A_{AC} = 0$ and $A_{BC} = 1$, and Figure 16b shows the initial interfacial concentration profiles for which $A_{AC} = 1$ and $A_{BC} = 0$. For the former case, the initial bulk phase mole fraction of component C in bulk phase II, the one rich in component A, is higher than its concentration in bulk phase I, the one rich in component B, given that components A and C form ideal mixtures ($A_{AC} = 0$), in contrast to components B and C for which the Porter coefficient A_{BC} is assigned a value of 1 ($A_{BC} = 1$), as was assumed. For the latter case, the same behavior is observed, but the bulk phases are now interchanged.

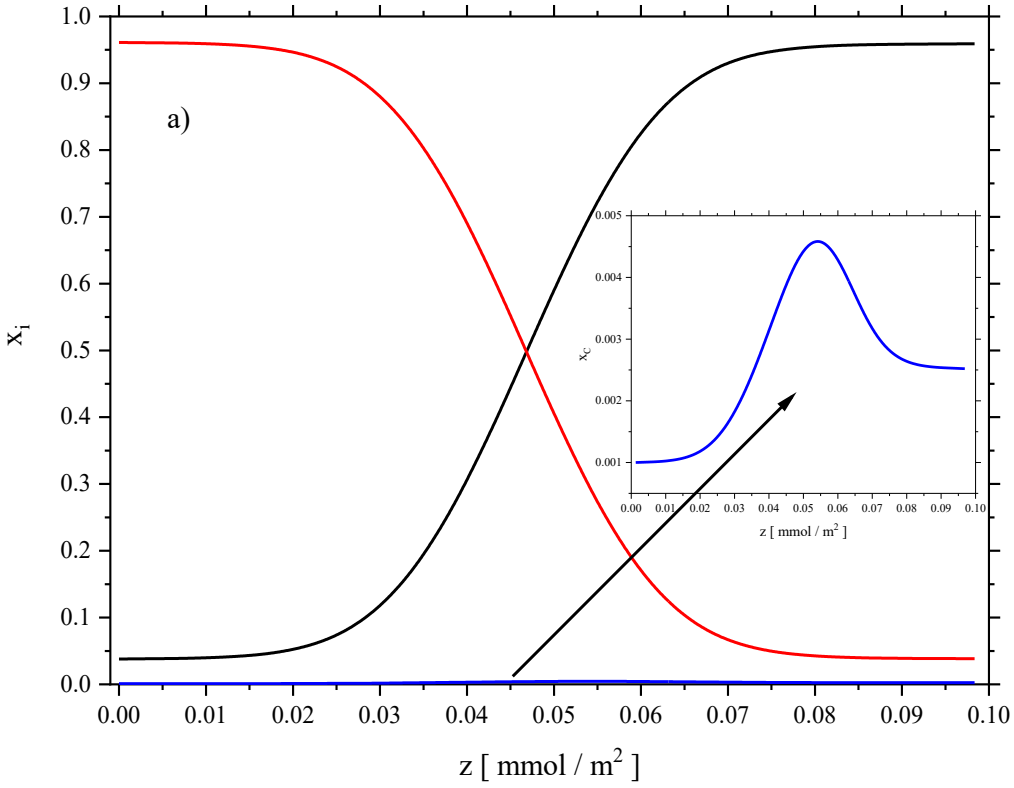

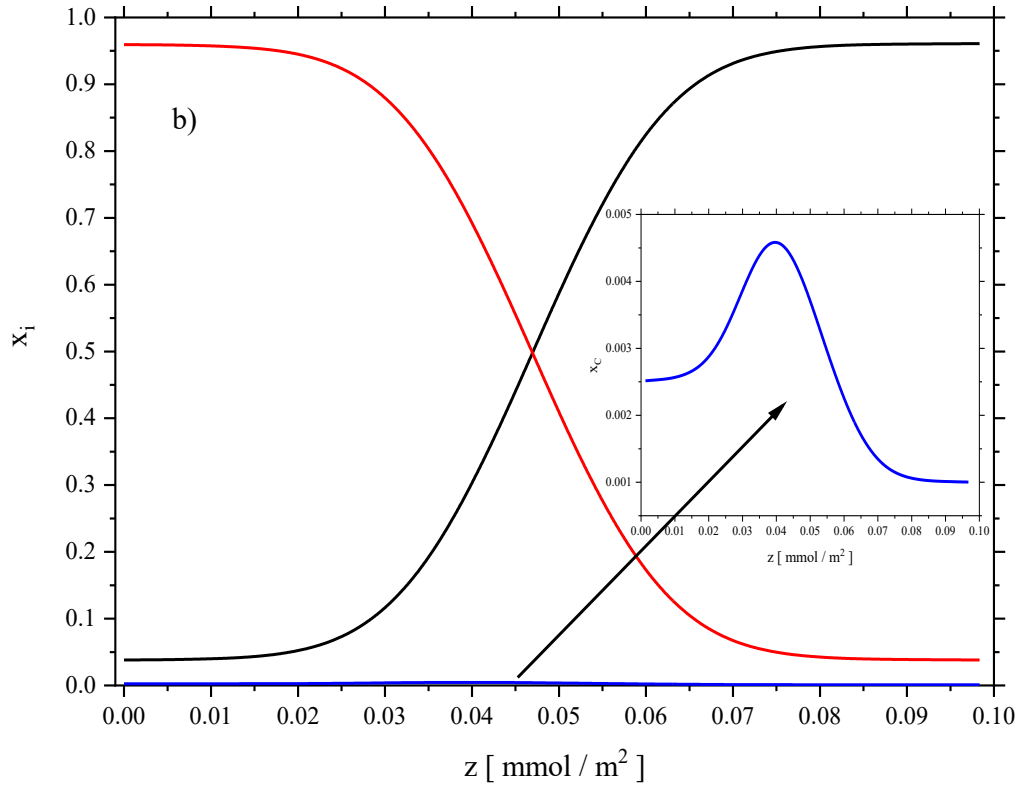

Figure 16. Equilibrium interfacial mole fraction profiles at $t = 0$ for components A (black line), B (red line) and C (blue line) at infinite dilution of component C, calculated by eq. (116) and eq. (119), in combination with eq. (101) by using $A_{AB} = 3.5$ and for different values of A_{AC} and A_{BC} (a) $A_{AC} = 0$, $A_{BC} = 1$ and b) $A_{AC} = 1$, $A_{BC} = 0$) at $T = 298.15$ K and $\kappa_{AB} = 12 \cdot 10^{-7} \frac{\text{J·mol}}{\text{m}^4}$. The inserted figures show the mole fraction profile of component C.

Therefore, the initial bulk phase mole fraction of component C in bulk phase I is higher than its concentration in bulk phase II, because components B and C form ideal mixtures ($A_{BC} = 0$), in contrast to components A and C for which the Porter coefficient A_{AC} is assigned a value of 1 ($A_{AC} = 1$). The relative enrichment of component C in the interface for both cases will thus be less pronounced than its enrichment in Figure 4. Moreover, Figure 15a and Figure 15b as well as Figure 16a and Figure 16b show mirror symmetry due to the Porter equation (eq. (101)) and the applied Porter coefficients. The equilibrium concentration profiles at $t = 0$ (Figure 16) are the ones that will initiate the chemical reaction. They will thus correspond to the initial condition ($t = 0$) required to solve the set of partial differential equations given by eq. (123) and eq. (124).

The mole fraction profiles that result from the occurring chemical reaction will now be considered. Figure 17, Figure 18 and Figure 19 show the predictions at the various equilibration times of the ternary reactive system.

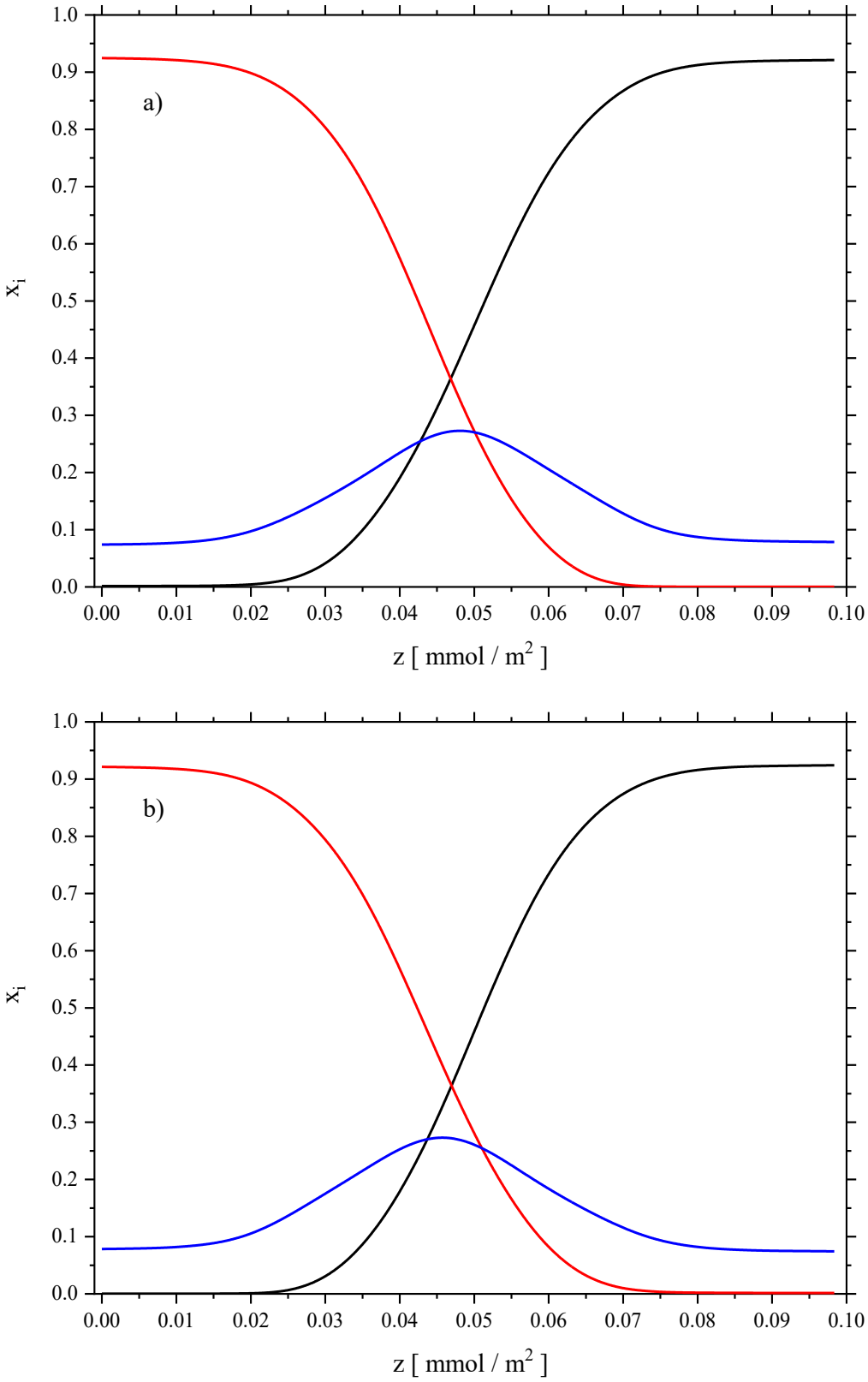

Figure 17. Interfacial mole fraction profiles at $t = 0.25$ s for components A (black line), B (red line), and C (blue line), calculated by solving eq. (123) and eq. (124) at $T = 298.15$ K with

$A_{AB} = 3.5$ and for different values of A_{AC} and A_{BC} (a) $A_{AC} = 0$, $A_{BC} = 1$ and b) $A_{AC} = 1$, $A_{BC} = 0$) in eq. (101), $\kappa_{AB} = 12 \cdot 10^{-7} \frac{\text{J·mol}}{\text{m}^4}$, $k_1 = k_2 = 1\ \text{s}^{-1}$, and $M_{AB} = M_{AC} = M_{BC} = 0$.

Typical reactive features can be again observed in Figure 17, Figure 18 and Figure 19. Concerning the case in which $A_{AC} = 0$ and $A_{BC} = 1$, the chemical reaction reaches chemical equilibrium first in bulk phase II at approximately $t = 0.25$ s, then in bulk phase I at approximately $t = 0.34$ s, and lastly at the interface between them after approximately 2.55 s have elapsed since the chemical reaction started. The interfacial mole fraction profiles that correspond to these three equilibrium system states are shown in Figure 17a, Figure 18a, and Figure 19a, respectively. The reaction will not reach equilibrium in both liquid bulk phases at the same time anymore, in contrast to the predictions made in subsubchapter 4.1.1, because the symmetry is now broken and, given that components A and C form ideal mixtures and the initial bulk phase concentration of component C in bulk phase II is higher than its concentration in bulk phase I, the reaction will thus reach equilibrium first in bulk phase II, then in bulk phase I. The same observations also apply to the second modeling case in which $A_{AC} = 1$ and $A_{BC} = 0$, but the bulk phases are now interchanged, given the mirror symmetry discussed above.

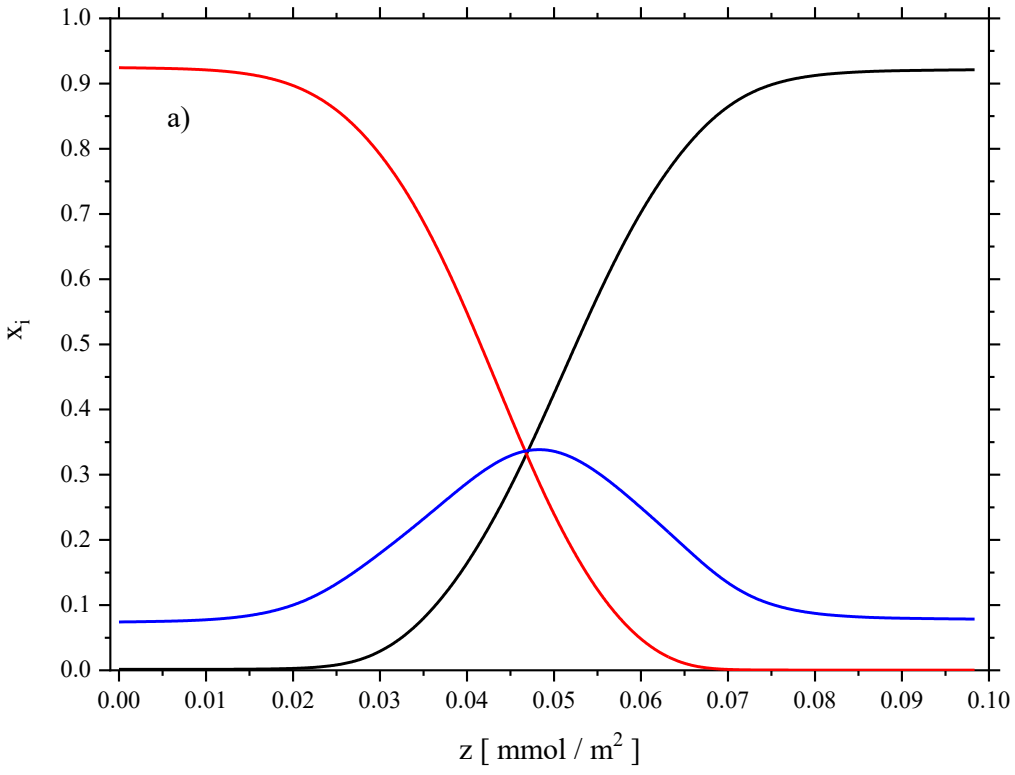

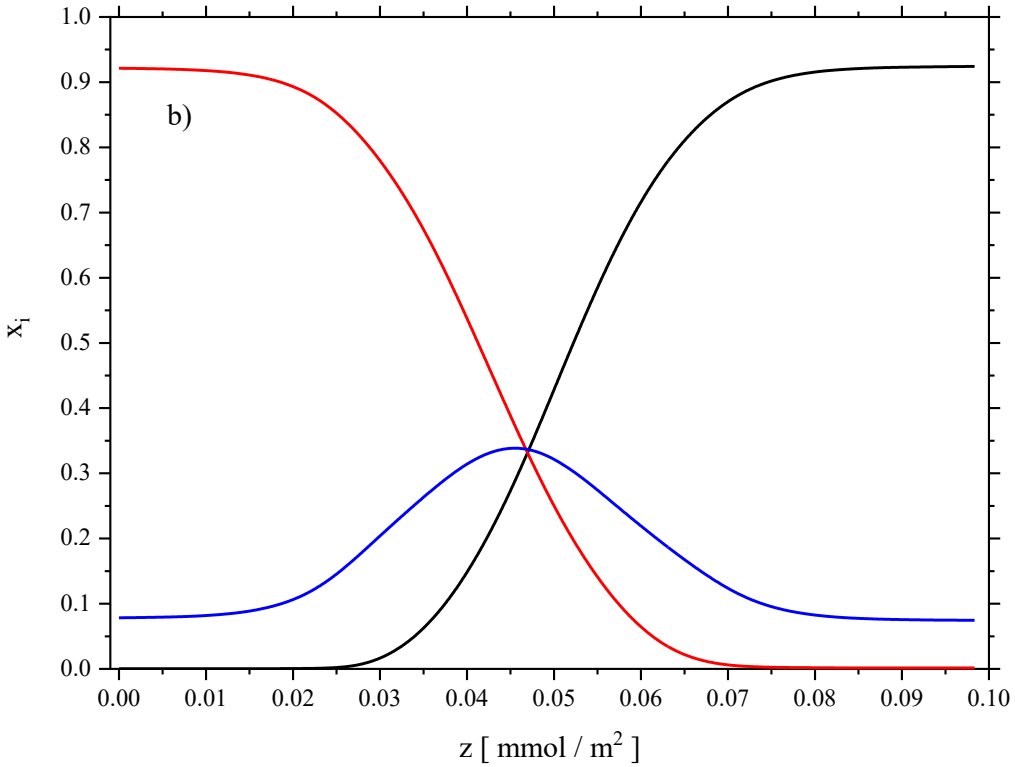

Figure 18. Interfacial mole fraction profiles at $t = 0.34$ s for components A (black line), B (red line), and C (blue line), calculated by solving eq. (123) and eq. (124) at $T = 298.15$ K with $A_{AB} = 3.5$ and for different values of A_{AC} and A_{BC} (a) $A_{AC} = 0$, $A_{BC} = 1$ and b) $A_{AC} = 1$, $A_{BC} = 0$) in eq. (101), $\kappa_{AB} = 12 \cdot 10^{-7} \frac{\text{J·mol}}{\text{m}^4}$, $k_1 = k_2 = 1\ \text{s}^{-1}$, and $M_{AB} = M_{AC} = M_{BC} = 0$.

Hence, the chemical reaction reaches chemical equilibrium first in bulk phase I at approximately $t = 0.25$ s, then in bulk phase II at approximately $t = 0.34$ s, and lastly at the interface between them at approximately $t = 2.55$ s. The corresponding interfacial mole fraction profiles are shown in Figure 17b, Figure 18b and Figure 19b, respectively, and are symmetric to those found in Figure 17a, Figure 18a and Figure 19a, respectively. In addition, and concerning both modeling cases, the reaction educts A and B have progressively vanished at the interface and their mole fractions are taking a value of nearly 0 across a big portion of the interfacial layer between both liquid bulk phases I and II, as can be seen in Figure 17, Figure 18 and Figure 19.

The stationary state, which the system evolved into, more precisely the stationary spatial distribution of the mole fractions of all three components in Figure 19, will now be closely investigated.

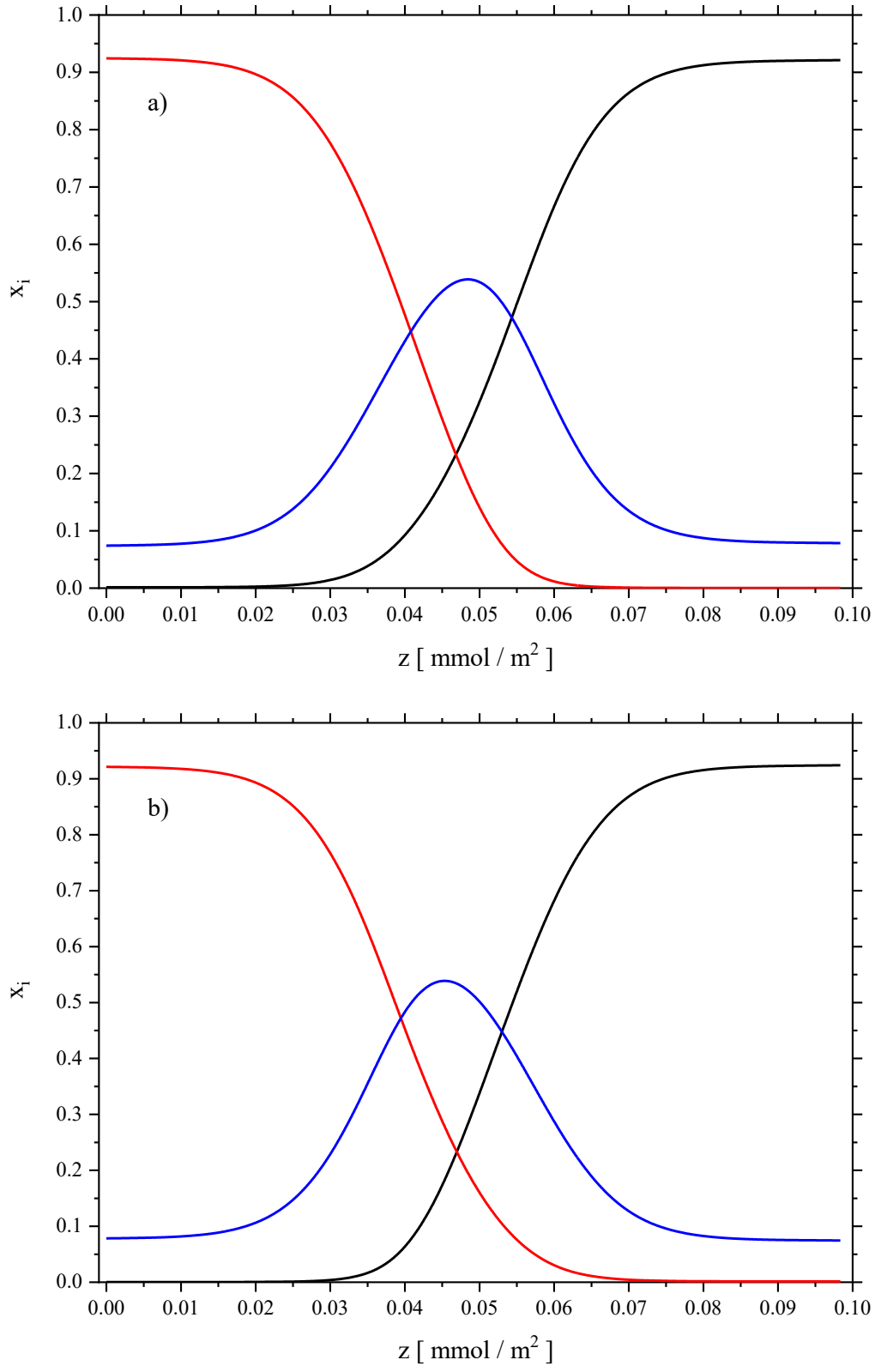

Figure 19. Interfacial mole fraction profiles at $t = 2.55$ s for components A (black line), B (red line), and C (blue line), calculated by solving eq. (123) and eq. (124) at $T = 298.15$ K with

$A_{AB} = 3.5$ and for different values of A_{AC} and A_{BC} (a) $A_{AC} = 0$, $A_{BC} = 1$ and b) $A_{AC} = 1$, $A_{BC} = 0$) in eq. (101), $\kappa_{AB} = 12 \cdot 10^{-7} \frac{\text{J·mol}}{\text{m}^4}$, $k_1 = k_2 = 1\ \text{s}^{-1}$, and $M_{AB} = M_{AC} = M_{BC} = 0$.

Figure 19a shows that the maximum in the interfacial mole fraction profile of product C is not found at the center of the interfacial layer, as predicted in subsubchapter 4.1.1, but is now shifted towards bulk phase II. This is exactly what can be expected, given that both components A and C form ideal mixtures, in contrast to components B and C ($A_{AC} = 0$, $A_{BC} = 1$). Therefore, a higher production of C, and consequently a bigger consumption of educts A and B, will be observed in bulk phase II as well as in the interfacial region close to it, compared to bulk phase I and the interfacial region adjacent to it, in which a lower production of C, and thus a smaller consumption of educts A and B, will be observed. Furthermore, and due to the mirror symmetry incorporated by the model examples, Figure 19b shows that the highest product actual yield has been shifted towards bulk phase I, because both components B and C form ideal mixtures, in contrast to A and C ($A_{AC} = 1$, $A_{BC} = 0$). Hence, a higher production of C, and thus a bigger consumption of educts A and B, will be predicted in bulk phase I as well as in the interfacial domain close to it, compared to bulk phase II and the interfacial region adjacent to it.

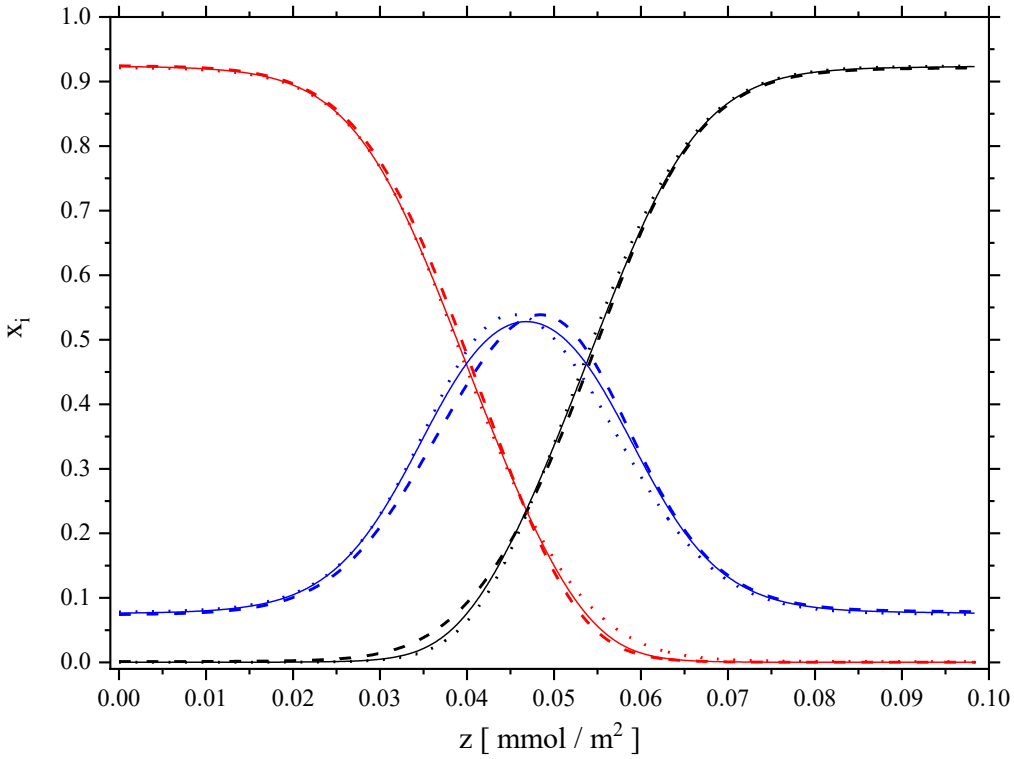

Figure 20. Interfacial mole fraction profiles for components A (black line), B (red line), and C (blue line), calculated by solving eq. (123) and eq. (124) at $T = 298.15$ K with $A_{AB} = 3.5$, for

different values of A_{AC} and A_{BC} in eq. (101), and at different times (solid line: $A_{AC} = 0$, $A_{BC} = 0$, $t = 2.4$ s; dashed line: $A_{AC} = 0$, $A_{BC} = 1$, $t = 2.55$ s; and dotted line: $A_{AC} = 1$, $A_{BC} = 0$, $t = 2.55$ s), with $\kappa_{AB} = 12 \cdot 10^{-7}\ \frac{\text{J·mol}}{\text{m}^4}$, $k_1 = k_2 = 1\ \text{s}^{-1}$, and $M_{AB} = M_{AC} = M_{BC} = 0$.

The reactive behavior and the corresponding results discussed above can also be clearly deduced from Figure 20 and Figure 21 by additionally plotting the interfacial mole fraction profiles of all three components and of component C, particularly, for the perfectly symmetrical case ($A_{AC} = 0$, $A_{BC} = 0$) of subsubchapter 4.1.1 at $t = 2.4$ s, at which the overall chemical equilibrium has been reached. These concentration profiles can thus be used as a reference for evaluating the observed differences in production of C and consumption of A and B between bulk phase I with the interfacial layer close to it, and bulk phase II with its interfacial region, and for both modeling cases investigated above.

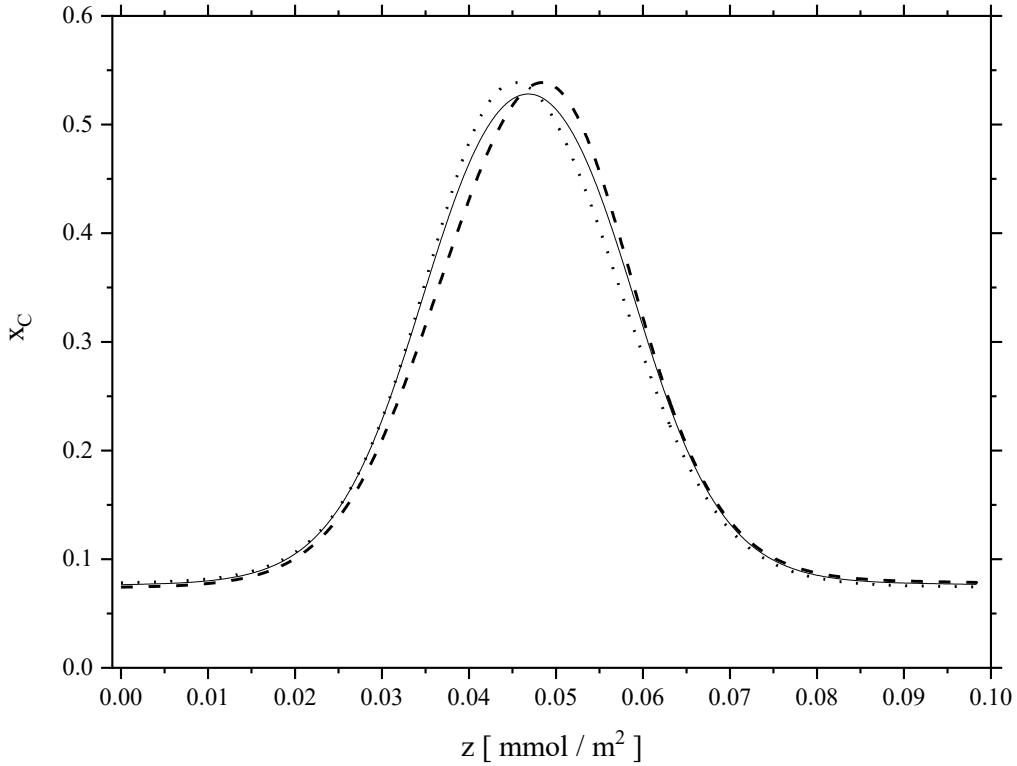

Figure 21. Interfacial mole fraction profiles for component C, calculated by solving eq. (123) and eq. (124) at $T = 298.15$ K with $A_{AB} = 3.5$, for different values of A_{AC} and A_{BC} in eq. (101), and at different times (solid line: $A_{AC} = 0$, $A_{BC} = 0$, $t = 2.4$ s; dashed line: $A_{AC} = 0$, $A_{BC} = 1$, $t = 2.55$ s; and dotted line: $A_{AC} = 1$, $A_{BC} = 0$, $t = 2.55$ s), with $\kappa_{AB} = 12 \cdot 10^{-7}\ \frac{\text{J·mol}}{\text{m}^4}$, $k_1 = k_2 = 1\ \text{s}^{-1}$, and $M_{AB} = M_{AC} = M_{BC} = 0$.

4.1.3 Impact of the reaction rate coefficients*

The following subsubchapter deals with model calculations and numerical solutions of the basic system given by eq. (123) and eq. (124), in which the values of the reaction rate coefficients will be varied in order to study their impact on the temporal evolution of the ternary reactive mixture, by comparing the obtained results and predictions with the standard example of subsubchapter 4.1.1. The initial system state at time $t = 0$ will again be the liquid-liquid phase equilibrium state (LLE) at infinite dilution of component C, at which no chemical reaction will take place. A thought experiment, in which a catalyst is added into the system to speed up the chemical reaction, will then be considered.

The impact of both reaction rate coefficients k_1 and k_2 on the temporal evolution of the reactive ternary system will be studied. Therefore, the Porter coefficients and the influence parameter of the binary subsystem A-B will be assigned the same values that have been assigned to them in subsubchapter 4.1.1, thus $A_{AB} = 3.5$, $A_{AC} = A_{BC} = 0$, and $\kappa_{AB} = 12 \cdot 10^{-7}\ \frac{\mathrm{J \cdot mol}}{\mathrm{m^4}}$.

Two modeling cases will be studied: the one in which the reaction rate coefficient of the forward chemical reaction k_1 is bigger than the one corresponding to the backward reaction k_2 ($k_1 = 1\ \mathrm{s^{-1}}$, $k_2 = 0.5\ \mathrm{s^{-1}}$), and the opposing case in which the reaction rate coefficient of the backward chemical reaction is bigger than the one related to the forward reaction ($k_1 = 0.5\ \mathrm{s^{-1}}$, $k_2 = 1\ \mathrm{s^{-1}}$). The chemical equilibrium constant given by eq. (126) will thus have a value of $K = 2$ for the former case, and $K = 0.5$ for the latter one. It is also worthwhile to mention that, for both reactive modeling cases, instantaneous reaction rates have been accounted for, and diffusive mass transfer in the considered reactive system can thus be neglected.

The ternary phase diagram as well as the equilibrium interfacial concentration profiles corresponding to the initial state ($t = 0$) of both involved mixtures are identical to the ones calculated in subsubchapter 4.1.1, and can be found in Figure 2 and Figure 4, respectively. The equilibrium concentration profiles at $t = 0$, shown in Figure 4, correspond to the initial condition required to solve the set of partial differential equations given by eq. (123) and eq. (124).

* Taken from [112]

The reaction dynamics will be investigated, and after approximately 0.21 s have elapsed since the chemical reaction started at $t = 0$, the reaction related to the modeling case in which $k_1 = 1\ \mathrm{s}^{-1}$ and $k_2 = 0.5\ \mathrm{s}^{-1}$ will reach chemical equilibrium in both bulk phases I and II. If the second modeling case is considered, this bulk phase equilibrium state will be reached at approximately $t = 0.58$ s. The interfacial mole fraction profiles of all three components corresponding to both intermediate equilibrium system states are found in Figure 22a ($k_1 = 1\ \mathrm{s}^{-1}$, $k_2 = 0.5\ \mathrm{s}^{-1}$) and Figure 22b ($k_1 = 0.5\ \mathrm{s}^{-1}$, $k_2 = 1\ \mathrm{s}^{-1}$), respectively. In addition, and regarding both studied reactive cases, the chemical reaction reaches equilibrium in both liquid bulk phases at the same time, given the symmetry incorporated in eq. (101) with $A_{AC} = A_{BC} = 0$.

The subsequent evolution of both systems will lead to the final overall equilibrium states at approximately $t = 3.5$ s if $k_1 = 1\ \mathrm{s}^{-1}$ and $k_2 = 0.5\ \mathrm{s}^{-1}$, and at approximately $t = 3$ s if $k_1 = 0.5\ \mathrm{s}^{-1}$ and $k_2 = 1\ \mathrm{s}^{-1}$, including the interface. Both systems evolved into stationary states, and the stationary spatial distributions of the mole fractions corresponding to these final system states are shown in Figure 23a ($k_1 = 1\ \mathrm{s}^{-1}$, $k_2 = 0.5\ \mathrm{s}^{-1}$) and Figure 23b ($k_1 = 0.5\ \mathrm{s}^{-1}$, $k_2 = 1\ \mathrm{s}^{-1}$), from which the equilibrium interfacial and bulk mole fractions can be obtained.

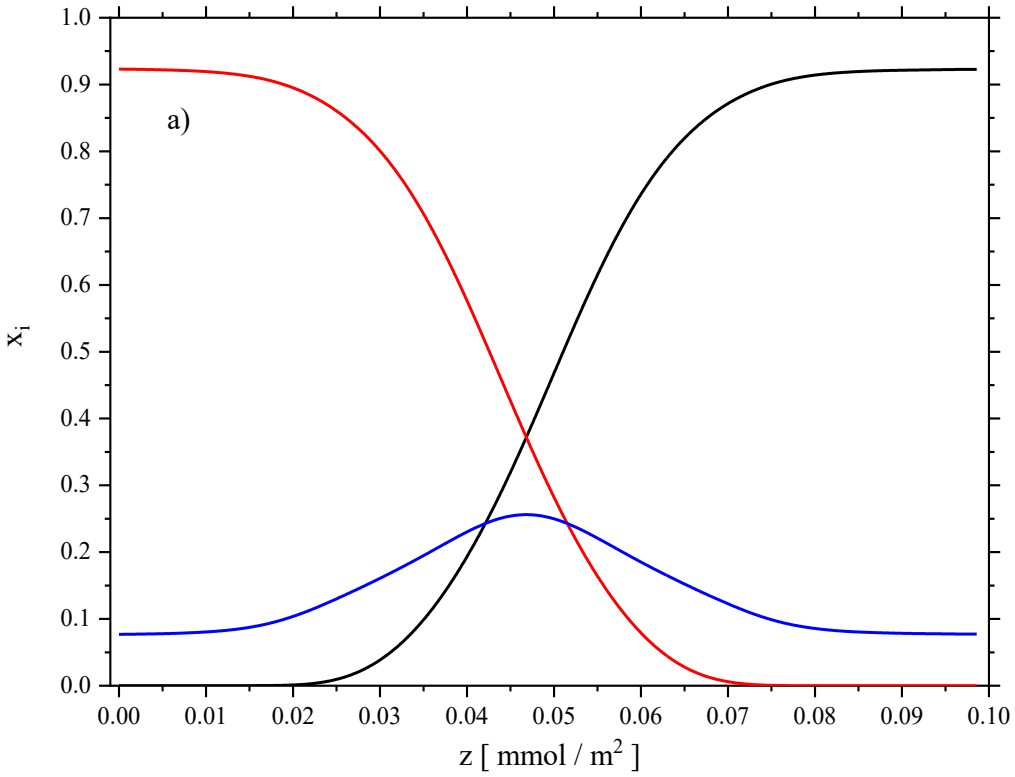

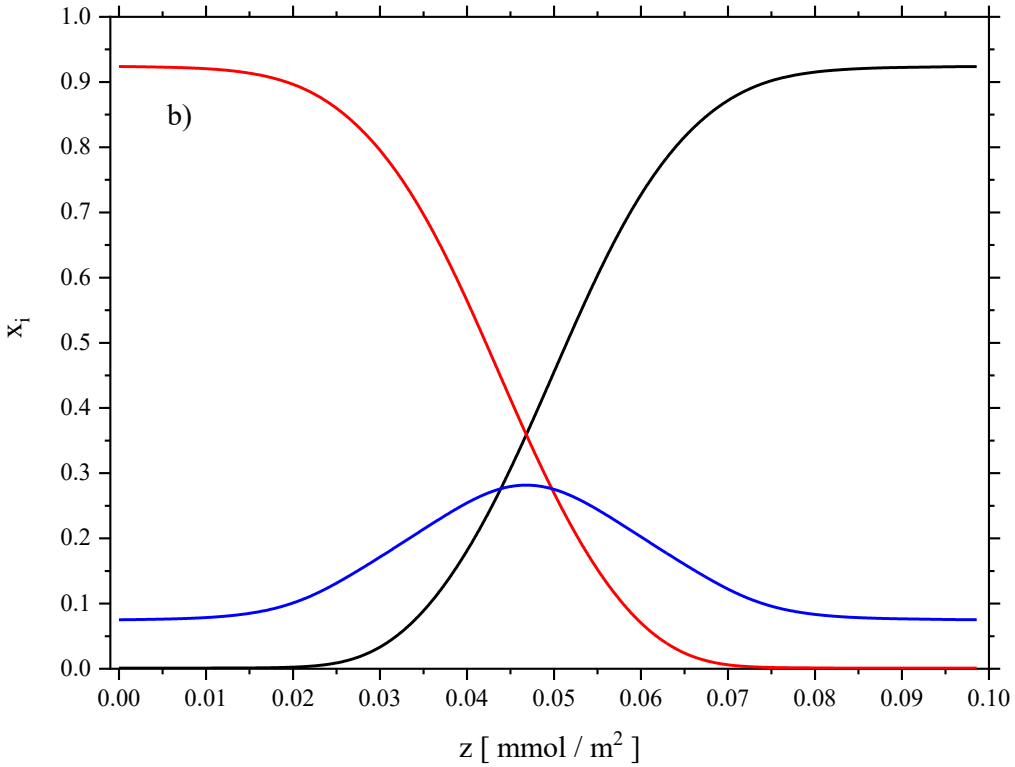

Figure 22. Interfacial mole fraction profiles for components A (black line), B (red line), and C (blue line), calculated by solving eq. (123) and eq. (124) at $T = 298.15$ K with $A_{AB} = 3.5$ and $A_{AC} = A_{BC} = 0$ in eq. (101), $\kappa_{AB} = 12 \cdot 10^{-7} \frac{\text{J·mol}}{\text{m}^4}$, for different values of k_1 and k_2 and at different times (a) $k_1 = 1\ \text{s}^{-1}$, $k_2 = 0.5\ \text{s}^{-1}$, $t = 0.21$ s and b) $k_1 = 0.5\ \text{s}^{-1}$, $k_2 = 1\ \text{s}^{-1}$, $t = 0.58$ s), and $M_{AB} = M_{AC} = M_{BC} = 0$.

At both time steps, namely at $t = 3.5$ s for the case in which $k_1 = 1\ \text{s}^{-1}$, $k_2 = 0.5\ \text{s}^{-1}$, and at $t = 3$ s for the case in which $k_1 = 0.5\ \text{s}^{-1}$, $k_2 = 1\ \text{s}^{-1}$, the final state will be such that the ratio of the activity of the product to the activities of the educts, all activities raised to the power of the absolute value of the corresponding stoichiometric coefficients given by eq. (126), will take a value of 2 for the former case and 0.5 for the latter case, and at every point of the grid located inside the interface, both values having already been reached in both liquid bulk phases at $t = 0.21$ s ($k_1 = 1\ \text{s}^{-1}$, $k_2 = 0.5\ \text{s}^{-1}$) and $t = 0.58$ s ($k_1 = 0.5\ \text{s}^{-1}$, $k_2 = 1\ \text{s}^{-1}$), respectively.

The differences between these calculations and the predictions made in subsubchapter 4.1.1, in which the modeling case characterized by both reaction rate coefficients having equal values of $k_1 = k_2 = 1\ \text{s}^{-1}$ is studied, will now be discussed and analyzed. Therefore, the predicted interfacial concentration profiles of all three components and of the reaction product C, specifically, will be plotted at the overall chemical equilibrium state, for all three modeling cases.

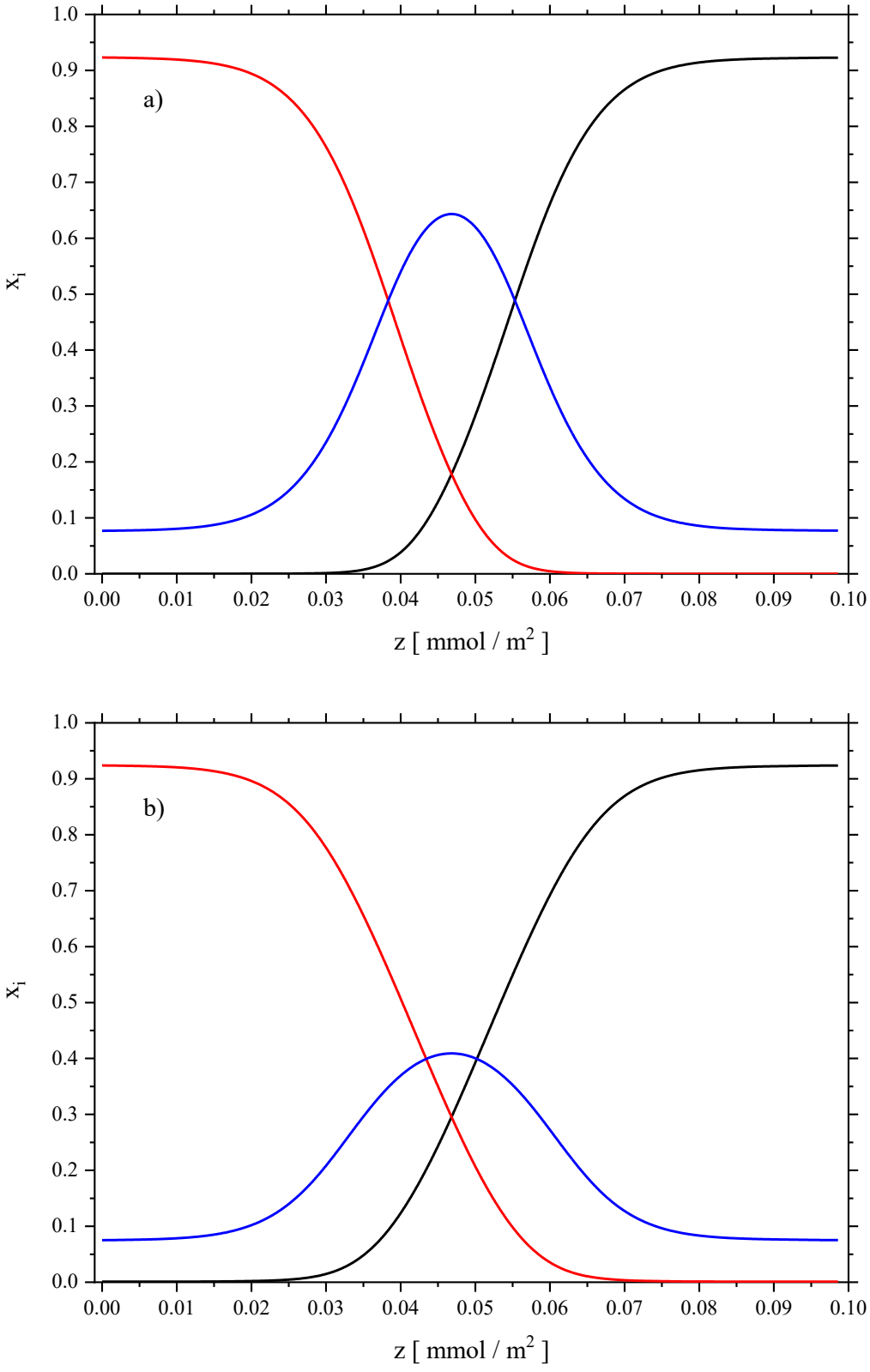

Figure 23. Interfacial mole fraction profiles for components A (black line), B (red line), and C (blue line), calculated by solving eq. (123) and eq. (124) at $T = 298.15$ K with $A_{AB} = 3.5$ and

$A_{AC} = A_{BC} = 0$ in eq. (101), $\kappa_{AB} = 12 \cdot 10^{-7} \frac{\text{J·mol}}{\text{m}^4}$, for different values of k_1 and k_2 and at different times (a) $k_1 = 1\ \text{s}^{-1}$, $k_2 = 0.5\ \text{s}^{-1}$, $t = 3.5\ \text{s}$ and b) $k_1 = 0.5\ \text{s}^{-1}$, $k_2 = 1\ \text{s}^{-1}$, $t = 3\ \text{s}$), and $M_{AB} = M_{AC} = M_{BC} = 0$.

The results are shown in Figure 24 for all three components A, B and C, and Figure 25 for component C. As was also deduced in subsubchapter 4.1.1, the highest actual yield of reaction product C is found at the center of the interface, while the lowest one will be in both bulk phases I and II, illustrated by minima in the mole fraction profiles of component C on the left-hand and the right-hand sides of Figure 25. However, and compared to the predictions and results made in subsubchapter 4.1.1, a higher production of product C, and consequently a higher consumption of both educts A and B, are observed not only in both liquid bulk phases but also at the interface between them for the modeling case in which $k_1 = 1\ \text{s}^{-1}$ and $k_2 = 0.5\ \text{s}^{-1}$.

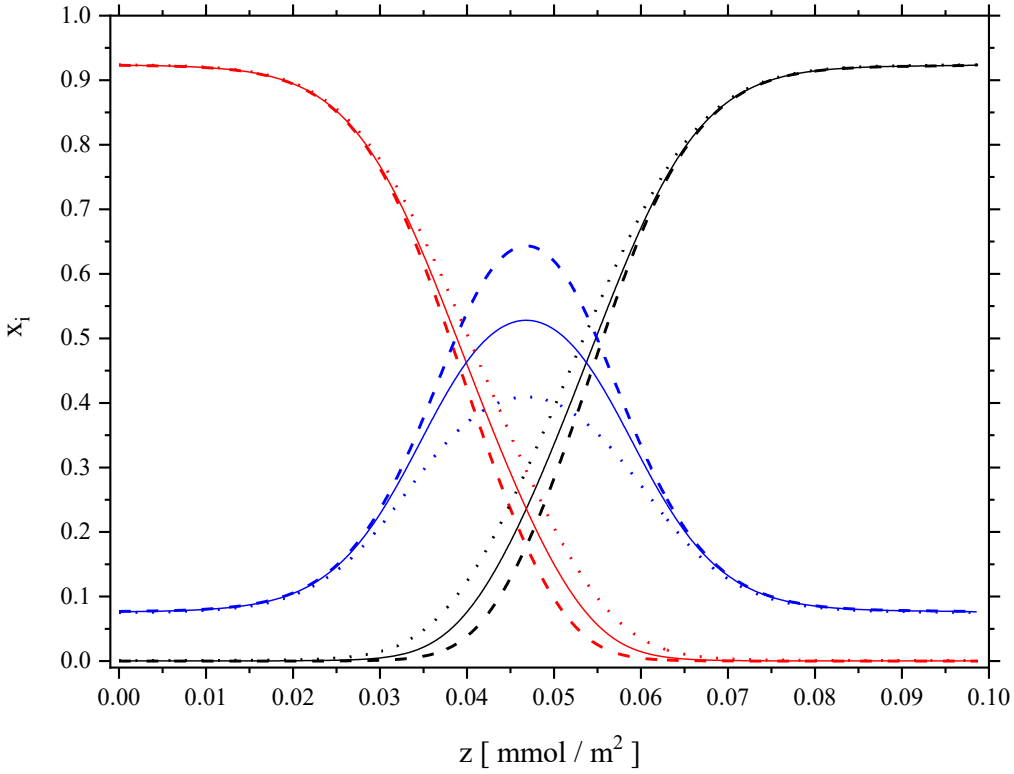

Figure 24. Interfacial mole fraction profiles for components A (black line), B (red line), and C (blue line), calculated by solving eq. (123) and eq. (124) at $T = 298.15$ K with $A_{AB} = 3.5$ and $A_{AC} = A_{BC} = 0$ in eq. (101), $\kappa_{AB} = 12 \cdot 10^{-7} \frac{\text{J·mol}}{\text{m}^4}$, for different values of k_1 and k_2 and at different times (solid line: $k_1 = k_2 = 1\ \text{s}^{-1}$, $t = 2.4$ s; dashed line: $k_1 = 1\ \text{s}^{-1}$, $k_2 = 0.5\ \text{s}^{-1}$, $t = 3.5$ s; and dotted line: $k_1 = 0.5\ \text{s}^{-1}$, $k_2 = 1\ \text{s}^{-1}$, $t = 3$ s), and $M_{AB} = M_{AC} = M_{BC} = 0$.

Furthermore, the opposite effect can be observed for the second modeling case in which $k_1 = 0.5\ \mathrm{s}^{-1}$ and $k_2 = 1\ \mathrm{s}^{-1}$. Hence, a smaller production of C, and thus a smaller consumption of A and B, are observed not only in both bulk phases but also at the interface between them, compared to the calculations made in subsubchapter 4.1.1. This is exactly what can be expected. It is a very interesting finding and obviously results from the chemical equilibrium which has now been shifted towards product C in eq. (97) for the former case ($K = 2$), and towards educts A and B in eq. (97) for the latter case ($K = 0.5$), compared to the chemical equilibrium state assumed in subsubchapter 4.1.1 ($K = 1$).

It is also important to mention that the observed differences are much more pronounced in the interfacial layer than the ones in both bulk phases I and II, given that the initial bulk phase mole fractions of educts A and B are close to 0 or 1 for all three modeling cases, and that the chemical reaction will thus totally consume one of its educts there.

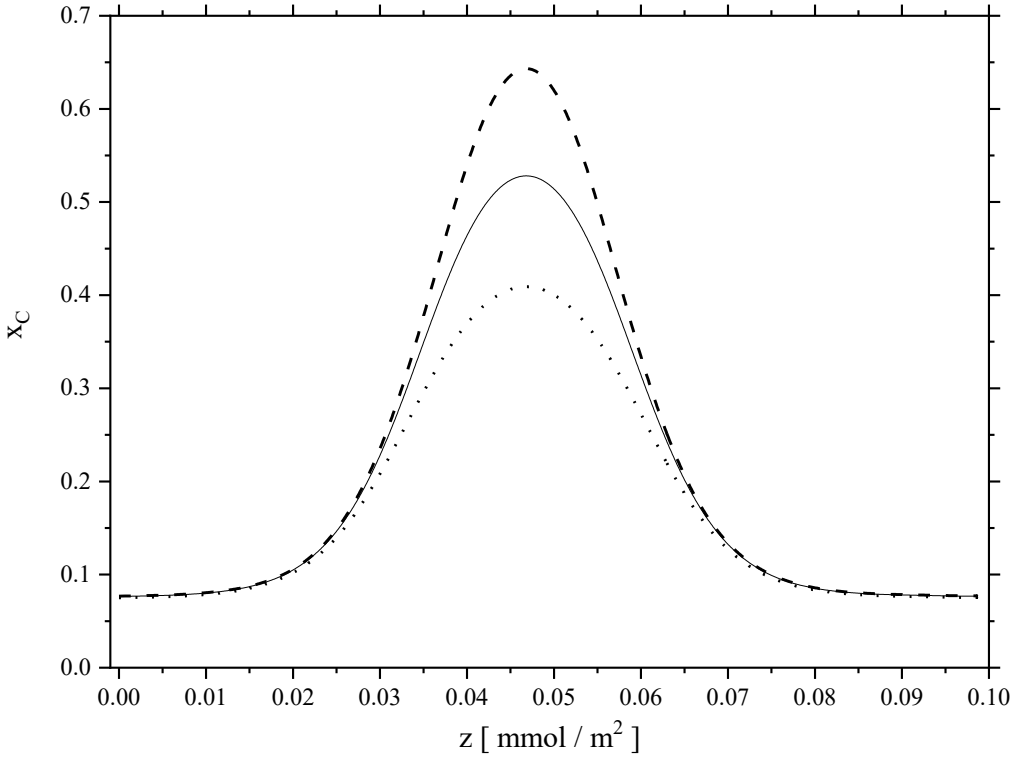

Figure 25. Interfacial mole fraction profiles for component C, calculated by solving eq. (123) and eq. (124) at $T = 298.15$ K with $A_{AB} = 3.5$ and $A_{AC} = A_{BC} = 0$ in eq. (101), $\kappa_{AB} = 12 \cdot 10^{-7}\ \frac{\mathrm{J \cdot mol}}{\mathrm{m^4}}$, for different values of k_1 and k_2 and at different times (solid line: $k_1 = k_2 = 1\ \mathrm{s}^{-1}$, $t = 2.4$ s; dashed line: $k_1 = 1\ \mathrm{s}^{-1}$, $k_2 = 0.5\ \mathrm{s}^{-1}$, $t = 3.5$ s; and dotted line: $k_1 = 0.5\ \mathrm{s}^{-1}$, $k_2 = 1\ \mathrm{s}^{-1}$, $t = 3$ s), and $M_{AB} = M_{AC} = M_{BC} = 0$.

4.1.4 Impact of the influence parameter*

Finally, in this subsubchapter, model calculations and numerical solutions of the basic system given by eq. (123) and eq. (124) will be provided, in which the value of the influence parameter of the binary subsystem A-B will be varied in order to study its impact on the temporal evolution of the ternary reacting mixture, by comparing the obtained predictions with the standard example of subsubchapter 4.1.1. The initial system state at time $t = 0$ will again be the liquid-liquid phase equilibrium state (LLE) at infinite dilution of component C, at which no chemical reaction takes place. Again, a thought experiment, in which a catalyst is added into the mixture in order to speed up the reaction, will then be considered.

The impact of the influence parameter κ_{AB} of the binary mixture A-B on the dynamics of the reactive ternary system will be studied. Hence, the Porter coefficients and the reaction rate coefficients will be assigned the same values that have been assigned to them in subsubchapter 4.1.1, thus $A_{AB} = 3.5$, $A_{AC} = A_{BC} = 0$, and $k_1 = k_2 = 1\ \mathrm{s}^{-1}$. The value of κ_{AB} will be increased by a factor of 10^4, and thus, κ_{AB} will be assigned the value of $\kappa_{AB} = 12 \cdot 10^{-3}\ \frac{\mathrm{J \cdot mol}}{\mathrm{m^4}}$.

The phase diagram of the ternary mixture is identical to the one calculated in subsubchapter 4.1.1 and can be found in Figure 2. Moreover, the initial equilibrium interfacial concentration profiles of components A, B, and C are calculated by solving eq. (116) in the interface and evaluating the integral in eq. (119), and are shown in Figure 26. It can be deduced that the initial mole fraction profiles are identical to the ones predicted in subsubchapter 4.1.1 (Figure 4). This is due to the assumption given by eq. (115), in which both influence parameters of the ternary mixture have equal values of $\frac{1}{4}\kappa_{AB}$. Therefore, the solutions of the Euler-Lagrange equation (eq. (116)) will not depend on the value of the influence parameter κ_{AB} of the binary mixture A-B, which explains why the interfacial mole fractions in Figure 26 are equal to the ones in Figure 4, in which $\kappa_{AB} = 12 \cdot 10^{-7}\ \frac{\mathrm{J \cdot mol}}{\mathrm{m^4}}$. However, the only difference between both figures is the thickness of the interface, which has now increased by a factor of 10^2, as shown in Figure 26, compared to its thickness in the standard example of subsubchapter 4.1.1 (Figure 4).

* Taken from [112]

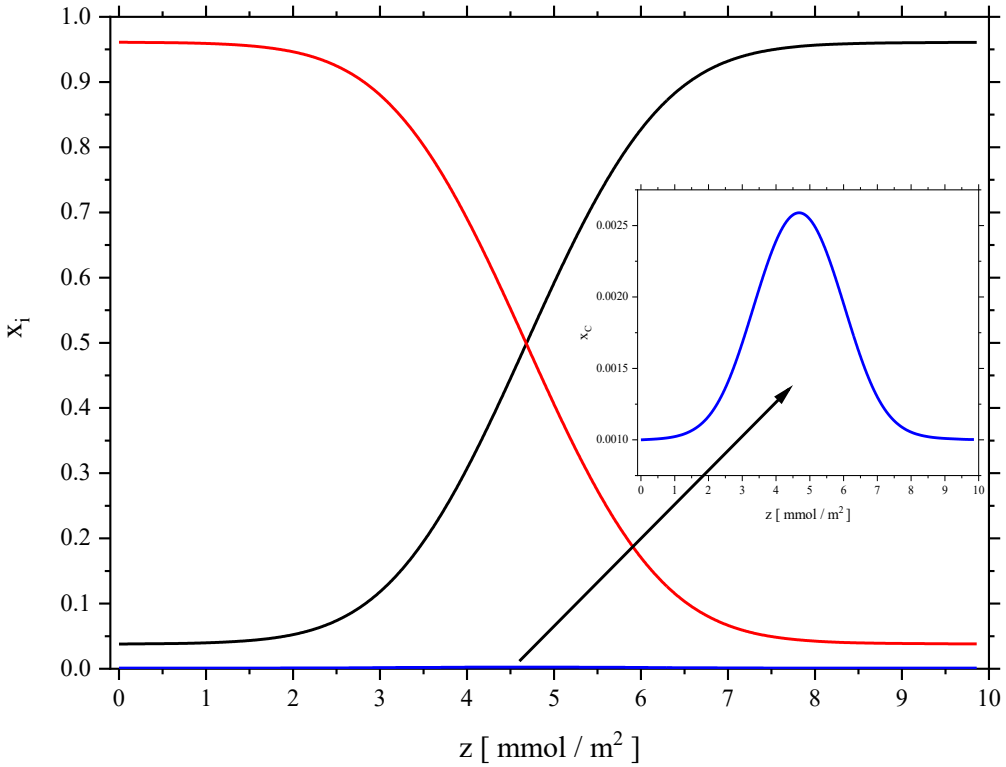

Figure 26. Equilibrium interfacial mole fraction profiles at $t = 0$ for components A (black line), B (red line) and C (blue line) at infinite dilution of component C, calculated by eq. (116) and eq. (119), in combination with eq. (101) by using $A_{AB} = 3.5$ and $A_{AC} = A_{BC} = 0$ at $T = 298.15$ K and $\kappa_{AB} = 12 \cdot 10^{-3} \frac{\text{J·mol}}{\text{m}^4}$. The inserted figure shows the mole fraction profile of component C.

This is exactly what can be expected because the interfacial coordinate z, given by eq. (119), is calculated by an integral of a square root function, and the influence parameter κ_{AB} of the binary subsystem A-B is found in the argument of this square root function. Furthermore, the grand thermodynamic potential $\Delta\Omega$, given by eq. (91) for a ternary mixture, as well as the ratio $\frac{dx_B}{dx_A}$, which are also found in that argument (eq. (119)), will not change, given that the solutions of the Euler-Lagrange equation (eq. (116)) do not depend on the value of κ_{AB}, as discussed above. Consequently, by increasing the value of κ_{AB} by a factor of 10^4, the value of z will increase by a factor of 10^2, compared to its value in subsubchapter 4.1.1. Therefore, the value of κ_{AB} will only have an impact on the thickness of the interface if the Porter coefficients are kept unchanged.

In addition, the equilibrium concentration profiles at $t = 0$, shown in Figure 26, correspond to the initial condition required to solve the set of partial differential equations given by eq. (123)

and eq. (124), with which the dynamics of the reactive system will be studied. The chemical reaction reaches chemical equilibrium in both liquid bulk phases I and II at approximately $t = 0.25$ s, and in the interface between them at approximately $t = 2.4$ s. The interfacial mole fraction profiles corresponding to these two equilibrium states are found in Figure 27a and Figure 27b, respectively. These mole fraction profiles, including the corresponding bulk phase concentrations as well as both equilibration times of the nonuniform system, coincide with the ones predicted in subsubchapter 4.1.1. The only difference between both modeling results is the interfacial thickness, which has now been increased by a factor of 10^2. The explanations concerning these predictions are as follows. By closely examining the argument of the exponential functions in eq. (123) and eq. (124), it is found that an increase or decrease of the influence parameter κ_{AB} will be exactly compensated by the increase or decrease of the spatial gradients of components A and B found in those arguments. This result only holds true if the equilibrium concentration profiles calculated with eq. (119) are taken as initial condition required to solve eq. (123) and eq. (124), because the dependence between the interfacial coordinate z and the influence parameter κ_{AB} discussed above will only be observed in this case.

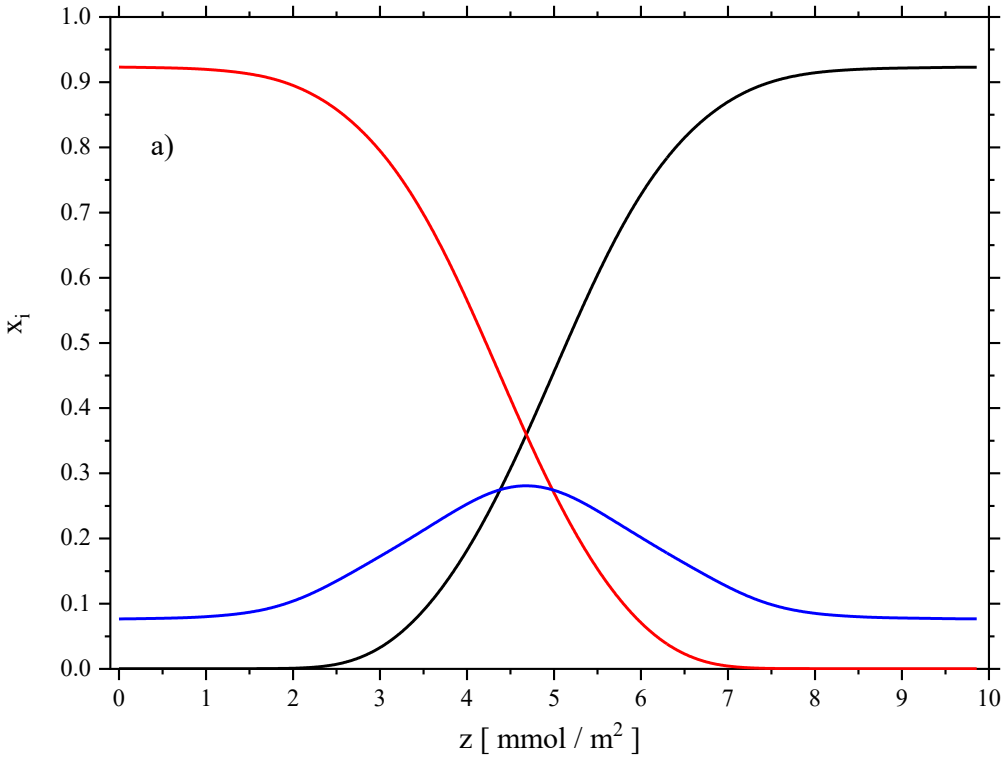

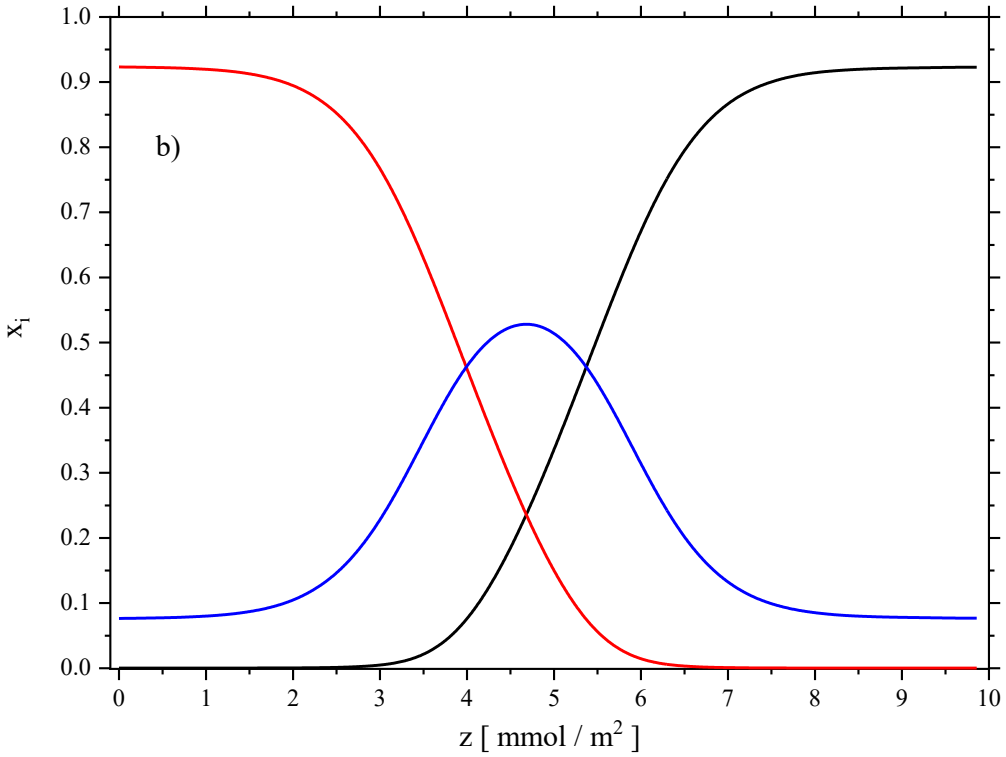

Figure 27. Interfacial mole fraction profiles at two different times (a) $t = 0.25\ \mathrm{s}$ and b) $t = 2.4\ \mathrm{s}$) for components A (black line), B (red line), and C (blue line), calculated by solving eq. (123) and eq. (124) at $T = 298.15\ \mathrm{K}$ with $A_{AB} = 3.5$ and $A_{AC} = A_{BC} = 0$ in eq. (101), $\kappa_{AB} = 12 \cdot 10^{-3}\ \frac{\mathrm{J \cdot mol}}{\mathrm{m^4}}$, $k_1 = k_2 = 1\ \mathrm{s^{-1}}$, and $M_{AB} = M_{AC} = M_{BC} = 0$.

Therefore, and given that the initial bulk phase and interfacial mole fractions of all three components A, B and C at $t = 0$ for both modeling cases ($\kappa_{AB} = 12 \cdot 10^{-3}\ \frac{\mathrm{J \cdot mol}}{\mathrm{m^4}}$ and $\kappa_{AB} = 12 \cdot 10^{-7}\ \frac{\mathrm{J \cdot mol}}{\mathrm{m^4}}$) are identical, the value of κ_{AB} will not affect the temporal evolution of the mole fractions of components A, B and C (eq. (123) and eq. (124)), and thus, it will not influence the dynamics of the reactive heterogeneous system. The value of the influence parameter κ_{AB} will only have an impact on the thickness of the interfacial layer between both liquid bulk phases I and II. These observations and results are only valid for the limiting case of reacting mixtures in which the reaction is much faster than the rate of diffusion, and thus in which the rate of reaction is effectively instantaneous and the diffusive mass transfer across the interface is not considered ($M_{AB} = M_{AC} = M_{BC} = 0$).

4.2 Dynamic modeling of the interfacial properties - Limiting case II*

In subchapter 4.1, reactive nonuniform systems in which the chemical reaction takes place instantaneously, and thus in which the reaction is much faster than the rate of diffusion were investigated. Therefore, the diffusion term was omitted from the component continuity equations. The influence of mobilities and how diffusive transport affects the dynamics of reactive mixtures will be the subject of the current subchapter, in which eq. (123) and eq. (124) are applied to study the second opposing limiting situation, in which the reaction rate is much smaller than the rate of diffusion.

In this subchapter, an exemplary model calculation and numerical solutions of the basic system given by eq. (123) and eq. (124) are provided, which will serve as a proof of concept. In what follows, a second standard model example will be introduced. A three-component mixture made of A, B and C, in which components A and B are practically immiscible and their phase diagram has a large miscibility gap at the assumed constant temperature $T = 298.15\,\mathrm{K}$, will be considered. Hence, and as was assumed in subsubchapter 4.1.1, the Porter coefficient A_{AB} will be assigned the following value of $A_{AB} = 3.5$ in eq. (101). Furthermore, the other two Porter coefficients are set to $A_{AC} = A_{BC} = 0$ so that the binary subsystems A-C as well as B-C will form ideal mixtures.

The corresponding phase diagram of the ternary mixture is identical to the one calculated in subsubchapter 4.1.1 (Figure 2) and is also shown in Figure 28. The initial state of the reactive system will again be defined as the liquid-liquid phase equilibrium state of the ternary system at infinite dilution of component C. Furthermore, the binodal mole fractions of both components A and B in the binary subsystem A-B will be close to 0 or 1 due to the Porter coefficient $A_{AB} = 3.5$ in eq. (101) assumed for the calculation of the phase equilibrium. The symmetrical phase diagram observed in Figure 28 is caused by both binary subsystems A-C and B-C, which form ideal mixtures. In addition, the influence parameter κ_{AB} of the binary subsystem A-B will be assigned a value of $\kappa_{AB} = 12.\,10^{-7}\ \frac{\mathrm{J.mol}}{\mathrm{m^4}}$, similarly to its value in subsubchapter 4.1.1.

* Taken from [102]

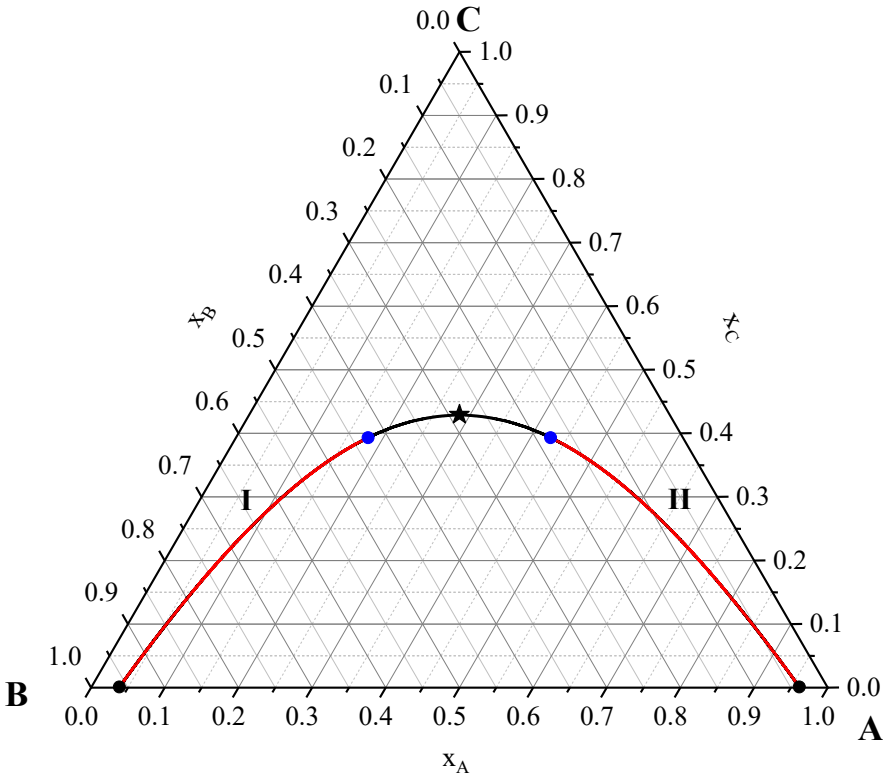

Figure 28. Phase diagram (binodal curve: black line, critical point: star) for the ternary mixture A-B-C at $T = 298.15$ K, calculated with eq. (101) by using $A_{AB} = 3.5$ and $A_{AC} = A_{BC} = 0$. The initial state is indicated by black points, the evolution of the bulk phase mole fractions (reaction path, calculated by solving eq. (123) and eq. (124) at $T = 298.15$ K with $A_{AB} = 3.5$ and $A_{AC} = A_{BC} = 0$ in eq. (101), $\kappa_{AB} = 12 \cdot 10^{-7} \frac{\text{J·mol}}{\text{m}^4}$, $k_1 = 0.5.\,10^{-8}\ \text{s}^{-1}$, $k_2 = 10^{-8}\ \text{s}^{-1}$, and $M_{AB} = M_{AC} = M_{BC} = 10^{-9}\ \frac{\text{mol}^3}{\text{J.m}^4\text{.s}}$) is depicted by red lines, and the final state is represented by blue points.

To account for diffusion rates that are much higher than reaction rates, it will be assumed that the reaction rate coefficients will have values of $k_1 = 0.5.\,10^{-8}\ \text{s}^{-1}$ and $k_2 = 10^{-8}\ \text{s}^{-1}$. The chemical equilibrium coefficient given by eq. (126) thus takes a value of $K = 0.5$. Moreover, the diffusive mobilities will be assigned equal values of $M_{AB} = M_{AC} = M_{BC} = 10^{-9}\ \frac{\text{mol}^3}{\text{J.m}^4\text{.s}}$. Having specified all the required parameters for modeling, the dynamics of the reactive system can now be evaluated by numerically solving eq. (123) and eq. (124).

The initial system state at time $t = 0$ is chosen to be an equilibrated (LLE) mixture of components A, B and C at infinite dilution of component C, as shown by both black points in Figure 28. These two points thus refer to the initial concentrations of bulk phase I and bulk

phase II at $t = 0$. The equilibrium interfacial concentration profiles that correspond to the initial system state at $t = 0$ of the chosen ternary reactive mixture will now be calculated by solving eq. (116) in the interface and then evaluating the integral in eq. (119). The result can be found in subsubchapter 4.1.1 and is shown in Figure 4. These equilibrium concentration profiles correspond to the initial condition ($t = 0$) needed to solve the set of partial differential equations given by eq. (123) and eq. (124).

The reaction dynamics will now be studied and the concentration profiles, $x_i(z,t)$, that result from the temporal evolution of the mole fraction of the various components will be investigated. Figure 29 shows the calculated interfacial mole fraction profiles at different time steps. Exemplary snapshots of the mole fraction distributions for the one-dimensional numerical solution of eq. (123) and eq. (124) at approximately $t = 149$ days and $t = 489$ days are illustrated in Figure 29a and Figure 29c, respectively. In addition, the equilibrium interfacial mole fraction profiles that result from the bulk phase concentrations corresponding to both time steps ($t = 149$ days and $t = 489$ days) are also calculated by solving eq. (116) in the interfacial layer and subsequently evaluating the integral of eq. (119) for both time steps.

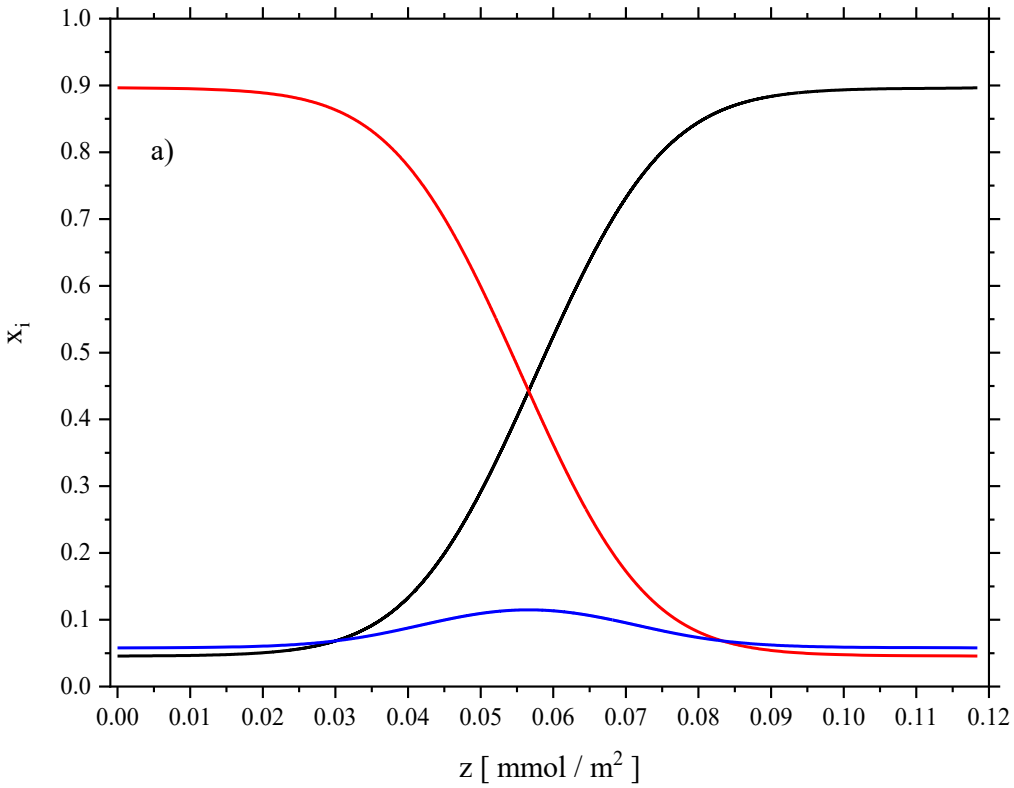

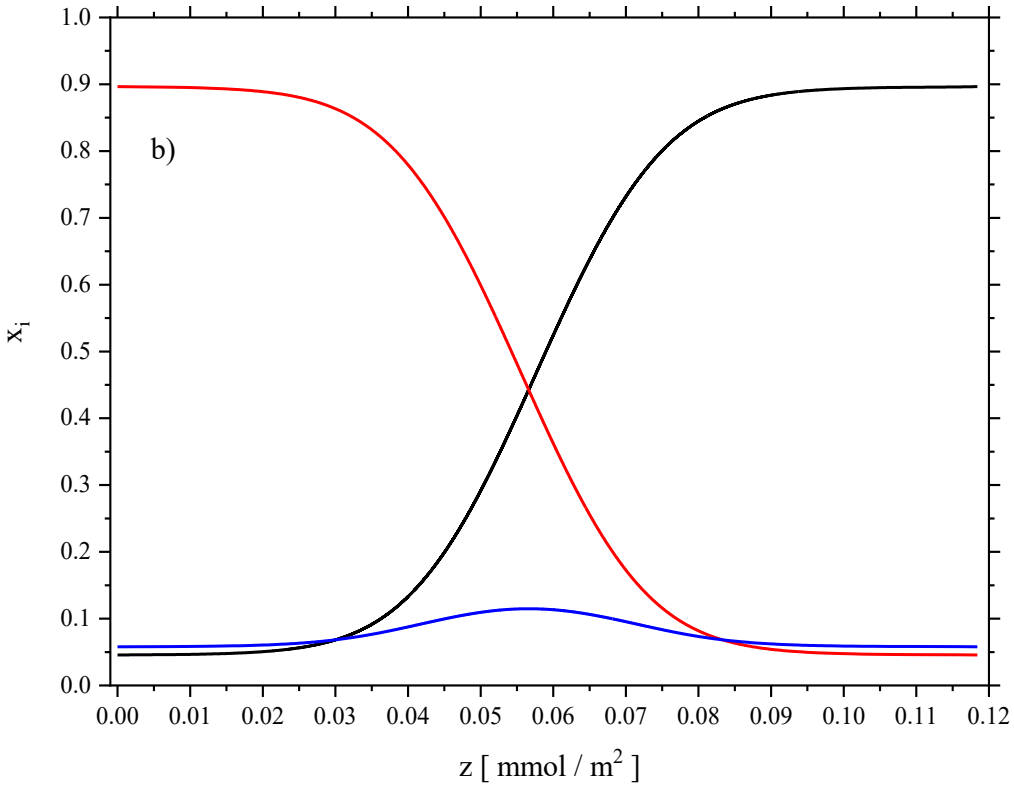
b)
x_i
z [mmol / m^2]

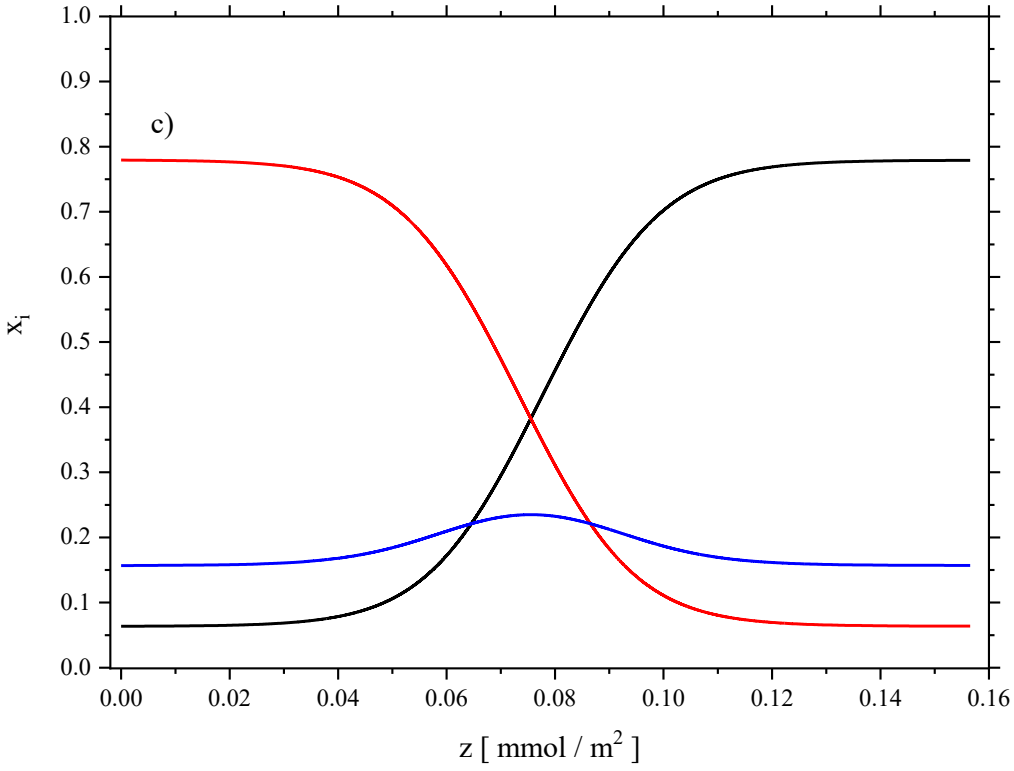
c)
x_i
z [mmol / m^2]

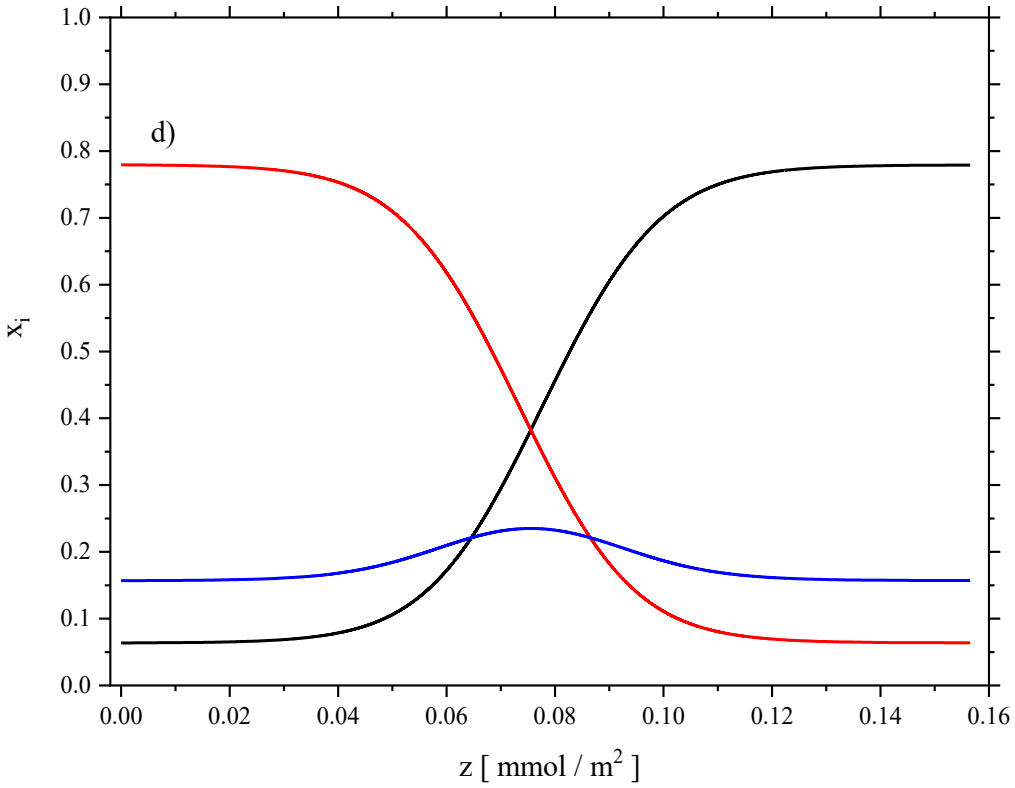

Figure 29. Interfacial mole fraction profiles at different times (a) approximately $t = 149$ days and c) approximately $t = 489$ days) for components A (black line), B (red line), and C (blue line), calculated by solving eq. (123) and eq. (124) at $T = 298.15$ K with $A_{AB} = 3.5$ and $A_{AC} = A_{BC} = 0$ in eq. (101), $\kappa_{AB} = 12 \cdot 10^{-7} \frac{\text{J·mol}}{\text{m}^4}$, $k_1 = 0.5.\,10^{-8}\ \text{s}^{-1}$, $k_2 = 10^{-8}\ \text{s}^{-1}$, and $M_{AB} = M_{AC} = M_{BC} = 10^{-9}\ \frac{\text{mol}^3}{\text{J.m}^4\text{.s}}$. The corresponding equilibrium interfacial mole fraction profiles are calculated by solving eq. (116) and eq. (119), in combination with eq. (101) by using $A_{AB} = 3.5$ and $A_{AC} = A_{BC} = 0$ at $T = 298.15$ K, and $\kappa_{AB} = 12 \cdot 10^{-7} \frac{\text{J·mol}}{\text{m}^4}$ (b) approximately $t = 149$ days and d) approximately $t = 489$ days).

The results for the interfacial concentration profiles at LLE are shown in Figure 29b and Figure 29d for approximately $t = 149$ days and $t = 489$ days, respectively. In other words, Figure 29a (approximately $t = 149$ days) and Figure 29c (approximately $t = 489$ days) are obtained by applying the diffusion term found in eq. (123) and eq. (124), while Figure 29b and Figure 29d are obtained by taking the resulting bulk phase compositions at approximately $t = 149$ days and $t = 489$ days, respectively, from the previous calculation method, and subsequently solving the Euler-Lagrange equation (eq. (116)) in the interface and calculating the equilibrium interfacial concentration profiles (eq. (119)) that correspond to these bulk phase compositions, thus without applying the diffusion term.

It can be deduced from Figure 29 that the interfacial concentration profiles calculated by both aforementioned methods coincide at the corresponding time step. This is a very interesting observation and results from the assumed diffusion rates being much higher than the reaction rates. The diffusion being much faster than the rate of reaction, and by solving the set of partial differential equations (eq. (123) and eq. (124)), the reactive system is thus evolving towards global equilibrium, more precisely towards the chemical equilibrium state, by constantly approaching numerous phase equilibrium system states. This observation can also be deduced from Figure 28. To trace the evolution of the uniform liquid bulk phases, more precisely of the bulk phase concentrations using the Gibbs triangle, the mole fractions of all three components A, B and C in both bulk phases will be permanently evaluated. The result is given by red lines in Figure 28, in which the red line on the left-hand side of the phase diagram corresponds to the evolution of bulk phase I, whereas the red line on the right-hand side of the phase diagram to the evolution of bulk phase II due to chemical reaction. It can be deduced from Figure 28 that both liquid bulk phases are evolving along the binodal curve of the ternary reactive system, and that the evolving bulk phase concentrations are thus equal to the corresponding equilibrium concentrations of the ternary phase diagram. Therefore, the reaction path for both bulk phases coincides with the binodal curve in Figure 28. Conversely, pronounced deviations between reaction path and binodal curve are observed in subchapter 4.1 (e.g., Figure 3), given that the opposite limiting case of the model, in which the rate of reaction is effectively instantaneous and the diffusion rates are negligible, is considered. In that case, the reactive system will evolve towards the chemical equilibrium state without approaching phase equilibrium system states.

An additional exemplary snapshot of the mole fraction distribution of the various components at approximately $t = 1243\ \text{days}$ is illustrated in Figure 30a. The subsequent evolution of the reactive ternary system will lead to the final global equilibrium system state at approximately $t = 4656\ \text{days}$, at which the Gibbs energy of the overall system takes its minimum value, given that both phase and chemical equilibria are simultaneously reached. After approximately $4656\ \text{days}$ have elapsed since the reactive system was in its initial state, the educts and product bulk concentrations become constant, and chemical equilibrium in both bulk phases will be reached, the system having already reached phase equilibrium at each time step. The reactive nonuniform system evolved into a stationary state, and the stationary spatial distribution of the mole fractions corresponding to this final stable system state is shown in Figure 30b.

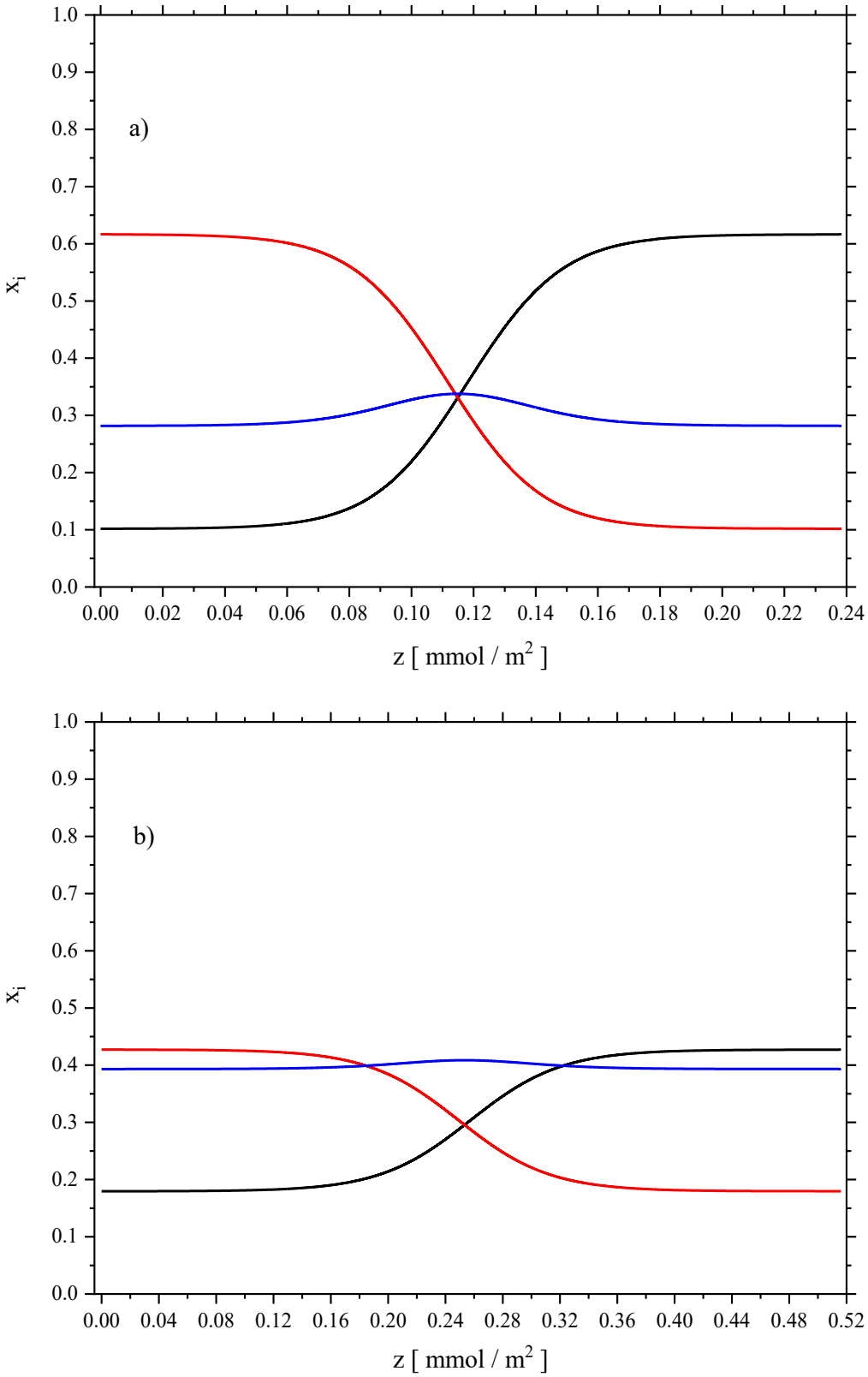

Figure 30. Interfacial mole fraction profiles at different times (a) approximately $t = 1243$ days and b) approximately $t = 4656$ days) for components A (black line), B (red line), and C (blue

line), calculated by solving eq. (123) and eq. (124) at $T = 298.15\,\mathrm{K}$ with $A_{AB} = 3.5$ and $A_{AC} = A_{BC} = 0$ in eq. (101), $\kappa_{AB} = 12 \cdot 10^{-7}\,\frac{\mathrm{J \cdot mol}}{\mathrm{m^4}}$, $k_1 = 0.5.\,10^{-8}\,\mathrm{s^{-1}}$, $k_2 = 10^{-8}\,\mathrm{s^{-1}}$, and $M_{AB} = M_{AC} = M_{BC} = 10^{-9}\,\frac{\mathrm{mol^3}}{\mathrm{J.m^4.s}}$.

Moreover, the equilibrium bulk phase concentrations can also be deduced from Figure 30b. The same state is indicated by two blue points in Figure 28, which refer to the final bulk system state. The corresponding values of the equilibrium mole fractions of components A, B and C in bulk phases I and II in Figure 30b agree with the ones taken from both blue points on the left-hand side and on the right-hand side of the phase diagram in Figure 28, respectively. Furthermore, the chemical reaction reaches chemical equilibrium in both liquid bulk phases at the same time after approximately $4656\,\mathrm{days}$. This can be intuitively explained by closely examining eq. (126). Given that the reactive system is evolving by constantly approaching phase equilibrium states, the chemical potentials, or more precisely the activities (eq. (38)), of each of the components in each of the phases that it is present are thus equal (isoactivity criterion). Therefore, the ratio of the activities given in eq. (126) will have the same value in both liquid bulk phases at each time step of the dynamic evolution, and chemical equilibrium will thus be reached in both bulk phases at the same time, irrespective of the symmetry of the system. Returning to both bulk phases, and at approximately $t = 4656\,\mathrm{days}$, the final bulk system state will be such that the ratio of the activity of the product to the activities of the educts, all activities raised to the power of the absolute value of the corresponding stoichiometric coefficients, which is also the equilibrium coefficient expression given by eq. (126), will take a value of 0.5 in bulk phases I and II. Hence, chemical equilibrium has been reached in both coexisting liquid bulk phases. In addition, Figure 29 and Figure 30 show that, upon reaction, the thickness of the interface is increasing, the relative enrichment of component C in the interface is decreasing, and the values of the mole fractions of each of the components A, B and C in bulk phase I are approaching their counterparts in bulk phase II. This is obviously due to the production of the solubilizer C and to the reactive system thus approaching, upon reaction and through numerous phase equilibrium system states, the critical point of the ternary mixture, as depicted in Figure 28.

The evolution of the composition of both liquid bulk phases over time is depicted in Figure 31a and Figure 31b. The former shows the change in mole fraction of components A, B and C in bulk phase I, while the latter shows the change in mole fraction of components A, B and C in bulk phase II.

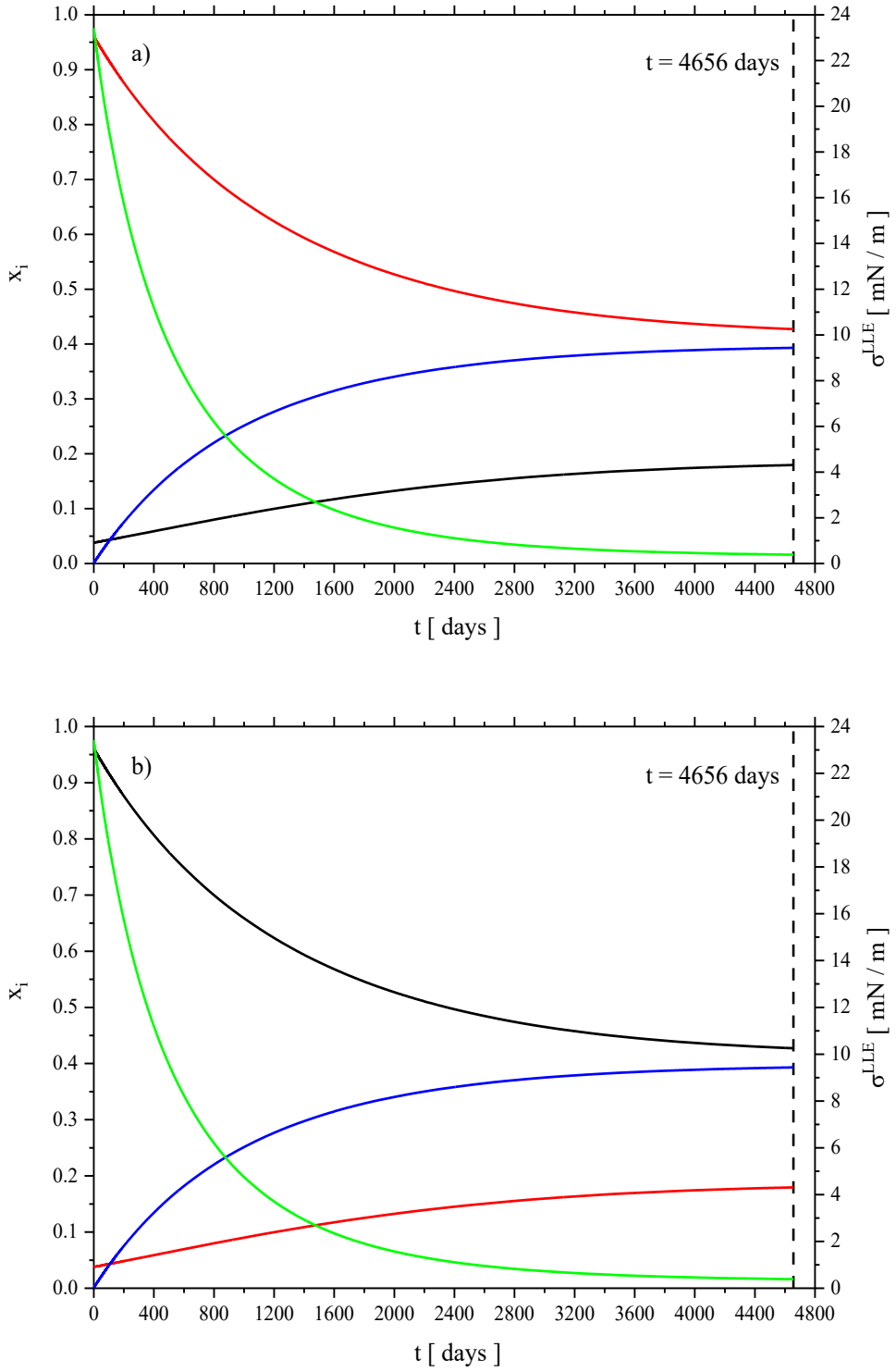

Figure 31. Time evolution of the mole fractions of components A (black line), B (red line) and C (blue line) in both bulk phases (a) bulk phase I and b) bulk phase II) and of the interfacial tension at LLE (green line) given by eq. (118), calculated by solving eq. (123) and eq. (124) at $T = 298.15\ \mathrm{K}$ with $A_{AB} = 3.5$ and $A_{AC} = A_{BC} = 0$ in eq. (101), $\kappa_{AB} = 12 \cdot 10^{-7}\,\frac{\mathrm{J \cdot mol}}{\mathrm{m^4}}$,

$k_1 = 0.5.10^{-8}\ \mathrm{s}^{-1}$, $k_2 = 10^{-8}\ \mathrm{s}^{-1}$, and $M_{AB} = M_{AC} = M_{BC} = 10^{-9}\ \frac{\mathrm{mol}^3}{\mathrm{J.m}^4.\mathrm{s}}$. The dashed line represents the time step at which global equilibrium is reached ($t = 4656$ days).

The temporal evolution of the concentrations in Figure 31 corresponds to the one depicted by both red lines in Figure 28. In addition, the temporal mole fraction profiles of educts A and B are interchanged by switching from phase I (Figure 31a) to phase II (Figure 31b). Therefore, a symmetrical behavior of the reactive nonuniform system can be observed. This behavior can be deduced from the symmetry of the Porter equation (eq. (101) with $A_{AC} = A_{BC} = 0$) and can also be observed in Figure 28, Figure 29 and Figure 30. The time derivatives of all three mole fractions in bulk phases I and II vanish after approximately 4656 days have elapsed since the reactive system was in its initial system state, signifying that global equilibrium has been reached. Consequently, the bulk phase concentrations will remain constant after approximately $t = 4656$ days. This time step is represented by a vertical dashed line in Figure 31.

Only the temporal evolution and the spatial distribution of the concentrations or mole fractions of all three components in both bulk phases as well as at the interface between them have been considered and investigated so far. Given that the reactive system is constantly approaching numerous phase equilibrium states on its way towards reaching the global equilibrium system state, the interfacial tension at LLE of the nonuniform system can be thus also calculated by numerically evaluating the integral in eq. (118) at each single time step of the dynamic evolution, and by plotting it in Figure 31 as σ^{LLE} over time. As can be deduced from Figure 31, the interfacial tension at LLE of the nonuniform system decreases with time, which is in accord with the second law of thermodynamics. Upon chemical reaction and through molecular diffusion, the reactive system will evolve to reach its final global equilibrium system state, at which the entropy of the system takes a maximum value and its Gibbs energy a minimum one. σ^{LLE} decreases with time to finally reach a constant value at global equilibrium and at approximately $t = 4656$ days. This constant value is slightly greater than 0 because the system is evolving towards global equilibrium by approaching the critical point of the mixture, at which, by definition, the interfacial tension vanishes, as can be observed in Figure 28.

A different dynamic modeling of the reactive heterogeneous system will now be presented by repeating the calculations performed above, but now without considering and predicting chemical reactions taking place at the interface between both coexisting liquid bulk phases.

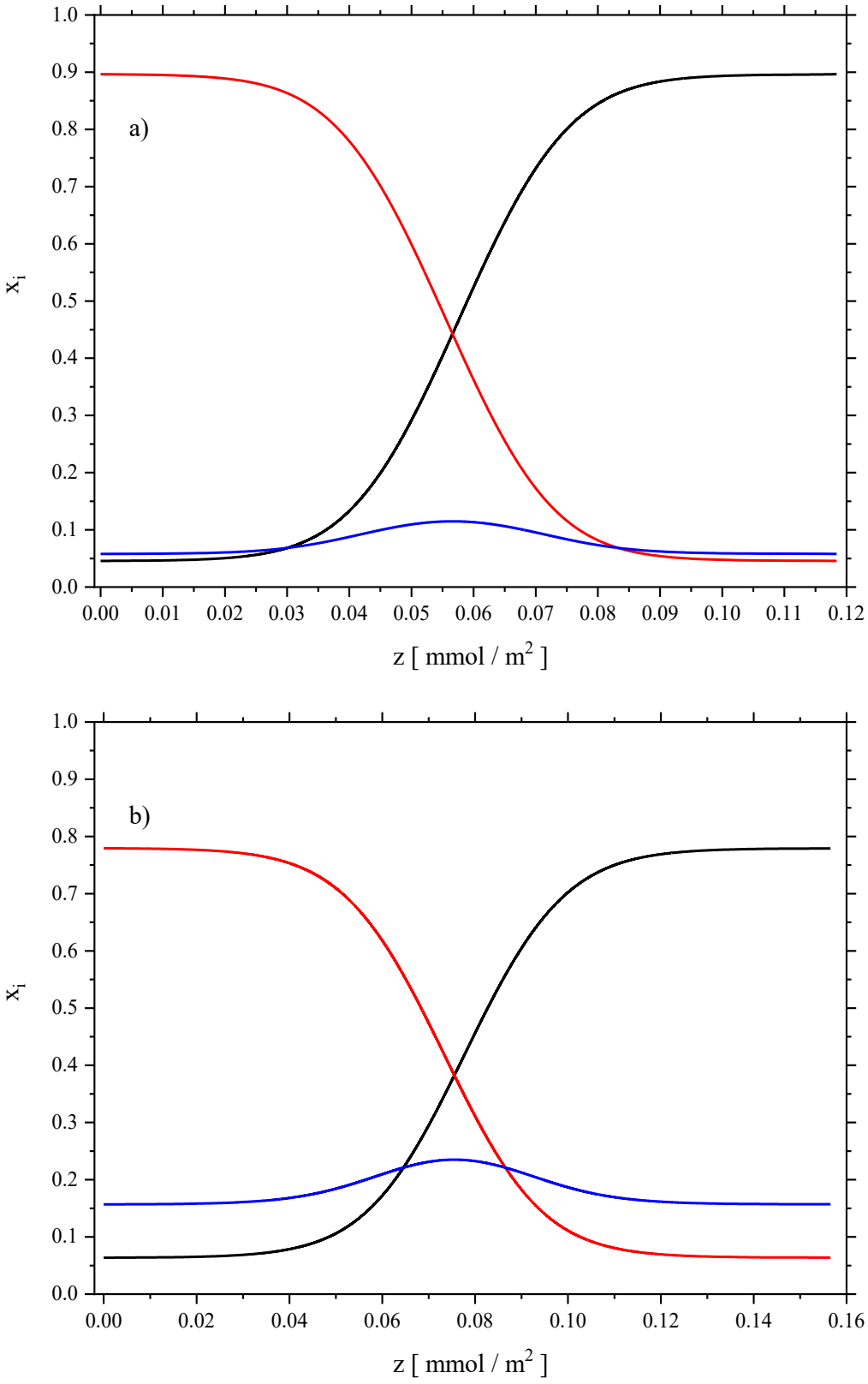

Figure 32. Interfacial mole fraction profiles at different times (a) approximately $t = 149$ days and b) approximately $t = 489$ days) for components A (black line), B (red line), and C (blue

line), calculated by solving eq. (130) and eq. (131) at $T = 298.15\,\mathrm{K}$ with $A_{AB} = 3.5$ and $A_{AC} = A_{BC} = 0$ in eq. (101), $\kappa_{AB} = 12 \cdot 10^{-7}\,\frac{\mathrm{J \cdot mol}}{\mathrm{m^4}}$, $k_1 = 0.5.\,10^{-8}\,\mathrm{s^{-1}}$, $k_2 = 10^{-8}\,\mathrm{s^{-1}}$, and $M_{AB} = M_{AC} = M_{BC} = 10^{-9}\,\frac{\mathrm{mol^3}}{\mathrm{J.m^4.s}}$.

The resulting governing equations for the mole fractions x_A and x_B are derived in subchapter 3.6 and are given by eq. (130) and eq. (131), respectively. The same initial and boundary conditions as the ones applied in the previous calculations for numerical solutions will be considered. The reaction dynamics will now be reevaluated, and the mole fraction profiles, $x_i(z,t)$, that result from the temporal evolution of the mole fraction of the various components will be investigated. Figure 32 shows the calculated interfacial mole fraction profiles at the same time steps as the ones found in Figure 29 and at which the calculations were performed there. Hence, exemplary snapshots of the mole fraction distribution for the one-dimensional numerical solutions of eq. (130) and eq. (131) at approximately $t = 149\,\mathrm{days}$ and $t = 489\,\mathrm{days}$ are illustrated in Figure 32a and Figure 32b, respectively.

Moreover, the evolution of the composition of both liquid bulk phases as well as the interfacial tension at LLE of the nonuniform system over time will also be portrayed. These evolutions are depicted in Figure 33a for bulk phase I and Figure 33b for bulk phase II. Both calculations were also performed by solving eq. (130) and eq. (131).

The interfacial mole fraction profiles in Figure 32, and the bulk phase concentrations as well as the interfacial tension at LLE in Figure 33 are identical to the ones found in Figure 29 and Figure 31, respectively. In addition, the system also reaches global equilibrium at approximately $t = 4656\,\mathrm{days}$ (Figure 33). It can be deduced from both figures (Figure 32 and Figure 33) that the same predictions concerning the ternary reactive system are obtained by neglecting the interfacial chemical reaction, compared to the ones obtained with the chemical reaction occurring at the interface between bulk phases I and II. Therefore, both modeling approaches presented above are equivalent. This is a very important finding that indicates that the interfacial chemical reaction has no impact on the dynamics and evolution of the reactive nonuniform system. The explanation is as follows. Because the diffusion rates across the interface are much higher than the reaction rates, components A, B and C will not have sufficient time to react with each other in the interfacial layer. The amount of reaction that takes place within the interface is thus negligible compared to the amount of reaction occurring in both uniform liquid bulk phases.

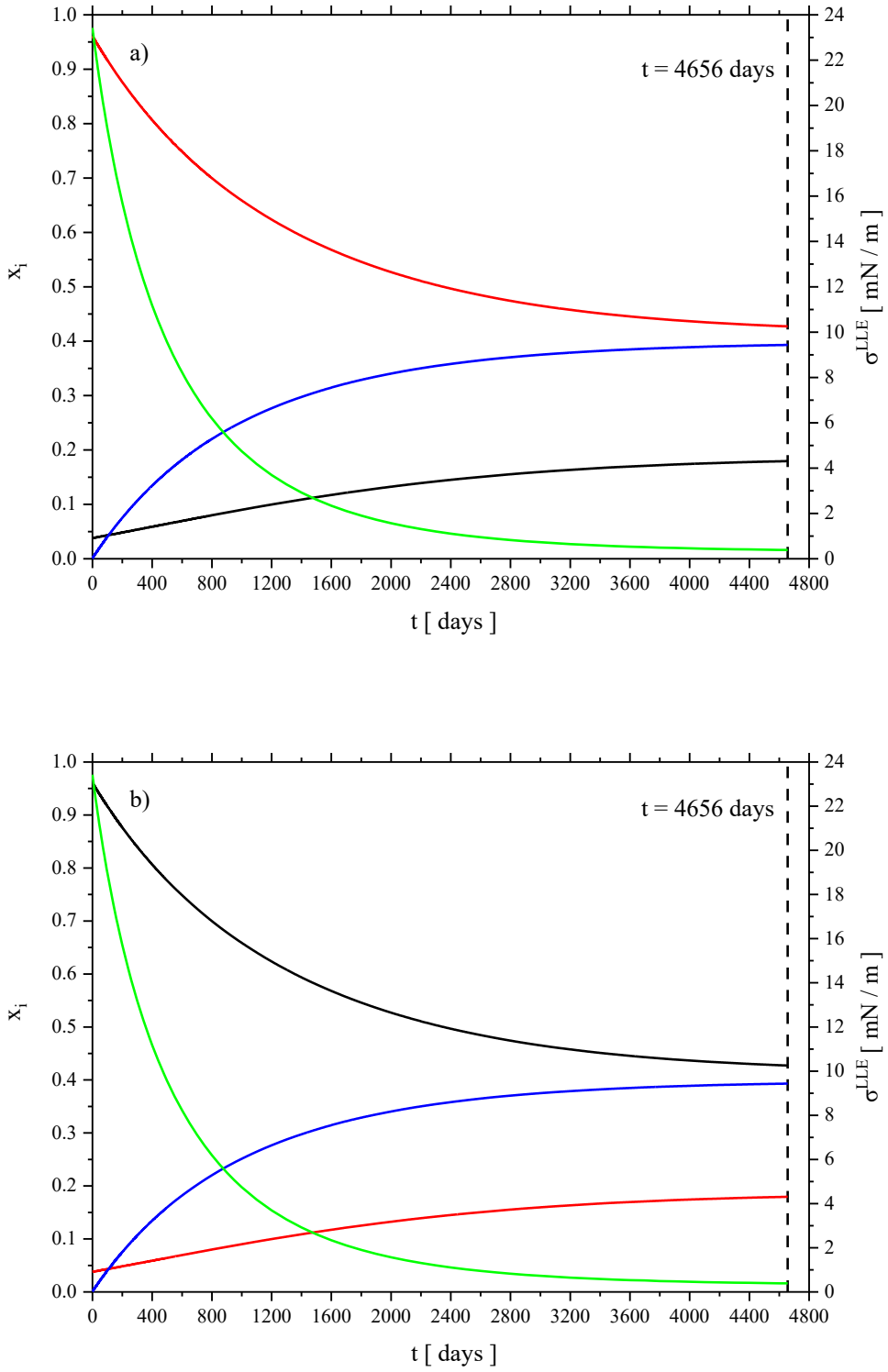

Figure 33. Time evolution of the mole fractions of components A (black line), B (red line) and C (blue line) in both bulk phases (a) bulk phase I and b) bulk phase II) and of the interfacial tension at LLE (green line) given by eq. (118), calculated by solving eq. (130) and eq. (131) at

$T = 298.15\,\mathrm{K}$ with $A_{AB} = 3.5$ and $A_{AC} = A_{BC} = 0$ in eq. (101), $\kappa_{AB} = 12 \cdot 10^{-7}\,\frac{\mathrm{J \cdot mol}}{\mathrm{m^4}}$, $k_1 = 0.5.10^{-8}\,\mathrm{s^{-1}}$, $k_2 = 10^{-8}\,\mathrm{s^{-1}}$, and $M_{AB} = M_{AC} = M_{BC} = 10^{-9}\,\frac{\mathrm{mol^3}}{\mathrm{J.m^4.s}}$. The dashed line represents the time step at which global equilibrium is reached ($t = 4656$ days).

As such, the chemical reaction within the interface between both bulk phases can be neglected, and there will be only diffusion taking place across the interface. This observation also confirms various assumptions made in the literature concerning the evolution of reactive heterogeneous systems (e.g., [98,99]). Danzer and Enders [98,99] studied the dynamics of the interfacial properties of a specific chemical reaction, namely the esterification reaction of 1-hexanol with acetic acid to hexyl acetate and water. Two liquid phases were involved in the reactive process, and the evolution of the interfacial properties of the reactive liquid system over time was modeled by combining the inc-DGT with rate equations, and compared to experimental data. In fact, Danzer and Enders [98,99] considered the beforementioned noncatalyzed esterification reaction, which is a very slow chemical reaction, and assumed that it can only take place in both liquid bulk phases that are present in the reactive system, thus, no reaction in the interface between them was modeled. The chemical reaction being extremely slow, they [98,99] thus opted for a quasistationary modeling approach by fulfilling the criteria for phase equilibrium after each reaction step in both bulk phases, hence, assuming instantaneous diffusion rates across the interface. For this reason, they [98,99] did not incorporate any diffusion equation into their model. Furthermore, Danzer and Enders [98] predicted the evolution of the interfacial tension at LLE of the nonuniform system over time, which was found to reproduce the experimental values accurately. Based on the predictions and observations made in this subchapter concerning reactive nonuniform systems characterized by diffusion rates being much higher than reaction rates, the assumption of neglecting the interfacial chemical reaction in [98,99] can thus be justified.

Finally, it is important to understand that the results presented above are only true for the limiting situation in which the reaction is much slower than the rate of diffusion in a reactive heterogeneous system. Opposing results emerge for the other limiting case of the model, in which the rate of reaction is effectively instantaneous. In this case, interfacial chemical reactions have a marked impact on the overall reacting system, as has been demonstrated in subchapter 4.1.

5 Conclusions and Outlook

In conclusion, a unified thermodynamic theory of reaction and diffusion in reactive heterogeneous liquid systems has been introduced. By combining the DGT in its incompressible version, which allows a continuous description of the chemical potential throughout the bulk phases and the interface between them, with thermodynamic consistent rate equations based on activities following a general stoichiometry, and the modified and generalized Cahn-Hilliard equation based on Onsager diffusion, a generalized theoretical treatment that can be applied to model the combined reaction and transport in nonuniform reactive systems has been proposed. In particular, this theoretical treatment is used to predict the interfacial concentration profiles of reacting liquid mixtures, in which chemical reactions will take place in uniform bulk phases as well as at the interface between them.

For this purpose, a generalized theoretical framework regarding the interfacial properties of reactive inhomogeneous liquid systems has been derived. The dynamics as well as the interfacial properties of a specific reactive ternary liquid system have been investigated for both limiting cases of reacting mixtures, in which, on the one hand, the reaction is much faster than the rate of diffusion, thus, the rate of reaction is effectively instantaneous, and, on the other hand, the diffusion across the interface is much faster than the rate of reaction.

Concerning the first limiting situation, in which the rate of reaction is effectively instantaneous, a suitable model example typical of many nonideal reactive systems has been studied. The approach revealed that interfacial chemical reactions have a large impact on the dynamics and evolution of reactive liquid systems characterized by reaction rates that are much higher than diffusion rates through the interface. In particular, the system in question must finally reach a stable chemical equilibrium state. If the miscibility gap between the reaction educts is assumed to be sufficiently large, then the reaction product will be mainly formed in the interface. Simultaneously, the product is enriched at the interface and acts as a solubilizer for the educts. It has been found that chemical equilibrium is reached first in both liquid bulk phases, and then at the interface between them, which is an effect more or less pronounced depending on the size

of the miscibility gap. The considered model examples were also used to perform sensitivity analysis in terms of the applied thermodynamic and kinetic parameters within the derived theoretical framework. The obtained predictions were compared with a standard model example. The impact of the Porter coefficients, the reaction rate coefficients, and the influence parameter on the dynamics of the investigated reactive systems was studied, while taking the standard model example as a reference for comparison. The predictions and results revealed that variations in the applied thermodynamic and kinetic parameters of the theoretical framework led to the expected reactive and phase behavior of the studied model examples.

Concerning the second limiting situation, in which diffusion is much faster than the rate of reaction, the theoretical treatment has been applied to predict the interfacial concentration profiles and the interfacial tension at LLE of a suitable ternary model example. The approach revealed that interfacial chemical reactions have no impact on the dynamics and evolution of reactive liquid systems characterized by reaction rates that are much smaller than diffusion rates across the interface. In particular, the studied reactive system must finally reach a stable global equilibrium state, at which the combined phase and chemical equilibria in both liquid bulk phases are reached. The reactive nonuniform system evolves towards this global equilibrium system state by constantly approaching phase equilibrium states, signifying that the mixture will remain in phase equilibrium upon reaction.

Some assumptions made within this work, more precisely within the dynamic modeling of reactive nonuniform liquid systems, have limitations regarding their validity concerning reactive extraction processes. For instance, the derived component continuity equations can be augmented with hydrodynamic interactions including convective flows that must be considered in practical production and extraction processes. Furthermore, the assumption of an isothermal process or a constant temperature upon reaction, and thus a vanishing heat of reaction, can be corrected by incorporating a temperature dependence of the various types of equilibria and kinetics within the derived model, and by including heat transfer models in the generalized theoretical framework, all of which must also be considered in practical separation processes. These model extensions result in a significant increase in the complexity of the theoretical framework, but would also lead to an even more detailed description and understanding of reactive extraction processes.

References

[1] N.L. Ricker, J.N. Michaels, C.J. King, Solvent properties of organic bases for extraction of acetic acid from water, J. Sep. Proc. Technol. 1 (1979) 36-41.

[2] C.J. King, Ch. 18.5 of "Handbook of Solvent Extraction", TC Lo, MHI Baird and C. Hanson, Wiley, New York (1983).

[3] M. Siebenhofer, R. Marr, Acid extraction by amines, Proceedings of the ISEC, Denver, CO, USA 28 (1983).

[4] M. Siebenhofer, R. Marr, Auswirkung der Extraktionsmittel-Zusammensetzung auf den Stoffaustausch und die Apparateauswahl am Beispiel der Essigsäure-Extraktion, Chem. Ing. Tech. 57 (1985) 558-559.

[5] B. Wojtech, M. Mayer, Synergistische Effekte bei der Extraktion mit tertiären Aminen, Chem. Ing. Tech. 57 (1985) 134-136.

[6] R. Wennersten, ISEC '80, Liege, Proc. 80-63 (1980).

[7] R. Wennersten, The extraction of citric acid from fermentation broth using a solution of a tertiary amine, J. Chem. Tech. Biotechnol. 33 (1983) 85-94.

[8] J. Yu-Ming, L. Dao-Chen, S. Yuan-Fu, Study on extraction of citric acid, Proc. Int. Solvent Extr. Conf., Denver, CO. (1983).

[9] J.P. Behr, J.M. Lehn, Transport in organic chemistry. I. Transport of amino acids through organic liquid membranes, J. Am. Chem. Soc. 95 (1973) 6108-6110.

[10] W. Halwachs, E. Schlichting, K. Schügerl, Reaktivextraktion von Salicylsäure und d,l-Phenylalanin, Chem. Ind. 36 (1984) 458.

[11] E. Schlichting, W. Halwachs, K. Schügerl, Reaktive extraction of salicylic acid and D, L-phenylalanine in a bench-scale pulsed sieve plate column, Chem. Eng. Proc. 19 (1985) 317-328.

[12] M. Reschke, K. Schügerl, Reactive extraction of penicillin I: Stability of penicillin G in the presence of carriers and relationships for distribution coefficients and degrees, Chem. Eng. J. 28 (1984) B1-B9.

[13] P. Vanura, L. Kuca, Extraction of citric acid by the toluene solutions of trilaurylamine, Collect. Czech. Chem. Commun. 41 (1976) 2857-2877.

[14] J.M. Wardell, C.J. King, Solvent equilibriums for extraction of carboxylic acids from water, J. Chem. Eng. Data 23 (1978) 144-148.

[15] R. Wennersten, The extraction of citric acid from fermentation broth using a solution of a tertiary amine, J. Chem. Tech. Biotechnol. 33 (1983) 85-94.

[16] T. Sato, H. Watanabe, H. Nakamura, Extraction des acides lactique, tartrique, succinique et citrique par la trioctylamine, Bunseki Kagaku 34 (1985) 559-563.

[17] W. Rückl, M. Siebenhofer, R. Marr, Separation of citric acid from aqueous fermentation solutions by extraction-reextraction processes, Proc. Int. Solv. Ext. Conf. (1986).

[18] J.A. Tamada, A.S. Kertes, C.J. King, Extraction of carboxylic acids with amine extractants. 1. Equilibria and law of mass action modeling, Ind. Eng. Chem. Res. 29 (1990) 1319-1326.

[19] V. Bizek, J. Horacek, R. Rericha, M. Kousova, Amine extraction of hydroxycarboxylic acids. 1. Extraction of citric acid with 1-octanol/n-heptane solutions of trialkylamine, Ind. Eng. Chem. Res. 31 (1992) 1554-1562.

[20] V. Bizek, J. Horacek, M. Kousova, A. Heyberger, J. Prochazka, Mathematical model of extraction of citric acid with amine, Chem. Eng. Sci. 47 (1992) 1433-1440.

[21] C.J. King, Amine-based systems for carboxylic acid recovery, Chemtech. 22 (1992) 285-291.

[22] R.S. Juang, W.T. Huang, Equilibrium studies on the extraction of citric acid from aqueous solutions with tri-n-octylamine, J. Chem. Eng. Jpn. 27 (1994) 498-504.

[23] E. Schlichting, W. Halwachs, K. Schügerl, Reactive extraction of salicylic acid and D, L phenylalanine in a stirred cell, Chem. Eng. Com. 51 (1987) 193-205.

[24] R. Marr, H.J. Bart, Metallsalz-Extraktion, Chem. Ing. Tech. 54 (1982) 119-129.

[25] W. Büchner, R. Schliebs, G. Winter, K.H. Büchel, Industrial inorganic chemistry. 2. rev. ed. Industrielle anorganische Chemie, VCH Verlagsges., Weinheim (1986).

[26] E. Hauer, R. Marr, Extraktive Stofftrennverfahren in der Biotechnologie, Chem. Ing. Tech. 63 (1991) 809-816.

[27] S.Y. Lee, J.M. Kim, H. Song, J.W. Lee, T.Y. Kim, Y.S. Yang, From genome sequence to integrated bioprocess for succinic acid production by Mannheimia succiniciproducens, Appl. Microbiol. Biotechnol. 79 (2008) 11-22.

[28] H. Ziegenfuß, G. Maurer, Distribution of acetic acid between water and organic solutions of tri-n-octylamine, Fluid Phase Equilibria 102 (1994) 211-255.

[29] T. Kirsch, G. Maurer, Distribution of oxalic acid between water and organic solutions of tri-n-octylamine, Ind. Eng. Chem. Res. 35 (1996) 1722-1735.

[30] T. Kirsch, H. Ziegenfuß, G. Maurer, Distribution of citric, acetic and oxalic acids between water and organic solutions of tri-n-octylamine, Fluid Phase Equilibria 129 (1997) 235-266.

[31] T. Kirsch, G. Maurer, Distribution of binary mixtures of citric, acetic and oxalic acid between water and organic solutions of tri-n-octylamine Part I. Organic solvent toluene, Fluid Phase Equilibria 131 (1997) 213-231.

[32] T. Kirsch, G. Maurer, Phasengleichgewichte bei der Reaktivextraktion von Carbonsäuregemischen, Chem. Ing. Tech. 69 (1997) 1104-1108.

[33] T. Kirsch, G. Maurer, Distribution of binary mixtures of citric, acetic and oxalic acid between water and organic solutions of tri-n-octylamine: Part II. Organic solvent methylisobutylketone, Fluid Phase Equilibria 142 (1998) 215-230.

[34] T. Kirsch, G. Maurer, Distribution of binary mixtures of citric, acetic and oxalic acid between water and organic solutions of tri-n-octylamine: Part III. Organic solvent chloroform, Fluid Phase Equilibria 146 (1998) 297-313.

[35] G.C. Jagirdar, M.M. Sharma, Recovery and separation of mixtures of organic acids from dilute aqueous solutions, J. Separ. Proc. Technol. 1 (1980) 40-43.

[36] G. Malmary, A. Vezier, A. Robert, J. Mourgues, T. Conte, J. Molinier, Recovery of tartaric and malic acids from dilute aqueous effluents by solvent extaction technique, J. Chem. Tech. Biotechnol. 60 (1994) 67-71.

[37] M.M. Anwar, A.S. Arif, D.W. Pritchard, Separation of closely related organic acids and bases dissociation extraction, Solvent Extraction and Ion Exchange 13 (1995) 127-142.

[38] K.S. Pitzer, Thermodynamics of electrolytes. I. Theoretical basis and general equations, J. Phys. Chem. 77 (1973) 268-277.

[39] C. Cianetti, P.R. Danesi, Kinetics and mechanism of the interfacial mass transfer of Zn2+, Co2+, Ni2+ in the system: bis(2-ethylhexyl)phosphoric acid, n-dodecane-KNO3, water, Solvent Extraction and Ion Exchange 1 (1983) 9-26.

[40] Z. Kolarik, M. Kunzmann, Extraction of zinc (II) with bis (2-ethylhexyl) phosphoric acid from perchlorate and sulfate media, EFCE Working Party Meeting (1989).

[41] T.C. Huang, R.S. Juang, Extraction equilibrium of zinc from sulfate media with bis(2-ethylhexyl) phosphoric acid, Ind. Eng. Chem. Fundamen. 25 (1986) 752-757.

[42] H.J. Bart, R. Berger, T. Misek, M.J. Slater, J. Schröter, B. Wächter, Recommended systems for liquid extraction studies, Liquid-Liquid Extraction Equipment (Eds: JC Godfrey, MJ Slater), John Wiley & Sons, Chichester 1 (1994).

[43] B. Wachter, H.J. Bart, T. Moosbrugger, R. Marr. Reactive liquid-liquid test system Zn/Di (2-ethyl hexyl) phosphoric acid/n-Dodecane. Equilibrium and kinetics, Chem. Eng. Technol. 16 (1993) 413-421.

[44] R. Grimm, Z. Kolarik, Properties of complexes formed by Cu (II), Ni (II), Zn (II) and Cd (II) with Di (2-ethylhexyl) phosphoric acid in organic solvents, J. Inorg. Nucl. Chem. 38 (1976) 1493-1500.

[45] Z. Kolarik, Critical evaluation of some equilibrium constants involving acidic organophosphorus extractants, Pure & Appl. Chem. 54 (1982) 2593-2674.

[46] J.M. Hildebrand, R.L. Scott, The Solubility of Nonelectrolytes, Reinhold Publishing Corporation, third edit. (1950).

[47] R.D. Neumann, S.J. Park, N.F. Zhou, P. Shah, Interfacial phenomena in hydrometallurgical solvent extraction systems, Solvent Extraction in the Process Industries 3 (1993) 1689-1696.

[48] H.J. Bart, Reaktivextraktion–Ein Statusbericht zur Simulation gerührter Kolonnen, Chem. Ing. Tech. 74 (2002) 229-241.

[49] H.J. Bart, Reactive Extraction, Springer Verlag, Berlin (2001).

[50] C.V.R. Murthy, E.S. Perez de Ortiz, Comparisons between single drop and stirred cell techniques in the modelling of the stripping of zinc from di (2-ethylhexyl) phosphoric acid, ISEC'86--International Solvent Extraction Conference. Preprints. (1986) 353-360.

[51] T.C. Juang, R.S. Juang, Kinetics and mechanism of zinc extraction from sulfate medium with di (2-ethylhexyl) phosphoric acid, J. Chem. Eng. Jpn 19 (1986) 379-386.

[52] H.F. Svendsen, G. Schei, M. Osman, Kinetics of extraction of zinc by di (2-ethylhexyl) phosphoric acid in cumene, Hydrometall. 25 (1990) 197-212.

[53] L.A. Ajawin, E.S. Perez de Ortiz, H. Sawistowski, Kinetics of extraction of zinc by di (2-ethylhexyl) phosphoric acid in n-heptane, Proc. Internat. Solvent Extraction Conf. 3 (1980) 80-112.

[54] W. Nitsch, K. Hillekamp, Zur Kinetic der Zinkionenextraktion aus Wasser in dithizonbeladene Solventien, Chem. Ztg. 96 (1972) 254-261.

[55] J.B. Lewis, The mechanism of mass transfer of solutes across liquid-liquid interfaces: Part I: the determination of individual transfer coefficients for binary systems, Chem. Eng. Sci. 3 (1954) 248-259.

[56] W.K. Lewis, W.G. Whitman, Principles of gas absorption, Ind. Eng. Chem. 16 (1924) 1215-1220.

[57] R. Higbie, The rate of absorption of pure gas into a still liquid during short periods of exposure, Trans. Am. Inst. Chem. Engrs. 31 (1935) 365-389.

[58] P.V. Danckwerts, Significance of liquid-film coefficients in gas absorption, Ind. Eng. Chem. 43 (1951) 1460-1467.

[59] J. Hajjar, S. Enders, Interfacial properties of fast chemical reactions occurring in demixed ternary mixtures, Fluid Phase Equilibria 568 (2023) 113758.

[60] C.I. Koncsag, A. Barbulescu, Liquid-liquid extraction with and without a chemical reaction, in: M. El-Amin (Ed.), Mass Transfer in Multiphase Systems and its Applications, IntechOpen (2011).

[61] M. Steensma, K.R. Westerterp, Thermally safe operation of a semibatch reactor for liquid-liquid reactions-fast reactions, Chem. Eng. Technol. 14 (1991) 367-375.

[62] K. Schügerl, R. Hänsel, E. Schlichting, W. Halwachs, Reaktivextraktion, Chem. Ing. Tech. 58 (1986) 308-317.

[63] K.D. Samant, K.M. Ng, Effect of kinetics and mass transfer on design of extractive reaction processes, AIChE J. 44 (1998) 2212-2228.

[64] D.S. Abrams, J.M. Prausnitz, Statistical thermodynamics of liquid mixtures: a new expression for the excess Gibbs energy of partly or completely miscible systems, AIChE J. 21 (1975) 116-128.

[65] J.C. Maxwell, IV. On the dynamical theory of gases, Phil. Trans. Roy. Soc. 157 (1867) 49-88.

[66] J. Stefan, Über das Gleichgewicht und die Bewegung, insbesondere die Diffusion von Gasgemengen, Sitzber. Akad. Wiss. Wien 63 (1871) 63-124.

[67] J. Wu, Z. Li, Density-functional theory for complex fluids, Annu. Rev. Phys. Chem. 58 (2007) 85-112.

[68] J.W. Cahn, J.E. Hilliard, Free energy of a nonuniform system. I. Interfacial free energy, J. Chem. Phys. 28 (1958) 258-267.

[69] J. D. van der Waals, Thermodynamische theorie der capillariteit onder de hypothese van een continue verandering van dichtheid, Verhandelingen der Koninklijke Nederlandsche Akademie van Wetenschappen te Amsterdam 1 (1893) 1-56.

[70] C.I. Poser, I.C. Sanchez, Interfacial tension theory of low and high molecular weight liquid mixtures, Macromolecules 14 (1981) 361-370.

[71] H. Kahl, S. Enders, Interfacial properties of binary mixtures, Phys. Chem. Chem. Phys. 4 (2002) 931-936.

[72] C. Miqueu, B. Mendiboure, C. Graciaa, J. Lachaise, Modelling of the surfactant tension of binary and ternary mixtures with the gradient theory of fluid interfaces, Fluid Phase Equilibria 218 (2004) 189-203.

[73] C. Miqueu, B. Mendiboure, A. Graciaa, J. Lachaise, Modeling of the surface tension of multicomponent mixtures with the gradient theory of fluid interfaces, Ind. Eng. Chem. Res. 44 (2005) 3321-3329.

[74] H. Lin, Y.-.Y. Duan, Q. Min, Gradient theory modeling of surface tension for pure fluids and binary mixtures, Fluid Phase Equilibria 254 (2007) 75-90.

[75] D. Fu, Y. Wei, Investigation of vapor-liquid surface tension for carbon dioxide and hydrocarbon mixtures by perturbed-chain statistical associating fluid theory combined with density-gradient theory, Ind. Eng. Chem. Res. 47 (2008) 4490-4495.

[76] C. Miqueu, B. Mendiboure, A. Graciaa, J. Lachaise, Petroleum mixtures: an efficient predictive method for surface tension estimations at reservoir conditions, Fuel 87 (2008) 612-621.

[77] O.G. Niño Amézquita, S. Enders, P.T. Jaeger, R. Eggers, Measurement and prediction of interfacial tension of binary mixtures, J. Supercrit. Fluids 55 (2010) 724-734.

[78] E. Schäfer, F. Horbach, S. Enders, Modeling of liquid–liquid interfacial properties of binary and ternary mixtures, J. Chem. Eng. Data 59 (2014) 3003-3016.

[79] S. Werth, M. Kohns, K. Langenbach, M. Heilig, M. Horsch, H. Hasse, Interfacial and bulk properties of vapor-liquid equilibria in the system toluene + hydrogen chloride + carbon dioxide by molecular simulation and density gradient theory + PC-SAFT, Fluid Phase Equilibria 427 (2016) 219-230.

[80] J. Mairhofer, J. Gross, Modeling of interfacial properties of multicomponent systems using density gradient theory and PCP-SAFT, Fluid Phase Equilibria 439 (2017) 31-42.

[81] S. Enders, K. Quitzsch, Calculation of interfacial properties of demixed fluids using density gradient theory, Langmuir 14 (1998) 4606-4614.

[82] T. Zeiner, P. Schrader, S. Enders, D. Browarzik, Phase- and interfacial behavior of hyperbranched polymer solutions, Fluid Phase Equilibria 302 (2011) 321-330.

[83] T. Grunert, H. Rudolph, S. Enders, Experimental and theoretical investigation of interfacial properties of demixed ternary systems, Z. Phys. Chem. 227 (2013) 269-284.

[84] T. Grunert, S. Enders, Prediction of interfacial properties of the ternary system water + benzene + butan-1-ol, Fluid Phase Equilibria 381 (2014) 46-50.

[85] H. Cárdenas, M. Cartes, A. Mejía, Atmospheric densities and interfacial tensions for 1-alkanol (1-butanol to 1-octanol) +water and ether (MTBE, ETBE, DIPE, TAME and THP) +water demixed mixtures, Fluid Phase Equilibria 396 (2015) 88-97.

[86] A. Kulaguin Chicaroux, A. Górak, T. Zeiner, Demixing behavior of binary polymer mixtures, J. Mol. Liquids 209 (2015) 42-49.

[87] A.K. Chicaroux, T. Zeiner, Investigation of interfacial properties of aqueous two-phase systems by density gradient theory, Fluid Phase Equilibria 407 (2016) 135-142.

[88] T. Goetsch, A. Danzer, P. Zimmermann, A. Köhler, K. Kissing, S. Enders, T. Zeiner, Liquid-liquid equilibrium and interfacial tension of hexane isomers - methanol systems, Ind. Eng. Chem. Res. 56 (2017) 9743-9752.

[89] A. Danzer, S. Enders, Comparison of two modeling approaches for the interfacial tension of binary aqueous mixtures, J. Mol. Liquids 266 (2018) 309-320.

[90] A. Danzer, S. Enders, Theoretical and experimental investigation of the interfacial properties in the ternary mixture water + 1-hexanol + acetic acid and water + hexylacetate + acetic acid using density gradient theory and spinning-drop tensiometry, J. Mol. Liquids 283 (2019) 482-490.

[91] A. Danzer, S. Enders, Prediction of phase equilibrium and interfacial properties in the quaternary system water + 1-hexanol + hexylacetate + acetic acid, Fluid Phase Equilibria 493 (2019) 50-57.

[92] E. Nauman, D.Q. He, Nonlinear diffusion and phase separation, Chem. Eng. Sci. 56 (2001) 1999-2018.

[93] K.F. Kruber, M. Krapoth, T. Zeiner, Interfacial mass transfer in ternary liquid-liquid systems, Fluid Phase Equilibria 440 (2017) 54-63.

[94] A. Kulaguin-Chicaroux, T. Zeiner, Interfacial behavior of aqueous two-phase systems based on linear and hyperbranched polymers, J. Chem. Eng. Data 63 (2018) 2467-2476.

[95] A. Kulaguin Chicaroux, T. Zeiner, Theoretical and experimental investigation of mass transfer in aqueous two-phase systems based on linear and branched polymers, Fluid Phase Equilibria 479 (2019) 106-113.

[96] R. Nagl, P. Zimmermann, T. Zeiner, Interfacial mass transfer in water-toluene systems, J. Chem. Eng. Data 65 (2020) 328-336.

[97] R. Nagl, T. Zeiner, P. Zimmermann, Interfacial mass transfer in quaternary liquid-liquid systems, Chem. Eng. Proc. - Process Intens. 171 (2022) 108501.

[98] A. Danzer, S. Enders, The modelling of the time-dependency of interfacial properties due to chemical equilibrium reactions in demixed liquid systems, Fluid Phase Equilibria 499 (2019) 112240.

[99] A. Danzer, S. Enders, Thermodynamic modelling of time-dependent interfacial properties in reactive liquid-liquid systems close to the critical point, J. Chem. Eng. Data 65 (2020) 312-318.

[100] A.A. Alfarraj, E.B. Nauman, Reactive phase separation: Prediction of an occlusion morphology, Polymer 49 (2008) 339-344.

[101] R. Nagl, S. Stocker, P. Zimmermann, T. Zeiner, Study on mass transfer in reactive liquid-liquid systems, Chem. Eng. Res. Des. 186 (2022) 541-555.

[102] J. Hajjar, S. Enders, Combined reaction and diffusion across the interface in reactive nonuniform liquid systems, Fluid Phase Equilibria 578 (2024) 114001.

[103] A. Fick, Über Diffusion, Pogg. Ann. 94 (1855) 59-86.

[104] L. Onsager, Reciprocal relations in irreversible processes. I., Physical review 37 (1931) 405-426.

[105] E. Petrishcheva, R. Abart, Exsolution by spinodal decomposition in multicomponent mineral solutions, Acta Materialia 60 (2012) 5481-5493.

[106] J.W. Cahn, J.E. Hilliard, Spinodal decomposition: A reprise, Acta Metallurgica 19 (1971) 151-161.

[107] J.W. Gibbs, On the Equilibrium of Heterogeneous Substances, Transactions of the Connecticut Academy of Arts and Sciences 3 (1876) 108-248; (1878) 343-524.

[108] B. L. Beegle, M. Modell, R. C. Reid, Thermodynamic stability criterion for pure substances and mixtures, AIChE Journal 20 (1974) 1200-1206.

[109] R. C. Reid, B. L. Beegle, Critical point criteria in legendre transform notation, AIChE Journal 23 (1977) 726-732.

[110] R. P. Brent, Algorithms for minimization without derivatives, Courier Corporation (2013).

[111] J. Stoer, R. Bulirsch, Introduction to numerical analysis, Springer Science & Business Media 12 (2013).

[112] J. Hajjar, S. Enders, Dynamic modelling of the interfacial concentration profiles of fast chemical reactions in reactive liquid-liquid systems, Molecular Physics 121 (2023) e2229907.